Material migration during high pressure metamorphism(Dissertation_全文)

AUTHOR(S):

Goto, Atsushi

(2)

Material migration during high pressure metamorphism

by

Atsushi Goto

1992. 5. 18.

Thesis submitted for the Degree of Doctor of Science

Kyoto University

Contents

Material migration during high pressure metamorphism

General Introduction

The compositional differentiation will accompany the chemical processes.

Metamorphic processes have a reputation for being exceedingly slow and complicated. Thus the mechanism of material migration during metamorphism is also complex. It is often not clear what mechanism of material migration affected the chemistry and mineralogy of metamorphic rocks. I intend to examine the material migration during high pressure metamorphism using bulk rock compositions.

In part 1 of this thesis, I have attempted to decipher whether a substantial amount of materials migrated during the Sanbagawa high pressure metamorphism, using the bulk compositions of pelitic schists. The present data are capable of understanding the geochemical nature of the Sanbagawa pelitic schist. Since variations in chemical composition of metamorphic rocks result mainly from those of original rocks, it is difficult to make clear the compositional changes caused by metamorphism. However, the present data combined with available petrographical data should yield some important information on detecting material migration during the Sanbagawa metamorphism. The present data also allow us to examine the compositional dependece on phase equilibria. The importance of bulk rock chemistry in phase petrology lies on the following point:

Mineral assemblages of metamorphic rocks depend on pressure and temperature which they had undergone and also on the chemistry of rocks and fluids. For the Sanbagawa metamorphic

belt, mineral assemblages change across mineral zones. Up to recent, metamorphic petrologists used phase equilibria independent of or insensitive with bulk chemical compositions when they estimated pressure and temperature of metamorphism. They went ahead with their work on deducing pressure and temperature trajectory of the metamorphism using the chemical trend of zoned minerals such as garnet in pelitic schists (e.g., Banno et al., 1986) and amphibole in hematite-bearing basic schists (Otsuki and Banno, 1990). However, such an approach requires that the effective chemical environment is known at every stage of crystal growth or resorption. Unless the rocks in question are isochemical, or the mode of a particular mineral in question is small, the comparison of zonal structure yields little information on quantifying pressure and temperature trajectory.

Large amounts of H_2O and CO_2 are released when sedimentary rocks are metamorphosed. Thus metamorphic petrologists have assumed and believed that a free fluid is always present during at least prograde metamorphism. The fluid flows upward because of its low density. The amount of fluids present at certain time is too small to hydrate a rock. Thus, the fluid-saturated conditions are not always attained during retrograde or hydration processes. In part 2 of this thesis I and my co-worker, Professor Shohei Banno, examined the hydration of pre-Sanbagawa granulite facies rocks to garnet-epidote amphibolite under the conditions of the Sanbagawa metamorphism. To understand the conditions and mechanism of the hydration, we developed calculations using an infiltration metasomatic model. I contributed to the experiments

and calculations. The sampling, discussion and writing were our collaboration.

Water drastically lowers the solidus temperature of peridotite. In particular, the origin of subduction zone magmas has been related to the introduction of water generated by the breakdown of hydrous minerals in subducted lithosphere (e.g., Fyfe and McBirney, 1975). Tatsumi (1986, 1989) emphasized that water released from pargasitic amphibole and phlogopite in peridotite plays an essential role in producing magmas at the volcanic front and at the back arc side of a volcanic arc, respectively. In part 3 of this thesis I and my co-worker, Dr. Yoshiyuki Tatsumi, obtained the stability of chlorite in the upper mantle using thermodynamic calculations to understand the role of chlorite in subduction zone magmatism. I contributed to the calculations. The idea of the origin of subduction zone magmas was attributed to Dr. Yoshiyuki Tatsumi. The writing was our collaboration.

References

Banno, S., Sakai, C. and Higashino, T., 1986. Pressure-temperature trajectory of the Sanbagawa metamorphism deduced from garnet zoning. Lithos, 19, 51-63.

Fyfe, W. S., and McBirney, A. R., 1975. Subduction and the structure of andesitic volcanic belts. Am. J. Sci., 275-A, 285-297.

Otsuki, M. and Banno, S., 1990. Prograde and retrograde metamorphism of hematite-bearing basic schists in the Sanbagawa belt in central Shikoku. J. metam. Geol., 8, 425-439.

Tatsumi, Y., 1986. Formation of the volcanic front in subduction zones. Geophys. Res. Lett., 13, 717-720.

Tatsumi, Y., 1989. Migration of fluid phases and genesis of basalt magmas in subduction zones. J. Geophys. Res., 94, 4697-4707.

Acknowledgements

I wish to thank my supervisor, Professor Shohei Banno, for his continuous encouragements and stimulating discussions throughout this study and for critical reading of the manuscript. I wish to thank Drs. Toshio Higashino, and Chihiro Sakai for their providing me many rock samples and also kind advice.

Thanks are also due to; Dr. Takeshi Mori, who trained me for electron microprobe analyses; Dr. Yoshiyuki Tatsumi, who shared the improvement of an X-ray fluorescent analysis with me; Dr. Kazumi Yokoyama, who provided rock samples and helped a sampling of granulite and its hydrated derivatives; Dr. Simon R. Wallis who improved the part 2 of this thesis; Dr. A. J. Crawford who improved the part 3 of this thesis; Messrs. Hisao Tsutsumi and Kinzo Yoshida for providing thin sections; Rigaku Corporation, which provided me the opportunity of using the XRF spectrometers.

A part of this study was supported by a Grant-in-Aid for Scientific Research from the Ministry of Education, Science and Culture of Japan (Grant Nos. 62103006, 62103007, 01790351, 03740419).

Finally I thank my family for their support.

主論文 1

Part 1

Geochemistry of the Sanbagawa pelitic schists in central Shikoku, Japan

Abstract

Based on about 200 analyses of the Sanbagawa pelitic schists, the geochemistry and their effect on the metamorphic paragenesis have been examined. TiO_2, Al_2O_3, Fe_2O_3 and MgO are negatively correlated with SiO_2, while MnO, CaO, Na_2O and K_2O and the trace elements are poorly correlated with SiO_2. The mg-value, the K/Ba and K/Rb ratios are constant over different mineral zones without a few exceptional samples. The exceptional samples occur in the oligoclase-biotite zone in the Besshi-traverse and as pelitic schist clasts from the Kuma Group. They are higher in CaO, Sr and the mg-value, and are more scattered in K/Rb ratio than the others.

Taking into account compositional dependence, in particular the mg-value, on the chemical trend of zoned garnet for the Asemi-traverse, I concluded that the garnet zone schists experienced higher pressure and lower temperature than the albite-biotite and oligoclase-biotite zone schists at the onset of the garnet formation. The difference in pressure and temperature at the onset of the garnet formation is larger than that previously envisaged by Banno et al. (1986). The difference in the chemical trend of zoned garnet in the oligoclase-biotite schists between of the Asemi-traverse and of the Besshi-traverse can not tell the difference in pressure and temperature.

The bulk rock compositions are insensitive to detect material migration during the Sanbagawa high pressure metamorphism because of their large diversity. However dolomite-bearing pelitic and basic schists record an increase in X_{CO_2} during the Sanbagawa metamorphism as Enami and Higashino (1988) stated. The increase in X_{CO_2} can be caused by an oxidation reaction of graphite to release CO_2. The reaction is triggered not by the introduction of fluid with high f_{O_2} but by the mixing of graphite-bearing pelitic schists and basic schists with high f_{O_2} minerals such as hematite, magnetite and Fe^{3+}-rich epidote. The dolomite-bearing schists are hybrids from pelitic and basic schists. The hybridization took place under the Sanbagawa peak metamorphic conditions, and may be related to the formation of tectonic melange zones. Thus the bulk compositions of dolomite-bearing rocks are not isochemical during the Sanbagawa metamorphism.

Introduction

Metamorphism is caused by the changes of pressure, temperature and chemistry of rocks and coexisting fluids. Most metamorphic petrologists have attempted to estimate pressure and temperature of metamorphism selecting reactions presumably independent of chemical compositions of rocks and fluids. Thus they have left aside the chemical effect, assuming, often without reason, the isochemistry of rocks throughout a metamorphic area. Recently, it has been made clear that the analysis of the chemical trend of a zoned mineral yields much information on understanding pressure and temperature trajectory of rocks. This is based on the facts that the chemical trend of a zoned mineral crystallized by a net transfer reaction completely preserves the instantaneous changes of pressure and temperature. This is regarded as the metamorphic fractional crystallization (Spear, 1988). The net transfer reaction strongly depends on the chemistry of minerals and rocks, and on pressure and temperature of metamorphism as Spear (1988) stated. Further, such reactions are petrographically conspicuous because they lead to significant variations in modal abundances. Therefore, it is dangerous to apply such procedure to rocks without examining effects of bulk and fluid compositions on their phase equilibria.

Pelitic schists are the most dominant rock-type in the Sanbagawa metamorphic belt. Some authors (Banno, 1961; Banno, 1964; Ernst et al., 1970; Kurata and Banno, 1974) have reported bulk compositions of the Sanbagawa schists. The data are insufficient for geochemical discussion both in quality and in quantity yet. Moreover, pressure and temperature trajectory of

the Sanbagawa pelitic schists deduced by Banno et al. (1986) should be regarded temporary as they ignored the dependence of bulk rock compositions on the chemical trend of zoned garnet.

The purpose of this paper is to understand the geochemistry of the Sanbagawa pelitic schists, based on new analysis. I intend to examine the effect of the bulk compositions on the metamorphic paragenesis. In particular, the effects of MnO and CaO that we usually disregarded in analyzing the paragenesis of the Sanbagawa pelitic schists are discussed. I also attempt to decipher whether a substantial amount of material migrated during the Sanbagawa high pressure metamorphic belt. Abbreviations of mineral names in the text and figures are, unless otherwise stated, after Kretz (1983).

Outline of geology

The Sanbagawa metamorphic belt is a high pressure intermediate type metamorphic belt (Miyashiro, 1961). It extends from eastern Kyushu through Shikoku Island to the Kanto Mountains for a distance of about 800 km and a width less than 30 km as Fig. 1 shows.

Figure 2 is a geological map of the Sanbagawa metamorphic belt in central Shikoku after Higashino (1990a). This region is lithologically divided into four formations in ascending order; the Kawaguchi, Koboke, Minawa and Ojoin Formations (Kojima et al., 1956; Hide et al., 1956; Kenzan Research Group, 1984). Although the geological structure of the Sanbagawa belt cannot be described by the superposition of these formations, they are convenient to describe the lithology of the belt.

The Sanbagawa metamorphic rocks in this area are composed mainly of pelitic and basic schists, but also contain some psammitic and siliceous schists, and a rare calcareous schist. Mappable to hand specimen sizes of metagabbro, peridotite, serpentinite and actinolite rocks occur as exotic rocks, particularly in the upper Member of the Minawa Formation and in the lower part of the Ojoin Formation (Kunugiza et al., 1986; Higashino, 1990a, b).

Metamorphic zonation

The parageneses of pelitic and basic schists have defined metamorphic zones of the Sanbagawa belt in central Shikoku (e.g., Banno and Sakai, 1989). Garnet, biotite and oligoclase appear successively in the Sanbagawa pelitic schist during prograde

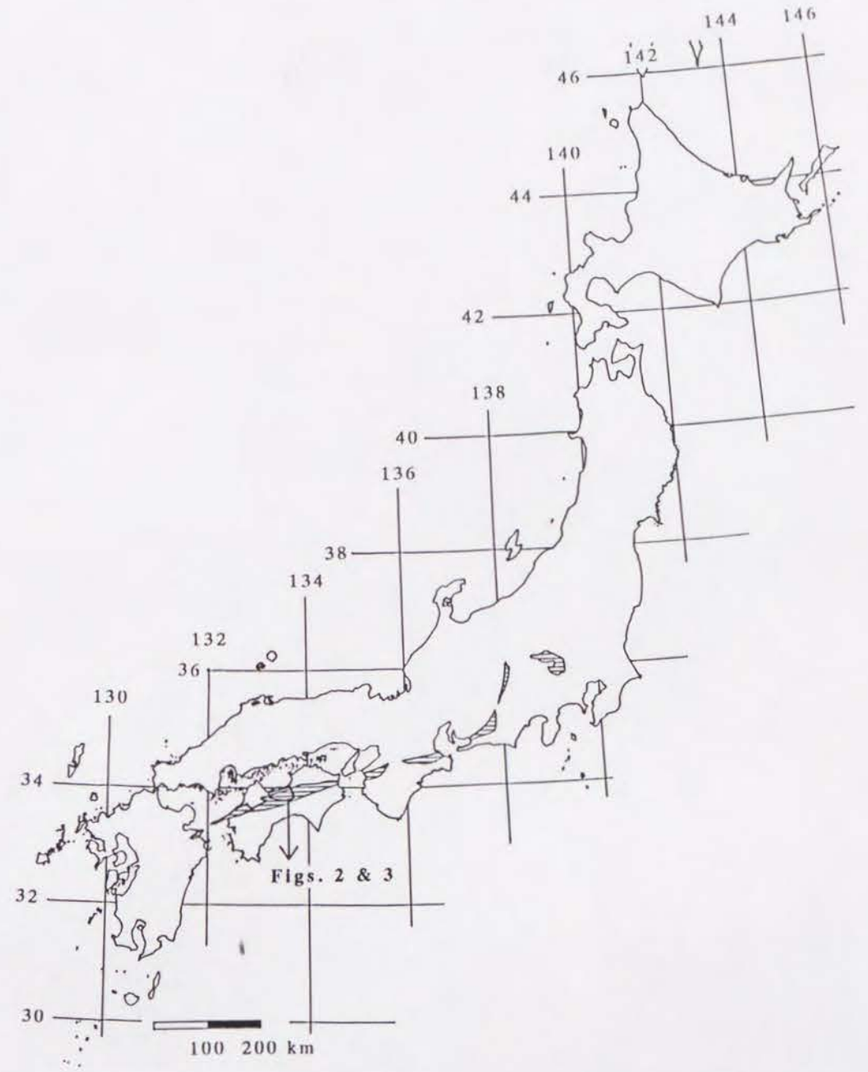

Figure 1. Distribution map of the Sanbagawa metamorphic rock.

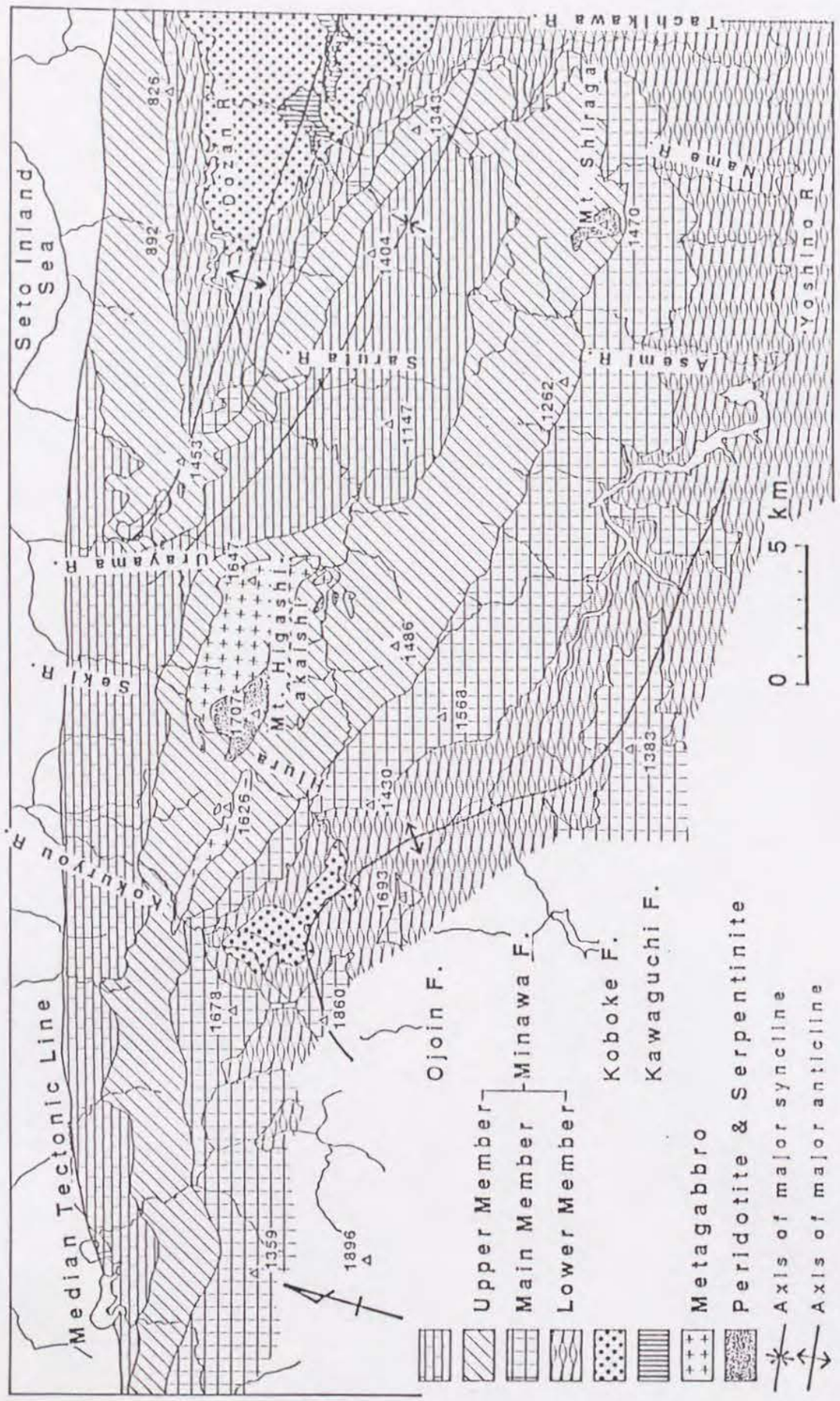

Figure 2. Geological map of the Sanbagawa metamorphic belt in central Shikoku (after Higashino, 1990a).

metamorphism (Higashino, 1990a, b). He mapped in detail a wide area of central Shikoku using the first appearance of these three minerals. Figure 3A is his new mineral zone map of the same area as in Fig. 2. Otsuki and Banno (1990) have discussed the parageneses of hematite-bearing basic schists.

Figure 3B shows the sample localities of pelitic schists to be discussed in this paper. I divided the localities into the Asemi-traverse and the Besshi-traverse. The former includes the Mishima area, the Dozan-river, the Urayama-river, the Saruta-river, the Name-river, the Tachikawa-river and the Asemi-river and its tributaries, and the latter does the Seki-river, the Kokuryo-river, the Hiura-valley and the Tokonabe-valley.

I also analyzed three pelitic schist clasts, which were of Sanbagawa provenance, in Middle Eocene conglomerates from the Kuma Group. It unconformably overlies the chlorite zone. Some clasts show the highest temperatures that have ever been reported for the Sanbagawa schists (Yokoyama and Itaya, 1990). They concluded that such highest grade rocks were exposed and eroded away by the Middle Eocene. All the analyzed samples contain quartz, albite (or oligoclase), muscovite and graphite.

Analytical procedures

I analyzed major elements and 9 trace elements (Rb, Sr, Y, Zr, Nb, Ba, Th, Pb and Ni) on about 200 pelitic schists by X-ray fluorescence spectrometers (Rigaku model Simultix 3530 for major elements and Rigaku model 3370 for trace elements). For major element analysis, I prepared fused glasses made from the mixture of 0.3 g rock powder and 3.0 g anhydrous lithium tetraborate

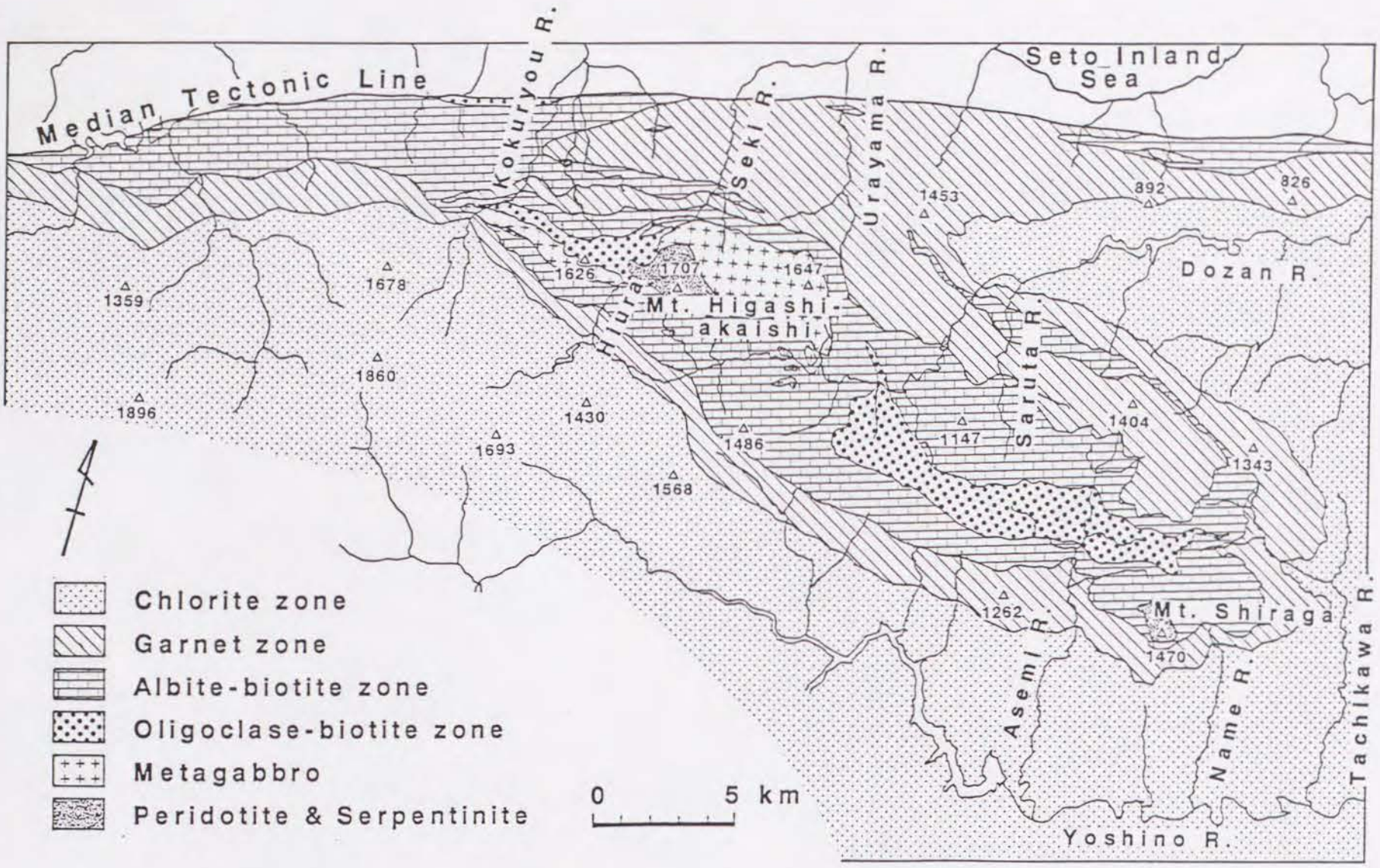

Figure 3A. Metamorphic zonal map of the Sanbagawa metamorphic belt in central Shikoku (after Higashino, 1990a and b).

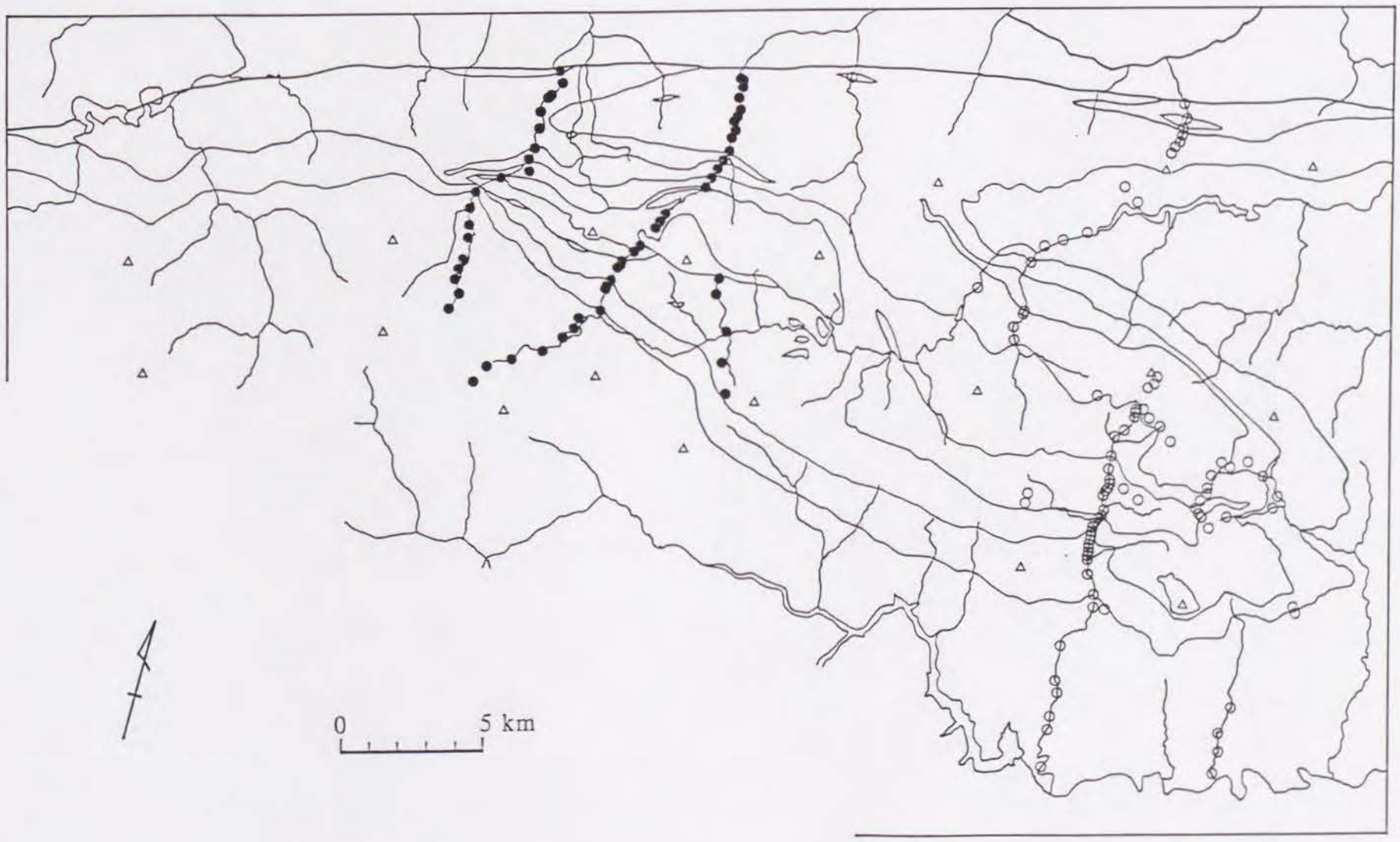

Figure 3B. Localities of analyzed samples from the Asemi-traverse (open circle) and from the Besshi-traverse (closed circle).

($Li_2B_4O_7$), and prepared pressed powder pellets for trace element analysis. Goto and Tatsumi (1991, 1992) reported sample preparations and analytical details. I also measured the loss on ignition of samples gravimetrically.

Table 1 lists the analytical errors (relative error; %), and the compositional ranges of the standards for the major and trace element analyses. I prepared 10 fused glasses for each of 2 pelitic schists, CS82102709 and CS82102901, and analyzed them. Their averages and standard deviations represent the reproducibility of the major element analyses of this study (Table 2). The counting errors of the trace elements except Ba are less than 1 % and that of Ba less than 2 %. Table 3 lists major and trace compositions of pelitic schists. When a concentration is out of the compositional range of the standards, we cannot evaluate the analytical error rigorously. In Table 3 an asterisk (*) and double asterisks (**) show the data lower than a minimum concentration of the standards and those higher than a maximum one, respectively.

Table 1. Compositional ranges of standards and the analytical errors (relative %).

	Min	Max	error(%)
SiO2	44.33	85.41	0.65
TiO2	0.12	2.84	7.0
Al2O3	1.09	23.10	3.8
Fe2O3	0.71	13.07	3.7
MnO	0.02	0.78	12.0
MgO	0.37	41.01	1.9
CaO	0.47	33.61	1.9
Na2O	0.27	8.97	3.9
K2O	0.13	6.90	2.9
P2O5	0.108	0.504	1.8
Rb(ppm)	0.414	247	2.0
Sr	27.2	369	2.3
Y	8.56	26.1	2.4
Zr	7.73	320.7	2.9
Nb	5.13	100.6	1.4
Ba*	57.3	472	5.1
Th	3.56	33.45	6.6
Pb	5.1	33.2	9.8
Ni	47.6	640	1.3

*: The calibration line for Ba is applicable to samples with Ba upto 1000 ppm.

Table 2. Replicate analyses of pelitic schists.

Sample No.	CS82102709		CS82102901	
	Av.	1sigma	Av.	1sigma
SiO2	70.61	0.19	72.96	0.21
TiO2	0.52	0.00	0.37	0.00
Al2O3	14.71	0.04	13.24	0.04
Fe2O3	4.31	0.01	2.79	0.01
MnO	0.18	0.00	0.06	0.00
MgO	1.65	0.03	0.91	0.02
CaO	0.51	0.01	1.97	0.01
Na2O	2.25	0.06	2.93	0.10
K2O	3.05	0.02	2.50	0.02
P2O5	0.10	0.00	0.10	0.00
Total	97.91	0.26	97.83	0.29

Results

1. Geochemistry of the Sanbagawa pelitic schists

Table 4 lists the average, standard deviation, and maximum and minimum of the analyses of the pelitic schists from each mineral zone in the Asemi-traverse, those in the Besshi-traverse, and those of the pelitic schist clasts. Tables 3 and 4 tabulate total iron as Fe_2O_3. Although the oxidation state of iron in the pelitic schists was not figured out, the majority of Fe was FeO in the graphite-bearing pelitic schist. As I analyzed only graphite-bearing pelitic schists, the total iron will be treated as FeO in this paper. The analyses are plotted on SiO_2-variation diagrams (Fig. 4A, chlorite zone; 4B, garnet zone; 4C, albite-biotite zone; and 4D, oligoclase-biotite zone and pelitic schist clasts) to view geochemistry of the Sanbagawa pelitic schists.

The TiO_2, Al_2O_3, Fe_2O_3 and MgO are negatively correlated with SiO_2, while the MnO, CaO, Na_2O and K_2O and the trace elements are poorly correlated with SiO_2 (Fig. 4). In addition, the mg-value (Fig. 5), the molar MgO/(FeO + MgO), the K/Ba (Fig. 6) and K/Rb (Fig. 7) weight ratios of the pelitic schists are constant without a few exceptional samples. Variations in the bulk composition of the pelitic schists are small among some mineral zones and traverses (Table 4 and Fig. 4):

- SiO_2 of the chlorite zone in the Asemi-traverse, whose average is 67.42 wt. %, is lower than that in the Besshi-traverse, 70.44 wt. %, although they overlap each other (Fig. 4A). So, the averages of TiO_2, Al_2O_3, Fe_2O_3, MnO, MgO and loss on ignition of the former are higher than those of the latter (Table 4).
- A slightly low SiO_2 is characteristic of the oligoclase-biotite

Table 3A. Chemical compositions of pelitic schists from the Asemi-traverse.

Sample No.	CS8305 0605	CS8305 0706	CS8305 0703	CS8305 1701	CS8305 1801	CS8305 2002	CS8305 0705	CS8405 2505
Loc.	Asemi	Asemi	Asemi	Asemi	Asemi	Asemi	Asemi	Tachi
Mineral zone	Chl-Z	Chl-Z	Chl-Z	Chl-Z	Chl-Z	Chl-Z	Chl-Z	Chl-Z
SiO2	67.28	69.47	69.02	69.29	69.98	64.38	67.65	69.35
TiO2	0.56	0.59	0.48	0.55	0.56	0.63	0.46	0.57
Al2O3	15.07	15.58	15.26	14.60	14.37	16.20	16.55	15.24
Fe2O3	4.95	4.59	3.09	4.71	4.67	6.91	3.04	4.76
MnO	0.09	0.08	0.05	0.17	0.15	0.28	0.05	0.13
MgO	1.87	1.80	1.25	1.81	1.71	2.34	1.22	1.76
CaO	1.48	0.38*	2.00	0.50	0.43*	0.37*	1.63	0.32*
Na2O	2.74	2.85	4.85	2.73	2.15	2.75	5.52	2.08
K2O	2.63	2.58	1.76	2.76	2.82	2.59	1.61	2.84
P2O5	0.12	0.12	0.12	0.10*	0.10*	0.10*	0.10*	0.15
LOI	2.95	2.43	1.99	2.48	2.78	2.97	1.61	2.28
Total	99.74	100.47	99.87	99.70	99.72	99.52	99.44	99.48
Rb(ppm)	103	107	68.2	114	121	109	62.2	115
Sr	143	48.1	260	55.5	63.5	53.5	182	74.8
Y	18.5	19.4	15.5	23.1	17.1	18.4	15.2	50.3**
Zr	137	150	187	138	120	124	177	142
Nb	8.9	9.7	6.8	9.7	9.1	9.1	6.7	10.0
Ba	438	415	361	541	494	320	334	448
Th	10.8	12.5	8.3	13.2	12.1	13.3	8.6	13.7
Pb	23.0	18.5	17.5	15.8	17.0	34.1**	20.2	17.8
Ni	19.1*	20.4*	9.8*	15.0*	17.6*	29.9*	7.1*	5.3*
mg-value	0.428	0.437	0.445	0.432	0.420	0.401	0.443	0.423
Mn-ratio	1.16	1.09	1.00	2.25	2.05	2.66	1.02	1.74
K/Rb	212	199	214	202	194	198	215	206
K/Ba	49.8	51.6	40.4	42.3	47.4	67.2	40.0	52.7

mg-value; molar MgO/(FeO + MgO)
Mn-ratio; percent molar MnO/(FeO + MnO + MgO)
K/Rb and K/Ba; weight ratios

Sample No.	CS8405 2901	CS8405 2903	CS8405 2904	CS8405 2906	CS8405 2907	TH8108 1111	TH8108 1105	HK6908 1602
Loc.	Asemi	Name	Name	Name	Name	Mishima	Mishima	Dozan
Mineral zone	Chl-Z	Chl-Z	Chl-Z	Chl-Z	Chl-Z	Chl-Z	Chl-Z	Chl-Z
SiO2	59.63	62.21	69.91	61.04	64.81	64.87	71.15	71.88
TiO2	0.75	0.69	0.59	0.76	0.66	0.60	0.47	0.45
Al2O3	18.41	16.91	14.22	18.23	16.74	17.25	14.37	14.25
Fe2O3	7.80	6.16	4.73	6.49	5.43	5.27	3.68	3.78
MnO	0.30	0.21	0.10	0.14	0.10	0.11	0.05	0.05

Table 3A. (continued)

MgO	2.96	2.23	1.57	2.31	2.02	1.62	0.95	1.29
CaO	0.66	1.32	0.50	0.62	0.79	0.56	0.25*	0.07*
Na2O	2.41	1.81	3.53	2.52	2.65	2.98	3.75	2.92
K2O	3.43	3.73	1.84	3.59	3.34	3.65	2.35	2.75
P2O5	0.11	0.14	0.12	0.14	0.16	0.10*	0.09*	0.08*
LOI	3.15	3.60	2.22	3.31	2.51	3.00	3.03	2.34
Total	99.61	99.01	99.33	99.15	99.21	100.01	100.14	99.86
Rb	135	153	76.7	138	125	142	91.1	111
Sr	52.4	113	65.0	74.9	87.4	71.9	46.3	34.7
Y	21.5	18.8	17.3	24.2	22.8	11.7	25.9	9.3
Zr	147	136	137	176	175	166	135	136
Nb	10.9	10.1	9.5	12.4	11.0	10.2	10.0	9.6
Ba	538	623	286	543	521	641	340	394
Th	15.8	12.4	11.5	15.1	13.4	14.6	13.5	13.8
Pb	21.3	10.8	20.3	22.5	20.1	22.1	30.1	18.7
Ni	40.6*	29.2*	13.3*	24.4*	20.7*	12.6*	8.8*	0.6*
mg-value	0.429	0.418	0.397	0.414	0.424	0.378	0.338	0.403
Mn-ratio	2.41	2.19	1.42	1.40	1.18	1.44	1.00	0.88
K/Rb	211	203	199	215	221	214	214	206
K/Ba	53.0	49.7	53.4	54.9	53.2	47.3	57.4	57.9

Sample No.	HK6908 1607	HK6908 1609	CS8210 2602	CS8210 2604	CS8210 2606	CS8210 2701	CS8210 2708	CS8210 2709
Loc.	Dozan	Dozan	Asemi	Asemi	Asemi	Asemi	Asemi	Asemi
Mineral zone	Chl-Z	Chl-Z	Grt-Z	Grt-Z	Grt-Z	Grt-Z	Grt-Z	Grt-Z
SiO2	71.33	70.32	73.39	68.82	70.06	71.80	68.22	70.66
TiO2	0.46	0.51	0.46	0.59	0.55	0.54	0.58	0.53
Al2O3	14.98	14.41	13.81	16.20	14.63	14.31	15.43	14.74
Fe2O3	3.93	4.54	3.12	4.83	4.68	4.57	5.31	4.31
MnO	0.11	0.08	0.06	0.18	0.22	0.20	0.23	0.19
MgO	1.60	1.48	1.04	1.79	1.66	1.78	2.03	1.69
CaO	0.10*	0.13*	0.73	0.59	0.62	0.68	0.87	0.50
Na2O	1.09	3.24	3.51	2.29	2.27	1.66	2.02	2.29
K2O	4.09	2.35	2.36	3.29	2.92	3.19	3.32	3.04
P2O5	0.08*	0.11	0.08*	0.12	0.11	0.10*	0.12	0.10*
LOI	2.33	2.30	1.44	1.96	2.04	1.66	2.09	2.14
Total	100.10	99.47	100.00	100.66	99.76	100.49	100.22	100.19
Rb	155	99.0	95.9	139	123	134	131	124
Sr	22.9*	57.6	121	101	93.0	70.6	121	86.9
Y	14.8	18.6	20.8	24.2	24.4	17.6	19.9	21.7
Zr	142	138	140	155	136	130	134	137
Nb	10.2	9.6	8.6	10.3	10.2	9.6	9.0	9.5
Ba	696	416	415	563	444	469	619	461
Th	15.7	12.8	10.7	14.9	12.6	12.7	15.0	12.9
Pb	12.7	17.7	13.5	18.2	21.1	12.2	13.9	22.3
Ni	16.4*	10.5*	10.4*	15.1*	14.6*	17.7*	11.3*	15.7*
mg-value	0.446	0.392	0.398	0.423	0.413	0.436	0.431	0.437

Table 3A. (continued)

Mn-ratio	1.71	1.19	1.29	2.36	3.01	2.71	2.70	2.72
K/Rb	219	197	204	197	197	198	210	204
K/Ba	48.8	46.9	47.2	48.6	54.6	56.5	44.5	54.7

Sample	CS8210	CS8210	CS8210	CS8210	CS8211	CS8211	CS8211	CS8211
No.	3106	3121	3108	3118	0109	0111	0202	0302
Loc.	Asemi	Asemi	Asemi	Asemi	Asemi	Asemi	Asemi	Asemi
Mineral zone	Grt-Z	Grt-Z	Grt-Z	Grt-Z	Grt-Z	Grt-Z	Grt-Z	Grt-Z
SiO2	72.21	74.94	69.71	62.63	67.53	66.84	68.81	64.55
TiO2	0.39	0.30	0.52	0.74	0.53	0.55	0.58	0.66
Al2O3	12.48	13.55	14.43	17.36	15.81	14.62	15.30	15.97
Fe2O3	3.33	2.46	4.78	6.25	5.51	4.74	4.86	5.40
MnO	0.16	0.05	0.27	0.12	0.35	0.23	0.22	0.21
MgO	1.20	0.64	1.88	2.61	2.02	1.84	1.73	2.24
CaO	2.23	0.59	1.06	1.19	0.77	2.83	0.66	1.24
Na2O	2.27	4.36	1.89	2.58	2.04	2.88	2.24	2.33
K2O	2.82	1.84	2.81	3.10	3.21	2.23	3.16	3.22
P2O5	0.12	0.07*	0.13	0.15	0.10*	0.12	0.11	0.12
LOI	2.27	1.31	2.72	2.83	2.09	3.16	2.51	3.38
Total	99.48	100.11	100.20	99.56	99.96	100.04	100.18	99.32
Rb	103	71.0	121	121	134	89.6	128	131
Sr	139	174	129	210	93.0	195	132	142
Y	17.1	19.7	20.2	21.6	23.9	18.6	22.8	21.3
Zr	101	141	114	145	124	123	147	148
Nb	7.0	6.9	9.3	10.1	9.4	8.9	10.4	10.3
Ba	431	383	354	501	512	337	479	485
Th	9.7	12.9	11.3	13.3	15.1	11.5	13.9	13.7
Pb	18.2	10.7	26.2	14.4	10.7	37.7**	12.4	8.7
Ni	8.3*	0.2*	20.6*	7.7*	25.3*	21.0*	14.1*	28.0*
mg-value	0.417	0.340	0.438	0.453	0.421	0.435	0.414	0.451
Mn-ratio	3.06	1.49	3.45	1.17	3.98	2.99	2.90	2.35
K/Rb	227	215	193	212	200	207	206	205
K/Ba	54.3	39.9	65.9	51.4	52.0	55.0	54.8	55.1

Sample	CS8305	CS8305	CS8305	CS8305	CS8305	CS8305	CS8305	CS8305
No.	0413	0407	0801	1105	1201	1206	0410	1208
Loc.	Asemi	Asemi	Asemi	Asemi	Asemi	Asemi	Asemi	Asemi
Mineral zone	Grt-Z	Grt-Z	Grt-Z	Grt-Z	Grt-Z	Grt-Z	Grt-Z	Grt-Z
SiO2	65.63	64.65	68.27	70.31	68.00	68.82	68.71	67.29
TiO2	0.65	0.67	0.61	0.51	0.55	0.58	0.57	0.54
Al2O3	16.42	15.96	16.06	14.29	15.05	15.29	14.59	14.95
Fe2O3	5.76	5.35	5.66	4.69	4.54	4.54	5.20	4.67
MnO	0.24	0.12	0.32	0.20	0.16	0.13	0.23	0.16
MgO	2.29	2.44	2.07	1.71	1.81	1.81	1.96	1.69
CaO	0.94	2.25	0.82	0.99	1.72	0.71	0.68	1.64
Na2O	1.98	2.16	1.52	1.28	1.72	1.97	1.98	2.39

Table 3A. (continued)

K2O	3.32	2.89	3.26	3.22	3.35	3.26	2.95	3.05
P2O5	0.12	0.12	0.10*	0.11	0.11	0.11	0.11	0.12
LOI	2.65	2.66	2.34	2.66	2.43	2.32	2.66	2.64
Total	100.00	99.27	101.03	99.97	99.44	99.54	99.64	99.14
Rb	140	112	131	133	129	131	128	119
Sr	136	203	30.5	110	191	130	120	155
Y	19.5	21.1	20.3	20.5	19.2	22.3	21.4	22.3
Zr	144	142	136	122	134	142	122	142
Nb	10.1	9.6	10.2	10.7	9.2	10.4	9.8	9.5
Ba	470	466	418	474	517	553	442	537
Th	12.7	12.0	14.6	11.7	11.5	14.0	12.4	12.7
Pb	21.4	22.8	22.7	20.3	14.0	13.8	21.7	13.7
Ni	31.3*	28.9*	10.9*	10.3*	13.9*	4.6*	24.0*	16.4*
mg-value	0.441	0.475	0.420	0.419	0.441	0.441	0.427	0.418
Mn-ratio	2.56	1.31	3.56	2.71	2.17	1.77	2.77	2.20
K/Rb	197	214	207	202	216	207	192	213
K/Ba	58.7	51.5	64.7	56.4	53.8	48.9	55.4	47.2

Sample	CS8310	CS8310	CS8310	CS8310	CS8310	CS8310	CS8405	CS8405
No.	2703	2706	2802	2905	3002	3004	2504	3001
Loc.	Asemi	Asemi	Asemi	Asemi	Asemi	Asemi	Asemi	Saruta
Mineral zone	Grt-Z	Grt-Z	Grt-Z	Grt-Z	Grt-Z	Grt-Z	Grt-Z	Grt-Z
SiO2	69.70	69.97	70.97	72.48	68.87	67.19	62.82	66.15
TiO2	0.57	0.49	0.44	0.50	0.55	0.60	0.75	0.61
Al2O3	15.03	14.55	14.41	13.03	14.75	16.40	16.70	15.84
Fe2O3	3.86	4.23	3.43	4.76	5.04	5.13	6.75	5.62
MnO	0.07	0.18	0.10	0.26	0.25	0.33	0.28	0.23
MgO	1.39	1.38	1.14	1.82	1.85	1.84	3.07	1.58
CaO	0.76	1.58	1.22	0.53	0.41*	0.62	0.64	1.08
Na2O	2.82	1.84	3.27	1.48	2.13	1.89	2.12	3.54
K2O	2.59	3.11	2.76	2.69	2.92	3.68	3.36	2.22
P2O5	0.07*	0.09*	0.09*	0.11	0.11	0.13	0.13	0.10*
LOI	1.95	2.31	1.17	1.99	1.94	1.81	2.50	2.36
Total	98.81	99.73	99.00	99.65	98.82	99.62	99.12	99.33
Rb	106	130	114	114	120	156	128	91.7
Sr	188	176	127	57.3	54.9	122	112	162
Y	32.5**	23.8	22.3	21.8	14.2	26.8**	25.0	22.2
Zr	158	137	146	116	127	168	151	119
Nb	10.8	10.3	9.0	8.8	9.9	11.7	10.5	9.5
Ba	380	655	501	449	402	535	463	427
Th	15.2	13.7	12.2	11.1	13.3	17.7	13.1	13.1
Pb	16.7	19.5	18.6	14.4	20.1	18.4	29.0	12.5
Ni	-	12.1*	5.1*	22.2*	11.9*	24.2*	52.0	19.2*
mg-value	0.416	0.393	0.397	0.431	0.421	0.415	0.474	0.358
Mn-ratio	1.18	2.83	1.94	3.38	3.13	4.06	2.40	2.87
K/Rb	202	198	202	196	202	196	218	201

Table 3A. (continued)

K/Ba	56.5	39.4	45.7	49.7	60.3	57.1	60.3	43.2

Sample	CS8405	CS8405	CS8405	CS8406	CS8406	CS8406	TH7611	TH7611
No.	3003	3007	3013	0102	0206	0301	0415	0413
Loc.	Saruta	Saruta	Saruta	Saruta	Saruta	Asemi	Mishima	Mishima
Mineral zone	Grt-Z	Grt-Z	Grt-Z	Grt-Z	Grt-Z	Grt-Z	Grt-Z	Grt-Z
SiO2	72.62	69.66	68.78	72.79	73.96	63.76	65.79	70.89
TiO2	0.51	0.52	0.54	0.39	0.43	0.70	0.61	0.59
Al2O3	13.07	14.52	15.99	14.64	13.61	18.18	17.44	14.96
Fe2O3	4.34	3.99	4.38	2.45	3.77	5.77	4.73	3.10
MnO	0.22	0.06	0.18	0.03	0.12	0.20	0.08	0.05
MgO	1.54	1.63	1.62	0.84	1.42	2.13	1.58	1.35
CaO	0.60	0.92	1.06	1.34	0.33*	0.29*	0.20*	1.06
Na2O	2.03	3.88	2.47	2.92	2.15	2.45	2.58	0.85
K2O	2.63	1.94	3.49	3.29	2.81	3.87	3.91	4.26
P2O5	0.09*	0.12	0.11	0.08*	0.09*	0.13	0.16	0.07*
LOI	1.73	1.50	1.70	1.60	1.80	2.91	2.71	2.38
Total	99.38	98.74	100.32	100.37	100.49	100.39	99.79	99.56
Rb	106	71.9	132	114	118	152	150	161
Sr	94.7	186	155	292	72.3	80.6	68.9	177
Y	16.9	16.3	25.5	21.0	20.7	24.9	24.4	20.0
Zr	110	151	153	166	123	170	165	128
Nb	8.9	7.6	10.6	7.8	8.4	12.0	9.5	10.6
Ba	410	369	571	559	434	641	667	778
Th	11.2	8.3	16.5	11.0	12.1	15.4	17.2	12.6
Pb	19.7	22.8	11.4	21.2	20.7	15.7	17.1	14.3
Ni	10.2*	6.3*	2.9*	1.2*	12.6*	24.0*	4.2*	3.4*
mg-value	0.413	0.447	0.423	0.404	0.427	0.422	0.398	0.463
Mn-ratio	3.24	0.93	2.60	0.81	2.01	2.20	1.13	0.97
K/Rb	205	224	220	240	198	211	216	220
K/Ba	53.2	43.7	50.7	48.8	53.7	50.1	48.7	45.5

Sample	TH7611	TH7611	TH7611	TH7211	TH7211	TH7211	TH7108	TH7108
No.	0404	0417	0420	2936	3026	3014	1004	1005
Loc.	Mishima	Mishima	Mishima	Asemi	Asemi	Asemi	Asemi	Asemi
Mineral zone	Grt-Z	Grt-Z	Grt-Z	Grt-Z	Grt-Z	Grt-Z	Grt-Z	Grt-Z
SiO2	68.39	70.26	68.51	74.64	70.65	72.89	72.21	74.01
TiO2	0.54	0.55	0.64	0.35	0.49	0.53	0.55	0.41
Al2O3	14.78	16.18	15.31	14.12	15.18	13.74	13.48	13.87
Fe2O3	4.45	2.67	4.79	2.14	3.75	3.43	4.98	2.78
MnO	0.12	0.02	0.11	0.05	0.05	0.06	0.17	0.05
MgO	1.59	1.22	1.96	0.81	1.43	1.22	1.71	0.98
CaO	1.47	0.10*	0.17*	0.42*	0.63	0.73	0.72	0.59
Na2O	2.22	1.88	1.60	2.67	3.74	3.69	2.06	3.96
K2O	3.24	4.19	3.62	3.34	2.42	2.09	2.61	2.12
P2O5	0.11	0.09*	0.09*	0.07*	0.10*	0.09*	0.10*	0.07*

Table 3A. (continued)

LOI	2.02	3.43	2.81	1.07	1.27	1.35	1.37	1.15
Total	98.93	100.59	99.61	99.68	99.71	99.82	99.96	99.99
Rb	125	165	145	130	98.2	85.3	112	88.5
Sr	102	51.7	49.5	93.0	142	121	73.0	118
Y	23.1	5.0*	7.0*	22.3	17.4	16.4	19.3	17.6
Zr	140	135	127	147	133	156	139	132
Nb	9.8	10.8	10.7	7.6	7.5	7.5	9.5	7.1
Ba	470	639	570	691	436	394	471	393
Th	13.1	15.9	14.5	13.0	9.6	9.5	11.2	10.7
Pb	21.6	14.3	19.3	18.8	14.2	12.9	11.0	12.7
Ni	15.5*	0.0*	7.0*	6.4*	10.9*	12.1*	24.4*	7.5*
mg-value	0.414	0.475	0.448	0.429	0.430	0.413	0.405	0.411
Mn-ratio	1.75	0.44	1.41	1.48	0.85	1.14	2.24	1.18
K/Rb	216	211	207	213	205	203	194	199
K/Ba	57.2	54.4	52.7	40.2	46.1	44.1	46.0	44.7

Sample	TH7107	TH7107	TH7107	TH7108	TH7108	STL7211	CS8210	CS8210
No.	2702	2714	2721	1001	0201	3005	2801	2802
Loc.	Asemi	Asemi	Asemi	Asemi	Asemi	Asemi	Asemi	Asemi
Mineral zone	Grt-Z	Grt-Z	Grt-Z	Grt-Z	Grt-Z	Grt-Z	Abt-Z	Abt-Z
SiO2	74.32	67.28	69.81	73.73	71.10	77.48	70.64	70.60
TiO2	0.40	0.60	0.59	0.49	0.50	0.31	0.43	0.50
Al2O3	13.60	16.02	14.82	13.16	15.01	12.01	15.35	14.52
Fe2O3	2.84	5.06	4.39	3.87	3.61	1.99	3.96	4.26
MnO	0.06	0.19	0.07	0.12	0.09	0.06	0.10	0.12
MgO	1.11	1.94	1.77	1.51	1.41	0.63	1.33	1.64
CaO	0.51	0.54	0.40*	0.64	0.40*	0.72	0.49	1.00
Na2O	3.16	2.01	2.55	2.24	2.74	3.28	2.87	2.64
K2O	2.57	3.53	2.90	2.67	2.83	2.24	3.03	2.84
P2O5	0.08*	0.10*	0.09*	0.09*	0.09*	0.06*	0.09*	0.11
LOI	1.46	2.20	2.34	1.68	1.68	1.23	2.00	1.86
Total	100.11	99.47	99.73	100.20	99.46	100.01	100.29	100.09
Rb	104	144	118	112	123	n.a.	134	121
Sr	109	112	77.0	109	97.1	n.a.	101	129
Y	18.4	22.0	20.8	18.3	16.0	n.a.	23.5	17.2
Zr	137	137	146	115	131	n.a.	129	125
Nb	6.8	10.3	9.3	8.6	9.3	n.a.	9.9	8.2
Ba	426	579	461	448	437	n.a.	537	521
Th	10.3	14.1	13.2	11.8	12.1	n.a.	16.7	11.9
Pb	14.6	19.2	12.6	20.1	22.8	n.a.	15.6	27.8
Ni	4.5*	11.1*	15.0*	7.0*	11.1*	n.a.	10.9*	22.2*
mg-value	0.436	0.432	0.444	0.436	0.436	0.385	0.400	0.433
Mn-ratio	1.32	2.35	0.99	1.93	1.56	2.04	1.68	1.77
K/Rb	206	203	204	199	192		188	194
K/Ba	50.1	50.6	52.3	49.5	53.7		46.8	45.2

Table 3A. (continued)

Sample	CS8210	CS8210	CS8210	CS8210	CS8210	CS8210	CS8210	CS8210
No.	2805	2803	2807	2817	2809	2814	2901	2903
Loc.	Asemi	Asemi	Asemi	Asemi	Asemi	Asemi	Asemi	Asemi
Mineral zone	Abt-Z	Abt-Z	Abt-Z	Abt-Z	Abt-Z	Abt-Z	Abt-Z	Abt-Z
SiO2	69.72	72.15	68.60	66.95	64.67	67.41	72.94	71.49
TiO2	0.56	0.54	0.55	0.62	0.68	0.59	0.37	0.51
Al2O3	15.04	14.27	15.31	16.00	16.86	15.05	13.28	14.45
Fe2O3	5.04	4.71	4.25	6.15	6.08	5.70	2.80	3.76
MnO	0.16	0.21	0.08	0.33	0.26	0.25	0.06	0.06
MgO	1.97	1.89	1.26	2.25	2.27	2.31	0.92	1.31
CaO	0.77	0.19*	0.60	0.43*	0.98	0.88	1.97	0.65
Na2O	0.60	0.67	2.84	2.04	2.27	2.17	2.81	3.56
K2O	4.15	3.22	3.21	2.89	3.29	2.77	2.48	2.39
P2O5	0.11	0.12	0.10*	0.12	0.13	0.10*	0.10*	0.11
LOI	1.88	2.17	2.83	2.47	2.54	2.08	1.64	1.70
Total	100.00	100.14	99.63	100.25	100.03	99.31	99.37	99.99
Rb	140	130	130	120	133	103	96.8	94.4
Sr	56.4	84.9	87.2	113	129	70.2	201	145
Y	25.3	12.8	19.5	19.6	27.0**	18.5	25.0	21.6
Zr	128	115	152	128	139	139	134	165
Nb	9.4	8.7	9.7	10.0	11.6	9.9	9.3	9.1
Ba	599	373	460	394	477	359	393	348
Th	12.4	13.1	12.6	11.6	13.6	12.4	12.7	11.6
Pb	10.3	17.6	16.1	27.4	29.0	17.1	13.4	16.0
Ni	20.3*	14.4*	11.2*	24.2*	29.2*	27.2*	3.7*	11.7*
mg-value	0.436	0.443	0.370	0.420	0.425	0.445	0.394	0.408
Mn-ratio	1.97	2.72	1.32	3.38	2.69	2.67	1.44	1.05
K/Rb	245	206	205	201	205	224	213	210
K/Ba	57.5	71.6	57.9	60.9	57.3	64.1	52.4	57.0

Sample	CS8210	CS8210	CS8210	CS8210	CS8210	CS8210	CS8210	CS8305
No.	2906	2909	2912	2914	2919	2922	3003	0403
Loc.	Asemi	Asemi	Asemi	Asemi	Asemi	Asemi	Asemi	Asemi
Mineral zone	Abt-Z	Abt-Z	Abt-Z	Abt-Z	Abt-Z	Abt-Z	Abt-Z	Abt-Z
SiO2	67.22	70.02	67.31	67.31	74.67	69.73	64.36	69.33
TiO2	0.64	0.53	0.60	0.62	0.18	0.42	0.69	0.53
Al2O3	15.69	14.21	15.44	15.62	14.01	14.72	17.14	14.74
Fe2O3	5.93	4.69	5.44	5.06	1.99	3.70	5.85	3.93
MnO	0.40	0.17	0.22	0.17	0.06	0.06	0.25	0.07
MgO	1.88	1.78	2.21	1.99	0.58	1.20	2.07	1.51
CaO	0.77	0.95	0.84	0.95	0.47	0.93	0.66	1.77
Na2O	2.36	1.27	1.92	2.19	4.55	2.46	2.07	2.75
K2O	2.68	3.51	3.23	3.43	2.33	3.93	3.74	2.60
P2O5	0.12	0.10*	0.12	0.12	0.06*	0.09*	0.12	0.11
LOI	2.18	2.75	2.63	2.29	0.99	1.76	2.85	2.41
Total	99.87	99.98	99.96	99.75	99.89	99.00	99.80	99.75

Table 3A. (continued)

Rb	110	137	128	134	94.6	159	153	103
Sr	117	116	106	104	114	138	119	224
Y	28.5**	19.9	20.3	19.2	40.3**	29.3**	23.9	15.7
Zr	133	112	131	141	110	159	149	148
Nb	10.6	9.3	9.5	9.5	12.7	12.8	11.4	8.8
Ba	407	540	421	484	337	491	533	399
Th	12.4	11.4	12.8	12.6	25.0	17.0	15.5	10.9
Pb	27.9	16.4	20.9	9.8	24.3	21.7	20.7	17.8
Ni	38.8*	18.5*	26.4*	17.8*	2.5*	6.8*	11.8*	14.9*
mg-value	0.386	0.429	0.446	0.438	0.366	0.391	0.412	0.432
Mn-ratio	4.46	2.28	2.46	2.08	2.11	1.10	2.75	1.13
K/Rb	203	212	209	213	204	206	203	210
K/Ba	54.7	53.9	63.6	58.9	57.4	66.4	58.2	54.1

Sample	CS8305	CS8305	CS8305	CS8305	CS8305	CS8305	CS8310	CS8310
No.	0901	0412	0802	0907	0909	1104	2701	2702
Loc.	Asemi	Asemi	Asemi	Asemi	Asemi	Asemi	Asemi	Asemi
Mineral zone	Abt-Z	Abt-Z	Abt-Z	Abt-Z	Abt-Z	Abt-Z	Abt-Z	Abt-Z
SiO2	73.85	66.98	68.89	71.31	67.66	72.72	70.27	65.80
TiO2	0.31	0.59	0.56	0.43	0.60	0.48	0.43	0.64
Al2O3	14.83	15.69	15.43	14.95	15.18	14.05	14.63	16.11
Fe2O3	2.83	4.89	4.96	3.44	4.83	3.11	3.16	5.50
MnO	0.11	0.17	0.18	0.09	0.13	0.07	0.06	0.23
MgO	0.93	1.91	1.78	1.18	1.83	1.12	1.12	2.05
CaO	0.67	1.55	0.72	0.72	1.69	0.93	1.24	1.31
Na2O	1.74	2.39	2.09	2.81	2.26	3.56	3.45	2.10
K2O	3.23	3.01	3.16	3.09	2.98	2.34	2.61	3.21
P2O5	0.08*	0.12	0.11	0.08*	0.10*	0.09*	0.09*	0.12
LOI	1.22	2.22	2.16	1.55	2.10	1.35	1.40	1.75
Total	99.80	99.52	100.04	99.65	99.36	99.82	98.46	98.82
Rb	125	121	128	120	115	88.8	94.7	127
Sr	145	162	114	123	198	158	159	167
Y	27.1**	18.0	18.8	24.5	17.3	17.0	17.7	22.9
Zr	146	137	137	149	145	160	130	146
Nb	9.7	9.3	10.2	9.1	8.8	8.4	8.2	10.2
Ba	597	497	514	406	433	354	404	455
Th	18.2	12.5	13.1	13.2	11.0	10.4	11.2	13.2
Pb	24.5	13.7	15.1	19.3	19.4	15.2	18.5	22.4
Ni	8.3*	20.3*	10.1*	6.9*	16.1*	3.3*	3.3*	21.6*
mg-value	0.394	0.436	0.416	0.405	0.429	0.416	0.412	0.425
Mn-ratio	2.58	2.16	2.33	1.72	1.70	1.46	1.24	2.64
K/Rb	214	206	204	213	216	219	229	209
K/Ba	44.9	50.2	51.1	63.2	57.2	54.9	53.6	58.6

Table 3A. (continued)

Sample	CS8310	CS8310	CS8310	CS8310	CS8310	CS8310	CS8310	CS8310
No.	2705	2803	2804	2805	2806	2902	2904	3104
Loc.	Asemi	Asemi	Asemi	Asemi	Asemi	Asemi	Asemi	Asemi
Mineral zone	Abt-Z	Abt-Z	Abt-Z	Abt-Z	Abt-Z	Abt-Z	Abt-Z	Abt-Z
SiO2	65.05	63.54	63.63	68.83	64.54	71.94	70.50	73.51
TiO2	0.70	0.72	0.67	0.58	0.65	0.51	0.54	0.43
Al2O3	16.00	17.11	17.22	14.52	16.93	13.76	14.29	11.57
Fe2O3	5.72	6.02	5.46	5.22	5.04	4.80	4.25	4.36
MnO	0.20	0.12	0.12	0.15	0.13	0.25	0.12	0.15
MgO	2.14	2.03	2.00	1.60	1.87	1.87	1.59	1.60
CaO	1.82	1.87	0.79	1.62	1.72	0.67	1.59	1.46
Na2O	2.49	3.38	2.64	2.12	2.39	1.38	1.81	1.78
K2O	3.09	2.73	4.11	2.83	3.46	2.86	3.01	2.64
P2O5	0.14	0.13	0.10*	0.18	0.13	0.12	0.11	0.19
LOI	2.44	1.72	1.95	1.89	2.31	1.44	1.41	1.37
Total	99.79	99.37	98.69	99.54	99.17	99.60	99.22	99.06
Rb	123	106	128	117	133	124	115	115
Sr	160	214	177	172	204	96.0	178	112
Y	22.6	22.9	21.3	25.2	22.1	19.0	17.7	24.6
Zr	165	162	157	146	164	119	147	104
Nb	10.5	9.7	8.0	9.7	10.7	7.9	8.3	7.6
Ba	481	498	963	504	517	408	450	354
Th	14.4	13.8	14.3	12.0	13.7	11.9	11.5	9.1
Pb	21.8	20.1	15.0	17.1	22.8	22.9	17.4	14.7
Ni	22.5*	18.9*	17.4*	12.6*	14.2*	22.9*	10.5*	12.1*
mg-value	0.426	0.400	0.420	0.378	0.424	0.436	0.426	0.421
Mn-ratio	2.21	1.33	1.41	1.97	1.65	3.20	1.79	2.19
K/Rb	208	214	267	201	216	192	218	191
K/Ba	53.4	45.5	35.4	46.6	55.5	58.2	55.6	61.8

Sample	CS8405	CS8405	TH7611	TH7611	TH7108	TH7108	TH7108	TH7108
No.	2401	2603	0401	0409	1408	1416	1107	1110
Loc.	Asemi	Asemi	Mishima	Mishima	Asemi	Asemi	Asemi	Asemi
Mineral zone	Abt-Z	Abt-Z	Abt-Z	Abt-Z	Abt-Z	Abt-Z	Abt-Z	Abt-Z
SiO2	69.11	72.54	67.94	69.23	70.66	69.22	71.90	68.55
TiO2	0.59	0.43	0.58	0.50	0.56	0.59	0.45	0.57
Al2O3	15.35	14.02	16.18	15.63	14.77	15.20	14.83	15.41
Fe2O3	4.94	2.83	4.33	3.77	4.47	5.00	3.20	4.99
MnO	0.24	0.04	0.14	0.05	0.14	0.21	0.05	0.19
MgO	1.72	1.10	1.58	1.23	1.52	1.77	1.08	1.83
CaO	0.79	0.99	0.59	0.78	0.89	0.73	0.92	0.98
Na2O	2.16	3.03	2.10	0.63	1.52	2.09	2.88	1.96
K2O	3.12	2.72	3.68	4.92	3.52	3.15	3.31	3.30
P2O5	0.12	0.08*	0.11	0.08*	0.11	0.09*	0.08*	0.11
LOI	1.32	1.57	1.85	2.40	1.96	1.85	1.32	2.16
Total	99.46	99.35	99.08	99.22	100.12	99.90	100.02	100.05

Table 3A. (continued)

Rb	135	100	142	181	141	130	130	134
Sr	125	137	109	134	155	122	149	115
Y	25.3	22.5	17.5	23.2	22.5	19.6	26.7**	21.0
Zr	165	133	150	125	140	124	165	136
Nb	11.1	8.1	10.2	10.1	9.3	9.5	11.8	9.8
Ba	445	445	663	916	564	560	523	523
Th	15.1	11.1	13.9	14.0	12.5	13.4	15.6	12.8
Pb	19.7	15.5	17.8	21.4	18.8	16.4	18.4	19.5
Ni	22.7*	5.0*	6.2*	13.6*	14.0*	20.8*	2.6*	27.4*
mg-value	0.408	0.435	0.420	0.393	0.402	0.412	0.401	0.421
Mn-ratio	3.13	0.89	2.07	0.90	2.06	2.70	1.04	2.42
K/Rb	192	225	216	225	207	202	211	204
K/Ba	58.2	50.7	46.1	44.6	51.8	46.7	52.5	52.4

Sample	TH7108	TH7108	TH7108	TH7108	TH7108	TH7108	TH7108	TH7108
No.	1111	1404	1405	1418	1108	1003	1002	1102
Loc.	Asemi	Asemi	Asemi	Asemi	Asemi	Asemi	Asemi	Asemi
Mineral zone	Abt-Z	Abt-Z	Abt-Z	Abt-Z	Abt-Z	Abt-Z	Abt-Z	Abt-Z
SiO2	71.79	72.10	70.19	68.23	64.72	70.15	72.57	63.48
TiO2	0.48	0.49	0.53	0.58	0.69	0.53	0.48	0.72
Al2O3	14.37	14.20	15.52	15.47	16.00	15.16	13.70	16.40
Fe2O3	3.48	3.33	3.79	4.73	5.67	4.14	4.25	7.96
MnO	0.06	0.09	0.11	0.12	0.16	0.10	0.13	0.34
MgO	1.39	1.26	1.36	1.68	2.34	1.40	1.61	2.65
CaO	0.43*	0.85	0.78	1.11	1.85	0.61	0.51	1.03
Na2O	2.99	5.15	3.34	2.06	2.59	3.24	1.60	2.08
K2O	2.79	1.42	2.80	3.43	2.91	2.76	3.09	2.87
P2O5	0.07*	0.10*	0.09*	0.11	0.12	0.15	0.11	0.11
LOI	1.85	1.08	1.92	2.07	2.32	1.35	1.96	2.36
Total	99.70	100.07	100.43	99.59	99.37	99.59	100.01	100.00
Rb	118	62.4	112	132	111	111	127	113
Sr	143	129	155	234	186	127	81.5	121
Y	16.1	20.5	22.4	21.2	20.9	20.4	24.2	25.0
Zr	136	149	156	150	141	168	139	133
Nb	8.0	8.2	8.3	8.4	9.3	8.8	13.6	12.2
Ba	441	252	436	733	507	497	484	455
Th	11.6	12.2	12.8	12.2	10.6	13.2	13.1	12.9
Pb	25.1	21.0	23.0	18.1	16.9	21.3	14.4	11.1
Ni	4.6*	15.9*	17.8*	11.4*	29.4*	18.5*	16.1*	24.4*
mg-value	0.442	0.428	0.415	0.413	0.450	0.401	0.429	0.397
Mn-ratio	1.07	1.71	1.87	1.65	1.72	1.60	1.93	2.82
K/Rb	196	189	208	216	217	207	202	211
K/Ba	52.5	46.8	53.3	38.9	47.7	46.1	53.0	52.4

Table 3A. (continued)

Sample	TH7108	TH7108	TH7108	STL7504	CS8305	CS8305	CS8305	CS8305
No.	1103	1104	1109	1908	0807	0908	1006	1401
Loc.	Asemi	Asemi	Asemi	Urayama	Asemi	Asemi	Asemi	Asemi
Mineral zone	Abt-Z	Abt-Z	Abt-Z	Abt-Z	Obt-Z	Obt-Z	Obt-Z	Obt-Z
SiO2	68.31	69.89	66.74	66.84	62.65	66.75	68.30	71.14
TiO2	0.65	0.55	0.61	0.57	0.71	0.67	0.60	0.49
Al2O3	15.99	14.63	16.16	16.32	16.88	16.31	15.44	13.85
Fe2O3	4.55	4.43	5.90	4.56	5.82	5.37	4.76	3.49
MnO	0.09	0.19	0.31	0.13	0.13	0.08	0.16	0.06
MgO	1.59	1.68	2.22	1.51	2.96	1.85	1.75	1.25
CaO	0.88	0.84	0.83	0.24*	2.90	0.95	1.52	1.69
Na2O	2.86	0.88	2.02	2.69	2.58	2.42	2.23	2.84
K2O	3.19	4.12	3.38	3.27	3.02	2.90	2.96	2.73
P2O5	0.12	0.09*	0.10*	0.11	0.14	0.14	0.12	0.08*
LOI	1.70	1.55	1.82	3.57	1.85	2.63	1.73	2.08
Total	99.93	98.85	100.09	99.81	99.64	100.07	99.57	99.70
Rb	125	156	134	n.a.	99.2	117	117	102
Sr	184	116	98.9	n.a.	211	153	178	164
Y	22.3	20.5	17.7	n.a.	21.2	20.3	21.5	19.3
Zr	184	135	134	n.a.	151	159	145	134
Nb	9.5	9.7	9.8	n.a.	10.0	9.4	10.3	8.3
Ba	587	627	471	n.a.	577	421	464	431
Th	12.0	12.9	15.1	n.a.	13.3	12.5	12.1	10.5
Pb	17.3	12.2	15.4	n.a.	14.1	19.2	20.4	16.6
Ni	16.9*	23.1*	15.5*	n.a.	49.9	11.0*	13.4*	9.8*
mg-value	0.409	0.429	0.427	0.396	0.502	0.406	0.421	0.415
Mn-ratio	1.30	2.68	3.28	1.90	1.24	0.99	2.14	1.12
K/Rb	212	219	209		253	205	210	223
K/Ba	45.1	54.6	59.5		43.4	57.2	52.9	52.6

Sample	CS8305	CS8310	CS8310	AG12-1	TH7108	TH7108	TH7108	TH7108
No.	1402	2807	2903		1422	1311	1306	1315
Loc.	Asemi	Asemi	Asemi	Asemi	Asemi	Asemi	Asemi	Asemi
Mineral zone	Obt-Z	Obt-Z	Obt-Z	Obt-Z	Obt-Z	Obt-Z	Obt-Z	Obt-Z
SiO2	73.78	68.64	70.70	69.42	70.69	63.85	64.47	67.74
TiO2	0.47	0.58	0.54	0.58	0.49	0.68	0.59	0.57
Al2O3	13.00	15.09	14.75	15.21	14.80	16.59	15.15	15.32
Fe2O3	3.58	4.39	3.81	5.10	4.00	5.59	4.91	5.04
MnO	0.10	0.10	0.15	0.20	0.24	0.18	0.20	0.14
MgO	1.31	1.50	1.42	1.94	1.73	1.94	1.56	1.70
CaO	1.36	1.87	1.43	0.83	1.13	1.99	3.74	1.19
Na2O	1.98	2.71	2.76	2.16	1.81	2.89	2.83	3.38
K2O	2.61	2.77	2.60	2.84	3.41	3.05	2.73	2.71
P2O5	0.10*	0.10*	0.09*	0.11	0.09*	0.12	0.13	0.09*
LOI	1.39	1.63	1.01	2.01	2.06	2.54	2.44	1.61
Total	99.68	99.38	99.26	100.40	100.45	99.42	98.75	99.49

Table 3A. (continued)

Rb	106	108	102	120	133	117	103	117
Sr	193	215	191	128	108	208	288	164
Y	16.8	20.9	18.9	23.5	23.3	23.5	21.8	21.7
Zr	146	149	173	141	121	162	143	132
Nb	8.6	9.5	9.6	9.8	8.6	9.8	13.7	6.3
Ba	375	404	375	420	414	531	479	466
Th	8.3	10.7	11.3	12.0	13.7	14.1	10.6	13.8
Pb	16.3	19.2	19.7	20.5	25.3	24.7	23.0	29.9
Ni	5.3*	11.7*	7.7*	20.4*	16.1*	21.7*	13.0*	20.1*
mg-value	0.420	0.404	0.425	0.430	0.461	0.407	0.386	0.401
Mn-ratio	1.79	1.51	2.48	2.46	3.51	2.10	2.74	1.84
K/Rb	205	214	212	196	213	216	220	193
K/Ba	57.7	56.9	57.6	56.1	68.4	47.7	47.3	48.3

Sample	TH7108
No.	1303
Loc.	Asemi
Mineral zone	Obt-Z
SiO2	70.78
TiO2	0.50
Al2O3	14.37
Fe2O3	4.67
MnO	0.18
MgO	1.78
CaO	0.92
Na2O	1.88
K2O	2.92
P2O5	0.12
LOI	1.26
Total	99.38
Rb	126
Sr	149
Y	16.9
Zr	129
Nb	7.8
Ba	537
Th	12.8
Pb	22.4
Ni	26.2*
mg-value	0.430
Mn-ratio	2.41
K/Rb	192
K/Ba	45.1

Table 3B. Chemical compositions of pelitic schsits from the Besshi-traverse and of pelitic schist clasts from the Kuma Formation.

Sample	TH7705	TI7604	HI7805	HI7805	TI7604	HI7805	HI7805	TI7604
No.	2617	2516	2922	2909	2510	2917	2901	2504
Loc.	Hiura	Kokuryo	Hiura	Hiura	Kokuryo	Hiura	Hiura	Kokuryo
Mineral zone	Chl-Z	Chl-Z	Chl-Z	Chl-Z	Chl-Z	Chl-Z	Chl-Z	Chl-Z
SiO2	67.09	74.41	66.12	69.33	67.83	68.08	73.06	68.56
TiO2	0.47	0.39	0.60	0.53	0.54	0.56	0.39	0.53
Al2O3	16.79	13.35	17.25	15.00	13.92	16.14	13.32	14.66
Fe2O3	3.97	3.10	4.20	4.37	4.40	4.29	2.90	4.43
MnO	0.10	0.04	0.09	0.09	0.04	0.09	0.05	0.11
MgO	1.48	1.02	1.36	1.42	1.48	1.52	0.97	1.58
CaO	0.68	0.10*	0.32*	0.62	0.23*	0.11*	1.31	0.97
Na2O	3.07	3.09	3.32	2.51	0.60	3.13	3.20	2.55
K2O	3.90	2.37	3.43	3.30	4.53	3.13	2.82	3.32
P2O5	0.10*	0.08*	0.11	0.09*	0.10*	0.11	0.08*	0.11
LOI	2.21	2.16	2.65	2.02	5.58	2.71	1.90	2.80
Total	99.86	100.11	99.45	99.28	99.25	99.87	100.00	99.62
Rb	148	97.9	136	133	160	131	101	130
Sr	98.4	33.4	104	76.4	35.4	44.6	142	88.9
Y	26.0	22.9	20.3	25.5	25.7	18.9	18.5	22.6
Zr	164	150	155	146	171	168	134	150
Nb	8.8	8.5	11.2	10.5	10.1	10.8	6.5	9.2
Ba	564	381	567	517	713	551	526	577
Th	14.1	12.0	16.4	14.1	13.2	11.7	8.2	12.8
Pb	12.7	20.6	18.6	15.9	20.4	11.1	18.3	21.3
Ni	9.6*	7.9*	8.0*	14.6*	14.1*	9.6*	4.4*	16.0*
mg-value	0.425	0.395	0.391	0.392	0.400	0.412	0.399	0.414
Mn-ratio	1.60	0.87	1.45	1.39	0.61	1.37	1.15	1.61
K/Rb	218	201	209	206	235	198	232	213
K/Ba	57.4	51.7	50.3	53.0	52.7	47.2	44.5	47.7

Sample	TH7604	TH7604	TH7604	TH7604	TH7604	TH7604	TH7705	TH7705
No.	2529	2526	2515	2521	2507	2524	2701	2608
Loc.	Kokuryo	Kokuryo	Kokuryo	Kokuryo	Kokuryo	Kokuryo	Hiura	Hiura
Mineral zone	Chl-Z	Chl-Z	Chl-Z	Chl-Z	Chl-Z	Chl-Z	Chl-Z	Chl-Z
SiO2	72.80	73.30	70.82	74.21	67.88	73.34	69.07	72.05
TiO2	0.46	0.38	0.50	0.37	0.58	0.43	0.54	0.42
Al2O3	13.08	13.09	14.13	13.42	15.21	13.71	13.29	14.22
Fe2O3	3.05	2.62	4.43	3.15	4.98	2.69	4.75	3.60
MnO	0.06	0.04	0.12	0.08	0.20	0.03	0.16	0.06
MgO	0.80	0.76	1.65	0.93	1.77	0.82	2.99	1.12
CaO	1.54	2.04	0.22*	0.15*	0.46*	0.54	1.23	0.20*
Na2O	4.12	3.27	3.20	3.27	2.37	2.97	1.85	2.85
K2O	1.94	2.46	2.29	2.57	3.41	3.19	2.71	3.17
P2O5	0.08*	0.09*	0.09*	0.07*	0.11	0.09*	0.11	0.08*

Table 3B. (continued)

LOI	1.35	1.13	1.95	1.66	1.83	1.37	2.53	1.87
Total	99.28	99.18	99.40	99.88	98.80	99.18	99.23	99.64
Rb	72.6	84.1	93.8	105	129	117	110	135
Sr	198	290	50.9	32.3	49.5	147	107	22.0*
Y	16.6	16.0	17.8	22.2	23.5	17.2	20.0	17.9
Zr	175	142	133	144	142	162	131	143
Nb	6.3	6.0	8.9	8.3	10.2	7.9	9.3	8.6
Ba	350	454	375	475	480	497	429	486
Th	8.9	8.2	11.6	12.2	12.7	11.4	10.3	13.1
Pb	16.0	15.5	16.3	28.8	18.6	18.6	25.8	21.2
Ni	8.2*	1.9*	10.4*	6.7*	20.9*	1.1*	50.0	6.2*
mg-value	0.342	0.365	0.425	0.369	0.413	0.376	0.555	0.381
Mn-ratio	1.44	1.08	1.72	1.77	2.58	0.78	1.66	1.15
K/Rb	222	243	203	204	219	227	204	196
K/Ba	46.1	44.9	50.7	44.9	59.0	53.3	52.4	54.1

Sample	TH7604	TH7705	TH7504	TH7504	TH7705	TH7604	TH7504	TH7504
No.	2510	2614	2510	2515	2704	2504	2112	2136
Loc.	Kokuryo	Hiura	Kokuryo	Kokuryo	Hiura	Kokuryo	Seki	Seki
Mineral zone	Chl-Z	Chl-Z	Grt-Z	Grt-Z	Grt-Z	Grt-Z	Grt-Z	Grt-Z
SiO2	73.21	66.69	68.76	67.39	63.55	65.89	71.69	66.31
TiO2	0.40	0.59	0.56	0.61	0.69	0.63	0.35	0.64
Al2O3	13.86	15.98	15.17	15.11	17.60	16.86	15.49	16.65
Fe2O3	3.18	5.01	5.16	5.16	5.89	5.11	2.47	4.30
MnO	0.07	0.15	0.23	0.21	0.29	0.11	0.08	0.08
MgO	1.08	1.81	1.70	2.03	2.12	1.85	1.01	1.66
CaO	0.17*	0.65	0.50	1.30	0.62	0.53	0.44*	1.19
Na2O	3.11	2.30	1.84	2.06	3.44	2.82	3.98	2.16
K2O	2.57	3.36	3.37	3.24	3.08	3.26	2.68	3.56
P2O5	0.08*	0.12	0.12	0.12	0.11	0.13	0.07*	0.13
LOI	1.79	2.79	2.90	2.17	2.58	2.76	1.46	2.83
Total	99.52	99.45	100.31	99.40	99.97	99.95	99.72	99.51
Rb	105	135	137	128	125	125	110	136
Sr	40.0	78.4	99.1	128	133	152	133	199
Y	18.9	22.9	26.2**	22.7	31.6**	17.5	26.8**	28.4**
Zr	146	152	162	140	163	158	180	165
Nb	8.7	10.4	10.8	9.7	12.4	9.6	10.2	10.6
Ba	437	545	513	479	468	481	502	602
Th	11.0	13.2	13.1	13.1	15.8	13.0	16.2	14.4
Pb	12.3	17.3	19.7	21.6	14.0	17.1	30.1	19.7
Ni	7.2*	14.8*	11.0*	26.9*	25.5*	6.2*	1.8*	10.8*
mg-value	0.402	0.417	0.395	0.438	0.416	0.418	0.448	0.433
Mn-ratio	1.46	1.93	2.95	2.51	3.13	1.39	1.97	1.17
K/Rb	203	206	204	210	204	217	203	217
K/Ba	48.9	51.1	54.5	56.1	54.6	56.3	44.3	49.1

Table 3B. (continued)

Sample	TH7504	TH7504	TH7504	TH7504	TH7504	TH7504	TH7504	TH7504
No.	2124	2132	2121	2115	2134	2128	2107	2212
Loc.	Seki	Seki	Seki	Seki	Seki	Seki	Seki	Seki
Mineral zone	Grt-Z	Grt-Z	Grt-Z	Grt-Z	Grt-Z	Grt-Z	Grt-Z	Grt-Z
SiO2	69.42	69.65	72.56	66.91	70.63	70.39	71.03	66.28
TiO2	0.58	0.31	0.37	0.58	0.50	0.48	0.51	0.64
Al2O3	14.47	17.07	14.65	15.34	14.98	13.65	14.04	15.51
Fe2O3	4.52	2.70	2.48	5.27	3.43	4.79	3.65	5.08
MnO	0.18	0.03	0.05	0.37	0.07	0.06	0.13	0.08
MgO	1.93	0.90	0.93	2.30	1.50	1.66	1.35	2.02
CaO	0.53	0.05*	0.56	0.66	0.21*	0.94	0.53	0.58
Na2O	1.24	3.54	3.45	1.13	2.11	2.65	2.43	1.40
K2O	3.50	3.40	2.73	3.84	3.47	2.21	2.89	4.25
P2O5	0.10*	0.05*	0.05*	0.11	0.10*	0.13	0.10*	0.13
LOI	2.82	2.05	1.64	2.40	2.49	2.20	2.16	2.64
Total	99.29	99.75	99.47	98.91	99.49	99.16	98.82	98.61
Rb	144	136	110	142	136	91.5	118	144
Sr	80.0	67.6	135	73.4	55.6	110	102	36.3
Y	18.4	36.8**	22.6	22.8	19.8	21.8	19.1	19.9
Zr	123	143	151	138	128	128	136	138
Nb	10.0	9.8	8.4	10.3	8.8	7.8	9.1	10.0
Ba	538	564	445	685	505	396	432	547
Th	13.8	15.0	12.8	13.9	13.5	9.9	12.1	11.4
Pb	16.3	17.8	15.3	55.8**	15.5	15.2	16.7	9.4
Ni	17.3*	10.9*	9.9*	25.6*	4.6*	13.6*	7.0*	17.9*
mg-value	0.458	0.398	0.426	0.464	0.464	0.407	0.423	0.441
Mn-ratio	2.37	0.75	1.29	4.07	1.22	0.83	2.26	0.98
K/Rb	202	207	207	224	211	200	203	245
K/Ba	54.0	50.0	51.0	46.5	57.0	46.4	55.5	64.5

Sample	TH7705	TH8005	TH7504	TH7504	TH7504	TH7504	TH7504	TH7705
No.	2708	2202	2410	2429	2415	2423	2414	2713
Loc.	Hiura	Kokuryo	Kokuryo	Kokuryo	Kokuryo	Kokuryo	Kokuryo	Hiura
Mineral zone	Grt-Z	Abt-Z	Abt-Z	Abt-Z	Abt-Z	Abt-Z	Abt-Z	Abt-Z
SiO2	68.02	68.82	70.03	67.35	72.83	70.38	71.82	73.72
TiO2	0.59	0.56	0.57	0.57	0.45	0.52	0.51	0.42
Al2O3	15.31	15.66	15.01	16.28	13.75	14.69	14.67	13.48
Fe2O3	5.13	4.66	4.72	5.03	3.71	4.52	3.40	2.89
MnO	0.20	0.22	0.12	0.14	0.17	0.09	0.10	0.05
MgO	1.93	1.81	1.68	1.66	1.31	1.42	1.21	1.04
CaO	0.62	0.46*	0.34*	0.31*	0.40*	0.28*	0.46*	1.04
Na2O	2.38	2.18	0.88	2.63	3.53	2.78	2.70	3.64
K2O	3.12	3.35	3.99	3.32	2.03	2.83	2.83	2.10
P2O5	0.12	0.10*	0.10*	0.14	0.10*	0.11	0.11	0.08*
LOI	2.07	2.14	2.73	2.69	1.60	2.45	2.38	1.21
Total	99.49	99.96	100.17	100.12	99.88	100.07	100.19	99.67

Table 3B. (continued)

Rb	126	133	157	128	82.3	112	116	76.1
Sr	72.5	102	77.2	81.3	116	90.9	113	113
Y	21.2	23.3	20.8	23.4	16.8	17.2	14.4	19.4
Zr	145	156	131	143	147	144	194	129
Nb	10.9	11.2	10.7	10.0	8.7	9.2	12.0	7.8
Ba	483	511	632	453	281	489	463	323
Th	13.5	15.9	13.0	14.0	12.0	12.7	12.4	10.9
Pb	15.0	22.4	12.6	26.8	15.0	24.4	40.0**	12.3
Ni	23.8*	24.7*	14.6*	10.6*	4.4*	13.6*	7.3*	11.0*
mg-value	0.427	0.435	0.414	0.395	0.412	0.384	0.413	0.416
Mn-ratio	2.45	2.92	1.65	1.86	2.95	1.36	1.90	1.12
K/Rb	206	209	210	215	205	210	203	229
K/Ba	53.6	54.4	52.4	60.9	59.9	48.0	50.8	54.0

Sample	TH7705	TH7705	TH7705	TH7504	TH7504	TH7504	TH7504	TH7705
No.	2716	2710	2717	2216	2221	2206	3020	2807
Loc.	Hiura	Hiura	Hiura	Seki	Seki	Seki	Tokona.	Tokona.
Mineral zone	Abt-Z	Abt-Z	Abt-Z	Abt-Z	Abt-Z	Abt-Z	Abt-Z	Abt-Z
SiO2	71.56	68.13	64.81	67.14	64.25	68.44	67.21	67.14
TiO2	0.43	0.53	0.65	0.70	0.62	0.56	0.60	0.56
Al2O3	13.90	14.35	16.68	15.99	16.38	14.93	15.05	15.99
Fe2O3	3.24	3.82	6.29	5.41	4.37	4.65	5.92	4.38
MnO	0.06	0.10	0.27	0.17	0.18	0.15	0.31	0.05
MgO	1.12	1.75	2.37	1.92	1.75	1.62	2.19	1.60
CaO	1.32	2.36	0.86	0.25*	2.22	1.13	0.85	3.47
Na2O	3.04	2.80	1.77	1.07	2.59	1.84	2.08	0.47
K2O	2.73	2.81	3.44	3.93	3.37	3.39	2.61	3.61
P2O5	0.08*	0.12	0.14	0.11	0.14	0.12	0.11	0.16
LOI	1.66	3.02	2.14	2.57	3.11	1.81	2.29	1.88
Total	99.14	99.79	99.42	99.26	98.98	98.64	99.22	99.31
Rb	98.8	107	142	157	135	131	113	115
Sr	110	174	118	85.9	240	136	123	440
Y	19.1	16.2	20.6	20.3	22.3	21.9	21.7	17.0
Zr	128	148	129	145	158	137	130	166
Nb	8.4	7.6	9.7	13.7	12.0	9.2	9.9	7.1
Ba	469	456	412	565	459	589	334	751
Th	10.1	9.2	13.2	13.1	11.1	12.4	13.2	10.6
Pb	17.4	15.2	23.0	14.7	19.5	21.1	28.4	19.7
Ni	7.4*	10.6*	28.0*	11.1*	12.8*	15.6*	23.0*	2.9*
mg-value	0.406	0.476	0.427	0.413	0.442	0.408	0.423	0.420
Mn-ratio	1.22	1.52	2.69	2.03	2.52	2.10	3.29	0.74
K/Rb	229	219	201	208	207	215	192	260
K/Ba	48.4	51.1	69.4	57.7	60.9	47.8	64.8	39.9

Table 3B. (continued)

Sample	TH7505	TH7504	TH7504	TH7504	TH8007	TH8005	TH8007	TH8005
No.	0120	2834	2807	2404	2303	2719	2307	2705
Loc.	Tokona.	Tokona.	Tokona.	Kokuryo	Hiura	Seki	Hiura	Seki
Mineral zone	Abt-Z	Abt-Z	Abt-Z	Obt-Z	Obt-Z	Obt-Z	Obt-Z	Obt-Z
SiO2	72.39	65.13	71.84	67.80	67.47	68.47	65.95	66.77
TiO2	0.49	0.63	0.39	0.56	0.66	0.75	0.60	0.72
Al203	13.83	16.63	13.45	15.99	16.16	12.46	15.90	15.78
Fe203	2.80	5.39	2.79	4.73	5.05	5.46	4.41	5.92
MnO	0.02	0.20	0.06	0.21	0.09	0.19	0.13	0.22
MgO	0.89	1.83	0.98	1.77	1.78	2.54	2.24	2.37
CaO	0.59	0.83	1.95	0.44*	1.16	3.75	3.81	2.39
Na20	2.58	2.15	2.91	3.06	1.83	1.36	1.18	1.48
K20	3.13	3.75	2.78	3.00	3.22	2.28	3.14	2.52
P205	0.09*	0.11	0.11	0.10*	0.13	0.16	0.13	0.14
LOI	2.11	2.29	1.26	2.43	2.20	1.37	2.04	1.48
Total	98.92	98.94	98.52	100.09	99.75	98.79	99.53	99.79
Rb	110	149	106	114	115	83.6	103	78.6
Sr	109	121	190	76.2	171	182	277	254
Y	15.1	23.5	19.2	21.1	22.9	20.7	19.3	22.8
Zr	150	153	150	152	164	119	153	142
Nb	9.1	11.9	8.5	11.5	11.7	10.6	8.3	9.5
Ba	426	514	450	419	468	371	606	475
Th	9.8	15.2	11.2	12.8	14.3	9.6	11.2	11.9
Pb	12.1	17.9	12.3	22.5	16.0	14.4	18.0	17.8
Ni	7.2*	9.9*	2.6*	15.1*	46.3*	23.2*	8.8*	22.9*
mg-value	0.386	0.402	0.410	0.426	0.411	0.480	0.502	0.442
Mn-ratio	4.91	2.44	1.41	2.79	1.17	2.00	1.63	2.28
K/Rb	237	210	218	218	233	226	253	266
K/Ba	60.9	60.5	51.3	59.4	57.2	51.0	43.0	44.0

Sample	TH7504	TH8005	KY118	KY K-1	KY K-8
No.	2505	2712	996		
Loc.	Kokuryo	Seki	Kuma	Kuma	Kuma
Mineral zone	Obt-Z	Obt-Z			
SiO2	66.44	63.83	60.47	63.30	65.31
TiO2	0.65	0.73	0.82	0.66	0.74
Al203	16.01	15.61	17.77	13.97	16.87
Fe203	4.98	5.94	6.11	5.36	5.49
MnO	0.09	0.12	0.11	0.16	0.08
MgO	2.19	3.01	3.68	3.41	1.94
CaO	2.02	2.96	1.73	4.97	1.76
Na20	1.73	1.83	2.34	2.87	4.00
K20	2.94	3.08	3.56	2.20	2.05
P205	0.13	0.15	0.17	0.13	0.17
LOI	1.92	1.87	3.57	3.38	1.94
Total	99.10	99.13	100.33	100.41	100.35

Table 3B. (continued)

Rb	82.8	113	122	79.1	90.2
Sr	247	165	199	245	183
Y	22.3	23.7	24.0	20.3	25.6
Zr	155	146	173	123	186
Nb	9.8	10.6	10.7	7.6	13.7
Ba	587	446	559	569	328
Th	11.7	12.0	12.7	9.3	17.7
Pb	19.1	14.3	10.7	15.1	21.7
Ni	22.4*	48.2	67.7	70.5	27.5*
mg-value	0.466	0.501	0.544	0.558	0.412
Mn-ratio	1.08	1.12	0.92	1.46	0.96
K/Rb	295	226	243	231	189
K/Ba	41.6	57.4	52.9	32.1	51.9

Table 4A. Average chemical composition of pelitic schists in each mineral zone for the Asemi-traverse.

Mineral zone	Chl-Z				Grt-Z			
N	18				52*1			
	Av.	1sigma	Max.	Min.	Av.	1sigma	Max.	Min.
SiO2	67.42	3.72	71.88	59.63	69.68	3.24	77.48	62.63
TiO2	0.57	0.10	0.76	0.45	0.54	0.10	0.75	0.30
Al2O3	15.70	1.37	18.41	14.22	14.92	1.26	18.18	12.01
Fe2O3	4.92	1.28	7.80	3.04	4.36	1.07	6.75	1.99
MnO	0.13	0.07	0.30	0.05	0.16	0.09	0.35	0.02
MgO	1.77	0.48	2.96	0.95	1.64	0.47	3.07	0.63
CaO	0.67	0.56	2.00	0.07	0.87	0.54	2.83	0.10
Na2O	2.92	1.03	5.52	1.09	2.42	0.73	4.36	0.85
K2O	2.82	0.71	4.09	1.61	2.99	0.54	4.26	1.84
P2O5	0.11	0.02	0.16	0.08	0.10	0.02	0.16	0.06
LOI	2.63	0.50	3.60	1.61	2.10	0.59	3.43	1.07
Total	99.66	0.38	100.47	99.01	99.78	0.51	101.03	98.74
Rb	112	26.8	155	62.2	121	20.7	165	71.0
Sr	83.7	58.5	260	22.9	123	49.7	292	30.5
Y	20.1	8.6	50.3	9.3	20.4	4.3	32.5	5.0
Zr	148	19.6	187	120	138	15.2	170	101
Nb	9.6	1.3	12.4	6.7	9.4	1.2	12.0	6.8
Ba	464	118	696	286	490	93.9	778	337
Th	12.8	2.1	15.8	8.3	12.8	2.0	17.7	8.3
Pb	20.0	5.5	34.1	10.8	17.6	5.3	37.7	8.7
Ni	16.7	9.9	40.5	1.0	13.7*2	9.6	52.0	0.0
mg-value	0.415	0.027	0.446	0.338	0.425	0.025	0.475	0.340
Mn-ratio	1.54	0.55	2.66	0.88	2.15	0.89	4.06	0.44
K/Rb	208	8.4	221	194	206	9.7	240	192
K/Ba	50.8	6.6	67.2	40.0	51.4	5.9	65.9	39.4

*1, The averaged number for the trace elements is 51.
*2, N=50

Table 4A. (continued)

Mineral zone	Abt-Z				Obt-Z			
N	54*3				13			
	Av.	1sigma	Max.	Min.	Av.	1sigma	Max.	Min.
SiO2	69.04	2.85	74.67	63.48	68.38	3.24	73.78	62.65
TiO2	0.55	0.10	0.72	0.18	0.57	0.08	0.71	0.47
Al2O3	15.17	1.06	17.22	11.57	15.14	1.07	16.88	13.00
Fe2O3	4.58	1.08	7.96	1.99	4.66	0.76	5.82	3.49
MnO	0.15	0.08	0.40	0.04	0.15	0.05	0.24	0.06
MgO	1.66	0.42	2.65	0.58	1.75	0.43	2.96	1.25
CaO	0.97	0.44	1.97	0.19	1.66	0.84	3.74	0.83
Na2O	2.38	0.86	5.15	0.60	2.50	0.47	3.38	1.81
K2O	3.11	0.54	4.92	1.42	2.87	0.22	3.41	2.60
P2O5	0.11	0.02	0.19	0.06	0.11	0.02	0.14	0.08
LOI	1.95	0.50	3.57	0.99	1.86	0.49	2.63	1.01
Total	99.66	0.44	100.43	98.46	99.63	0.46	100.45	98.75
Rb	123	19.4	181	62.4	113	10.4	133	99.2
Sr	138	39.2	234	56.4	181	45.6	288	108
Y	21.8	4.3	40.3	12.8	20.7	2.3	23.5	16.8
Zr	142	16.3	184	104	145	14.3	173	121
Nb	9.7	1.3	13.6	7.6	9.4	1.7	13.7	6.3
Ba	491	125	963	252	453	63.5	577	375
Th	13.2	2.4	25.0	9.1	12.0	1.7	14.1	8.3
Pb	18.7	4.4	29.0	9.8	20.9	4.2	29.9	14.1
Ni	15.8	8.0	38.8	2.5	17.4	11.5	49.9	5.3
mg-value	0.416	0.019	0.450	0.366	0.424	0.030	0.502	0.386
Mn-ratio	2.03	0.73	4.46	0.89	2.03	0.72	3.51	0.99
K/Rb	210	13.1	267	188	212	15.7	253	192
K/Ba	53.3	6.9	71.6	35.4	53.2	6.8	68.4	43.4

*3, The averaged number for the trace elements is 53.

Table 4B. Average chemical composition of pelitic schists in each mineral zone for the Besshi-traverse.

Mineral zone	Chl-Z				Grt-Z			
N	18				15			
	Av.	1sigma	Max.	Min.	Av.	1sigma	Max.	Min.
SiO2	70.44	2.86	74.41	66.12	68.57	2.51	72.56	63.55
TiO2	0.48	0.08	0.60	0.37	0.54	0.12	0.69	0.31
Al2O3	14.47	1.31	17.25	13.08	15.46	1.13	17.60	13.65
Fe2O3	3.84	0.80	5.01	2.62	4.34	1.12	5.89	2.47
MnO	0.09	0.05	0.20	0.03	0.14	0.10	0.37	0.03
MgO	1.36	0.53	2.99	0.76	1.66	0.44	2.30	0.90
CaO	0.64	0.56	2.04	0.10	0.62	0.32	1.30	0.05
Na2O	2.82	0.75	4.12	0.60	2.44	0.88	3.98	1.13
K2O	3.03	0.63	4.53	1.94	3.24	0.50	4.25	2.21
P2O5	0.09	0.01	0.12	0.07	0.10	0.03	0.13	0.05
LOI	2.24	0.97	5.58	1.13	2.34	0.43	2.90	1.46
Total	99.50	0.34	100.11	98.80	99.46	0.46	100.31	98.61
Rb	118	23.1	160	72.6	127	14.9	144	91.5
Sr	91.0	68.7	290	22.0	105	42.5	199	36.3
Y	20.7	3.2	26.0	16.0	23.7	5.4	36.8	17.5
Zr	150	13.2	175	131	147	16.2	180	123
Nb	8.9	1.5	11.2	6.0	9.9	1.1	12.4	7.8
Ba	496	87.5	713	350	509	71.6	685	396
Th	12.0	2.1	16.4	8.2	13.4	1.6	16.2	9.9
Pb	18.3	4.5	28.8	11.1	20.0	10.9	55.8	9.4
Ni	11.8	10.8	50.0	1.1	14.2	8.2	26.9	1.8
mg-value	0.404	0.044	0.555	0.342	0.430	0.022	0.464	0.395
Mn-ratio	1.42	0.46	2.58	0.61	1.96	0.97	4.07	0.75
K/Rb	213	13.8	243	196	211	11.5	245	200
K/Ba	50.6	4.2	59.0	44.5	52.9	5.2	64.5	44.3

Table 4B. (continued)

Mineral zone	Abt-Z				Obt-Z			
N	18				7			
	Av.	1sigma	Max.	Min.	Av.	1sigma	Max.	Min.
SiO2	69.06	2.90	73.72	64.25	66.68	1.52	68.47	63.83
TiO2	0.54	0.08	0.70	0.39	0.67	0.07	0.75	0.56
Al2O3	15.04	1.11	16.68	13.45	15.42	1.32	16.16	12.46
Fe2O3	4.33	1.06	6.29	2.79	5.21	0.58	5.94	4.41
MnO	0.14	0.08	0.31	0.02	0.15	0.06	0.22	0.09
MgO	1.56	0.41	2.37	0.89	2.27	0.43	3.01	1.77
CaO	1.06	0.89	3.47	0.25	2.36	1.27	3.81	0.44
Na2O	2.31	0.86	3.64	0.47	1.78	0.62	3.06	1.18
K2O	3.11	0.56	3.99	2.03	2.88	0.35	3.22	2.28
P2O5	0.11	0.02	0.16	0.08	0.13	0.02	0.16	0.10
LOI	2.19	0.55	3.11	1.21	1.90	0.38	2.43	1.37
Total	99.46	0.54	100.19	98.52	99.45	0.46	100.09	98.79
Rb	120	23.1	157	76.1	98.6	16.4	115	78.6
Sr	141	84.9	440	77.2	196	69.1	277	76.2
Y	19.6	2.9	23.5	14.4	21.8	1.5	23.7	19.3
Zr	147	16.3	194	128	147	14.3	164	119
Nb	9.8	1.8	13.7	7.1	10.3	1.2	11.7	8.3
Ba	476	112	751	281	482	85.8	606	371
Th	12.2	1.8	15.9	9.2	11.9	1.4	14.3	9.6
Pb	19.7	7.2	40.0	12.1	17.4	2.9	22.5	14.3
Ni	12.1	7.1	28.0	2.6	26.7	15.0	48.2	8.8
mg-value	0.416	0.021	0.476	0.384	0.461	0.036	0.502	0.411
Mn-ratio	2.15	0.99	4.91	0.74	1.32	0.66	2.79	1.08
K/Rb	215	15.5	260	192	245	27.6	295	218
K/Ba	55.2	7.3	69.4	39.9	50.5	7.6	59.4	41.6

Table 4C. Average chemical composition of pelitic schist clasts from the Kuma Formation.

N		3		
	Av.	1sigma	Max.	Min.
SiO2	63.03	2.43	65.31	60.47
TiO2	0.74	0.08	0.82	0.66
Al2O3	16.20	1.99	17.77	13.97
Fe2O3	5.65	0.40	6.11	5.36
MnO	0.12	0.04	0.16	0.08
MgO	3.01	0.94	3.68	1.94
CaO	2.82	1.86	4.97	1.73
Na2O	3.07	0.85	4.00	2.34
K2O	2.60	0.83	3.56	2.05
P2O5	0.16	0.02	0.17	0.13
LOI	2.96	0.89	3.57	1.94
Total	100.36	0.04	100.41	100.33
Rb	97.0	22.0	122	79.1
Sr	209	32.7	245	183
Y	23.3	2.7	25.6	20.3
Zr	161	33.6	186	123
Nb	10.7	3.1	13.7	7.6
Ba	485	136	569	328
Th	13.2	4.2	17.7	9.3
Pb	15.8	5.5	21.7	10.7
Ni	55.2	24.1	70.5	27.5
mg-value	0.505	0.081	0.558	0.412
Mn-ratio	1.11	0.30	1.46	0.92
K/Rb	221	28.5	243	189
K/Ba	45.6	11.7	52.9	32.1

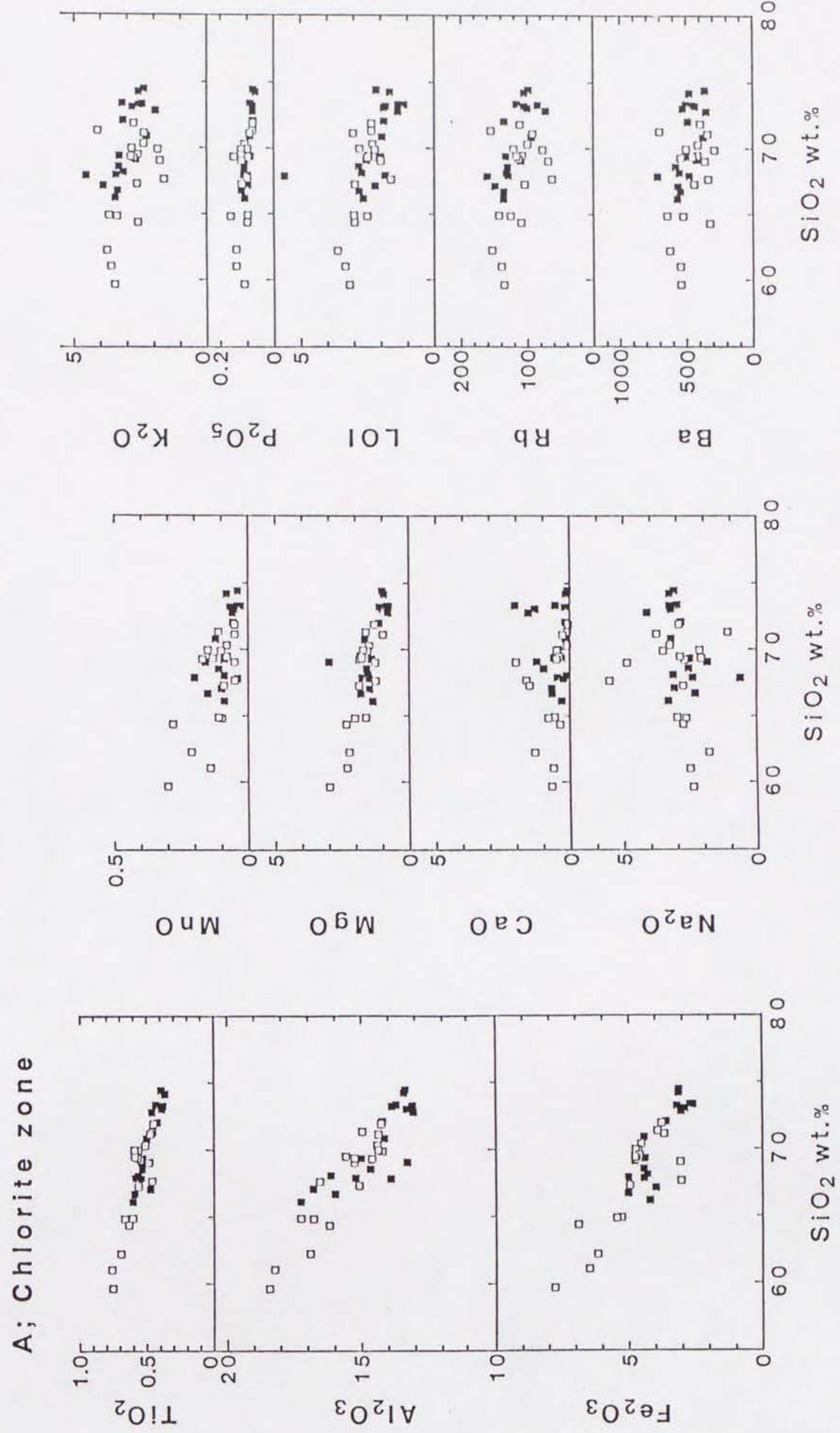

Figure 4. SiO_2-variation diagrams. A: Chlorite zone samples; B: Garnet zone samples; C: Albite-biotite zone samples; D: Oligocalse-biotite zone samples (hexagon) and pelitic schsit clasts from the Kuma Formation (filled diamond). Open-symboles (□,○,△,◇), the Asemi-traverse; Closed symboles (■,●,▲,◆), the Beshi-traverse.

A; Chlorite zone (continued)

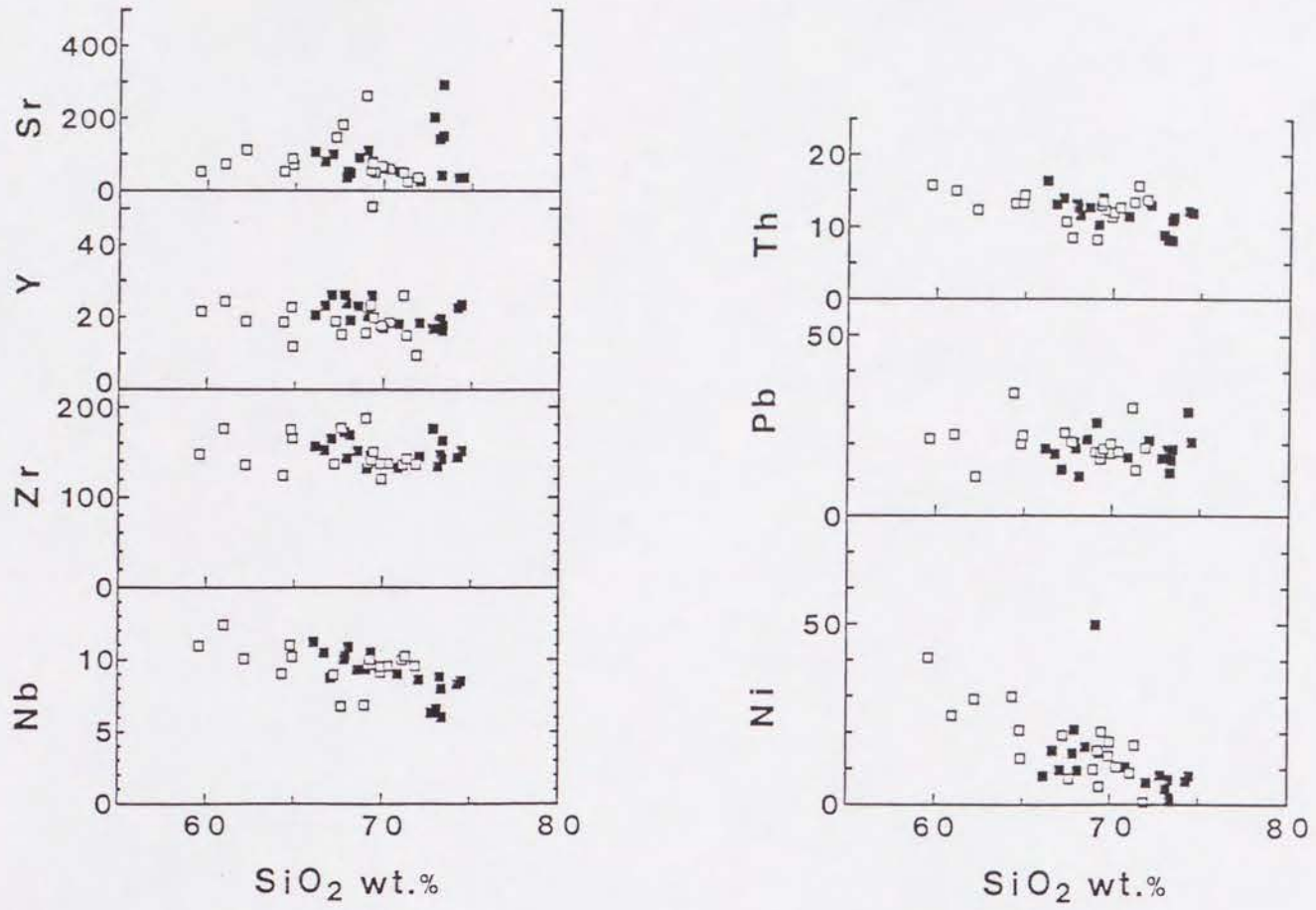

Figure 4. (continued)

B; Garnet zone

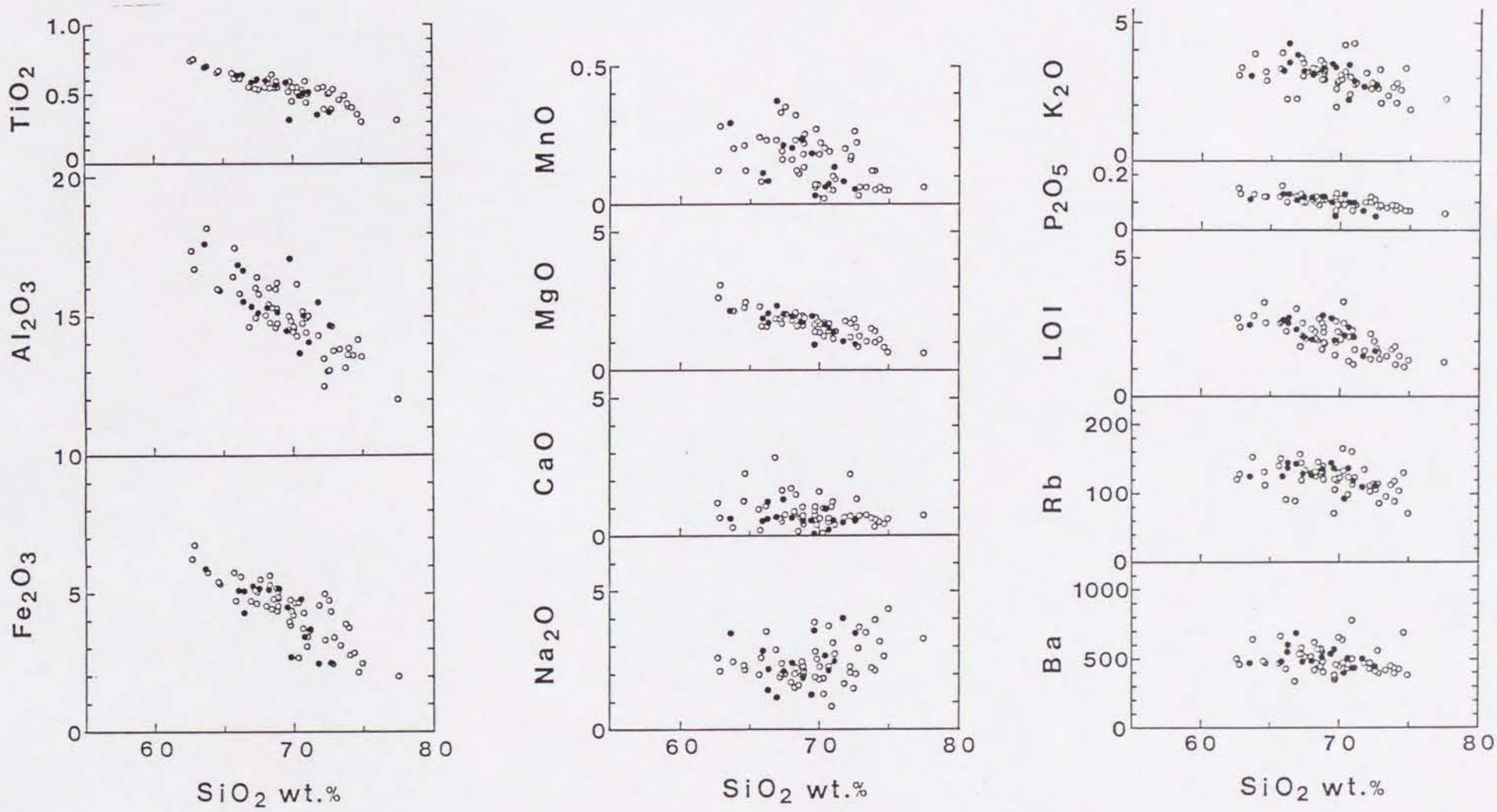

Figure 4. (continued)

B; Garnet zone (continued)

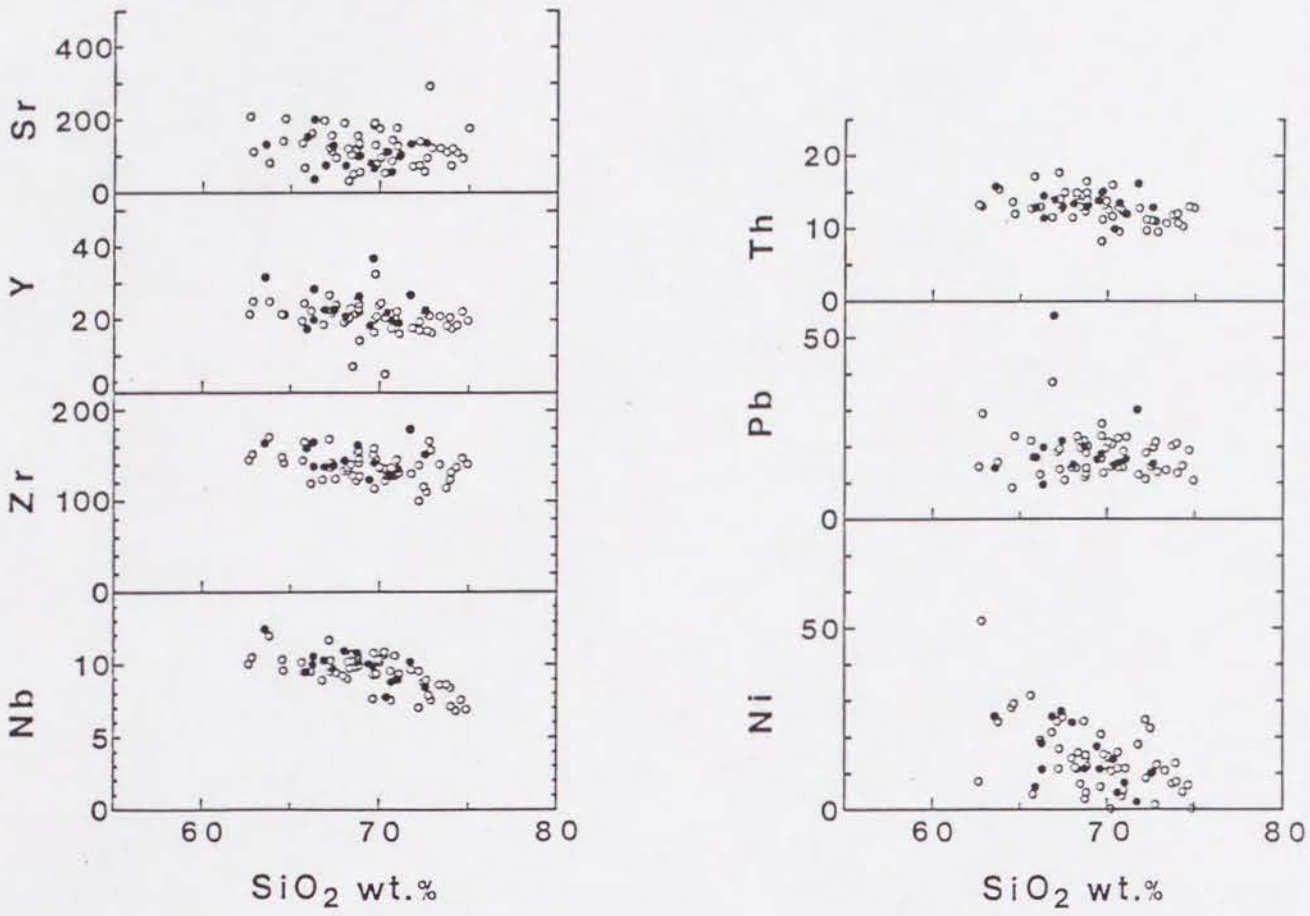

Figure 4. (continued)

C; Albite-biotite zone

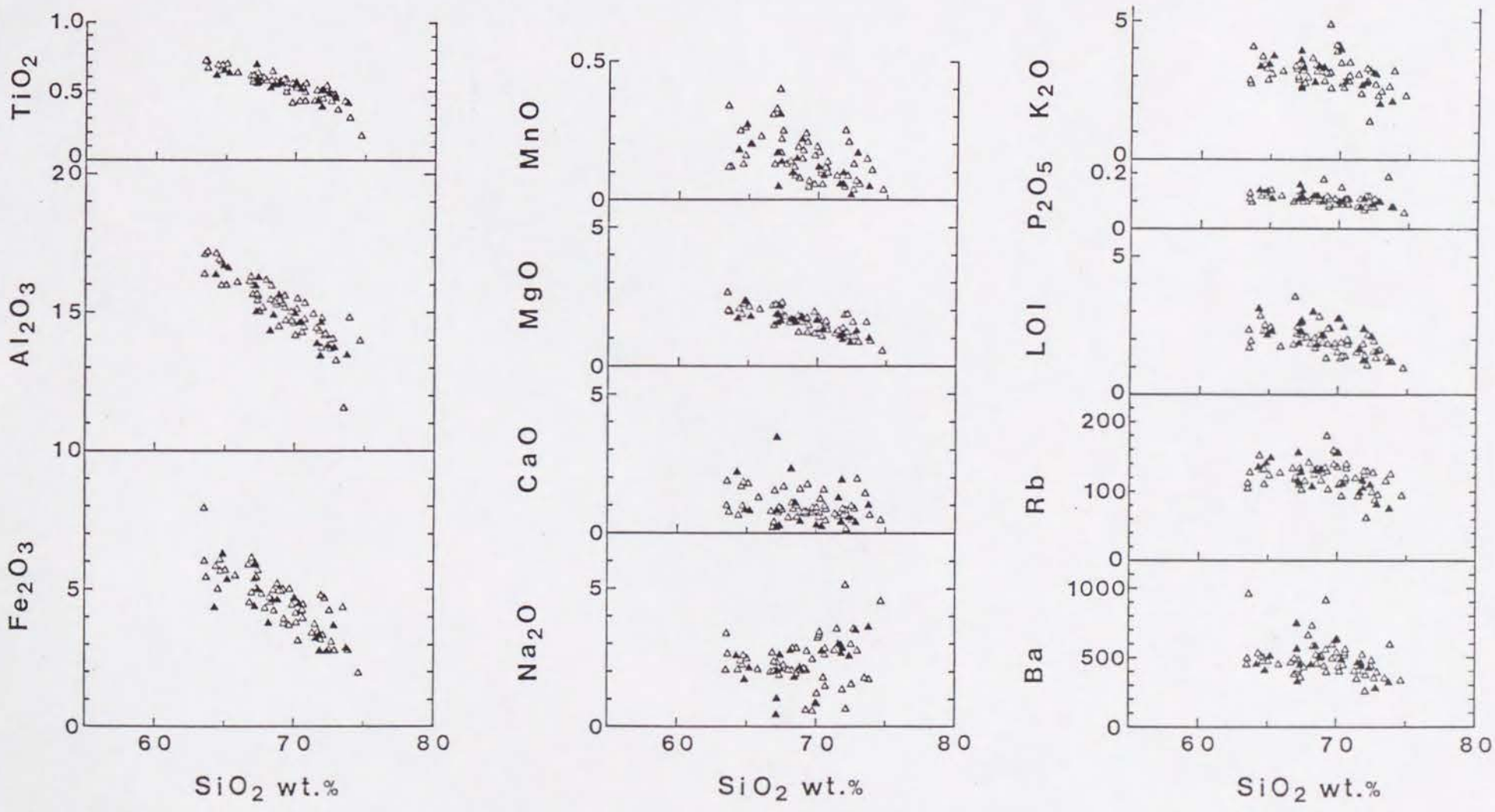

Figure 4. (continued)

C; Albite-biotite zone (continued)

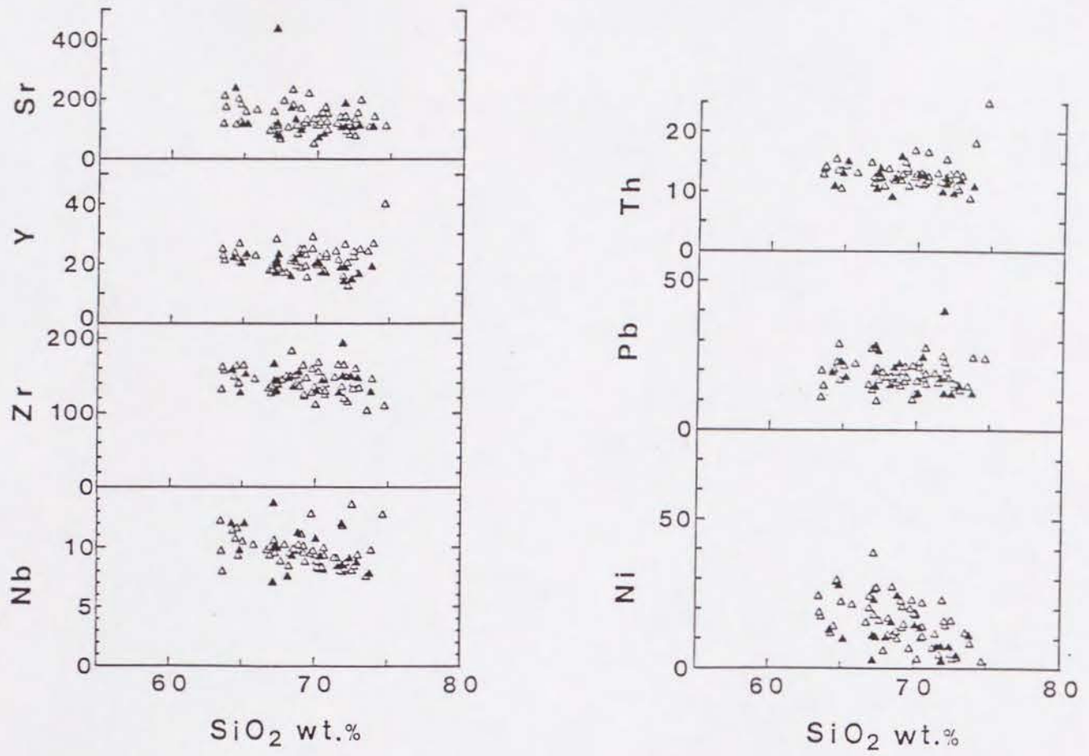

Figure 4. (continued)

D; Oligoclase-biotite zone & schist clasts

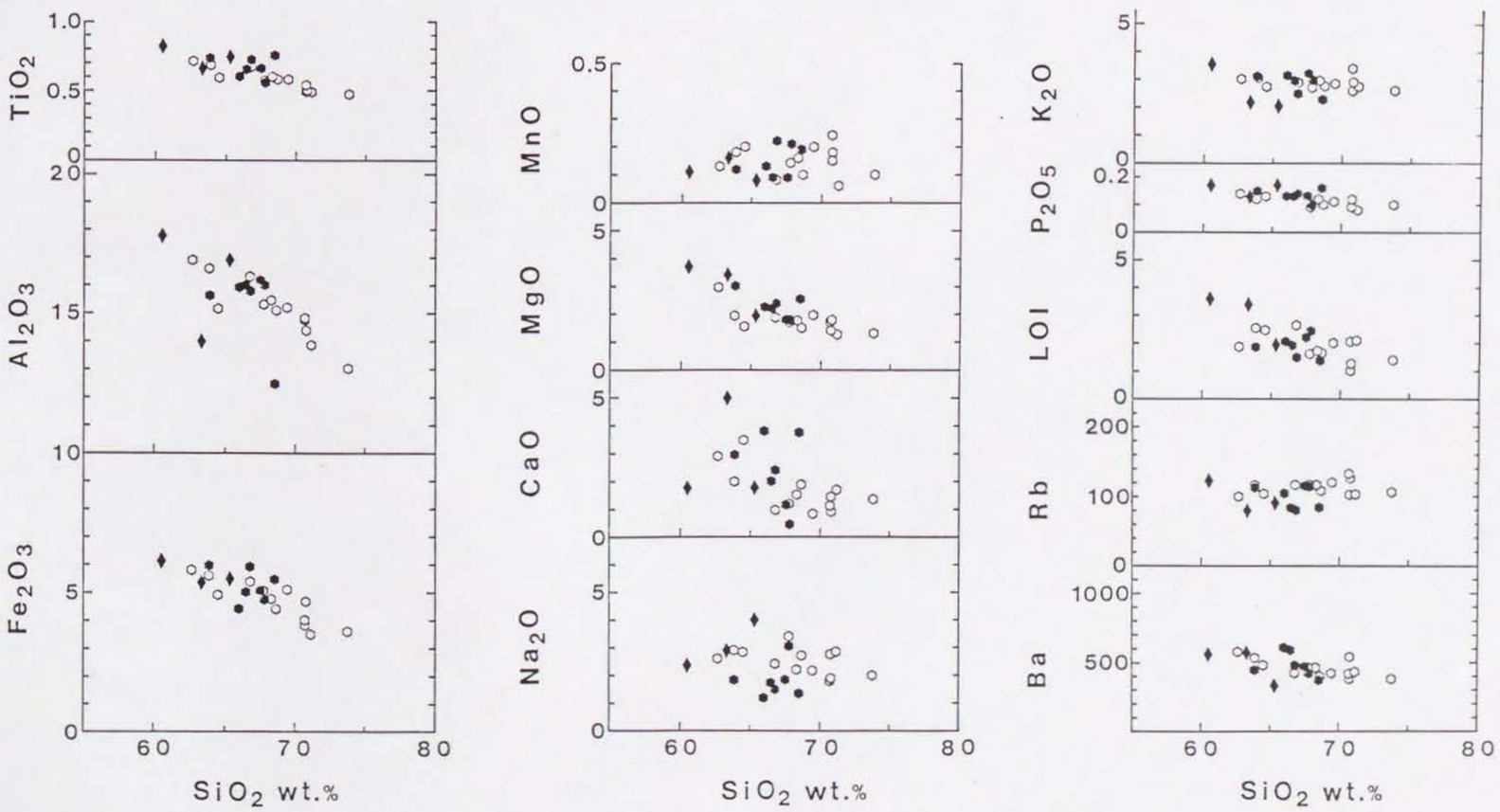

Figure 4. (continued)

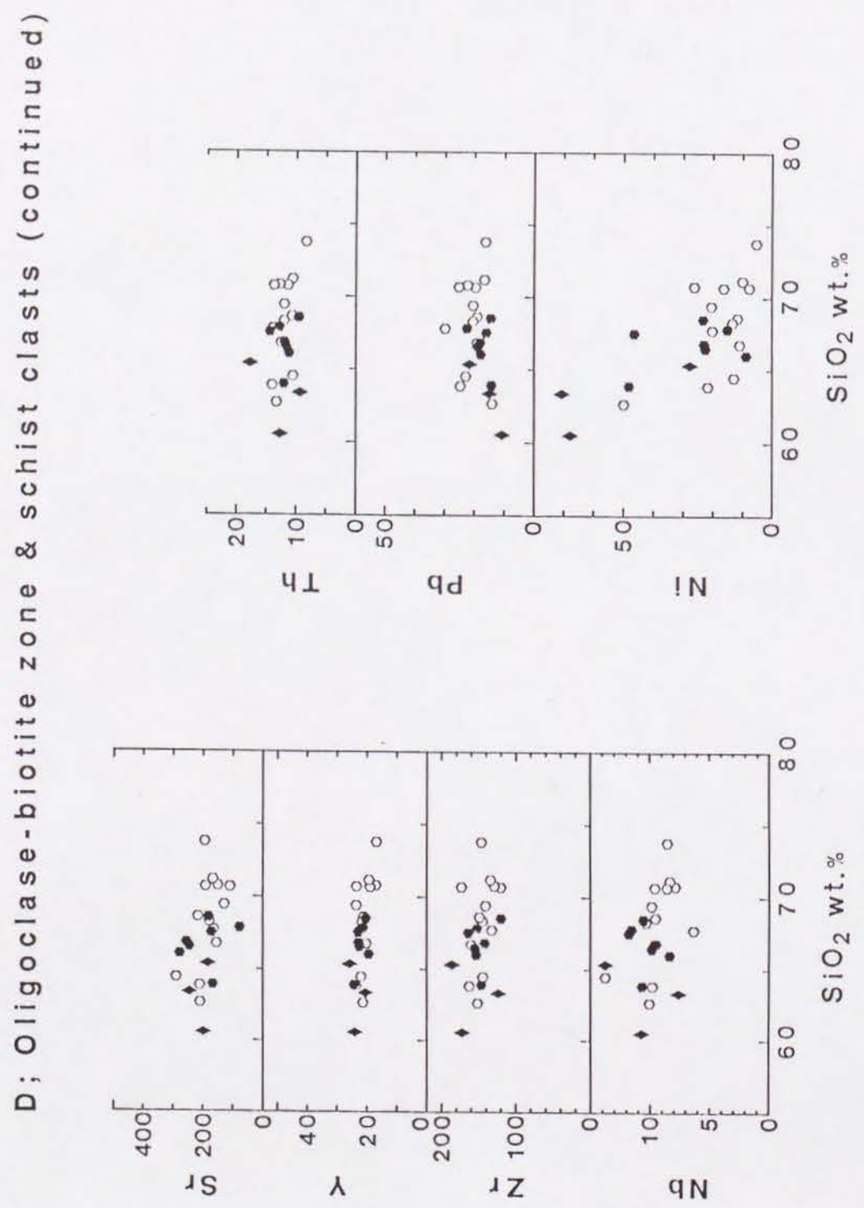

Figure 4. (continued)

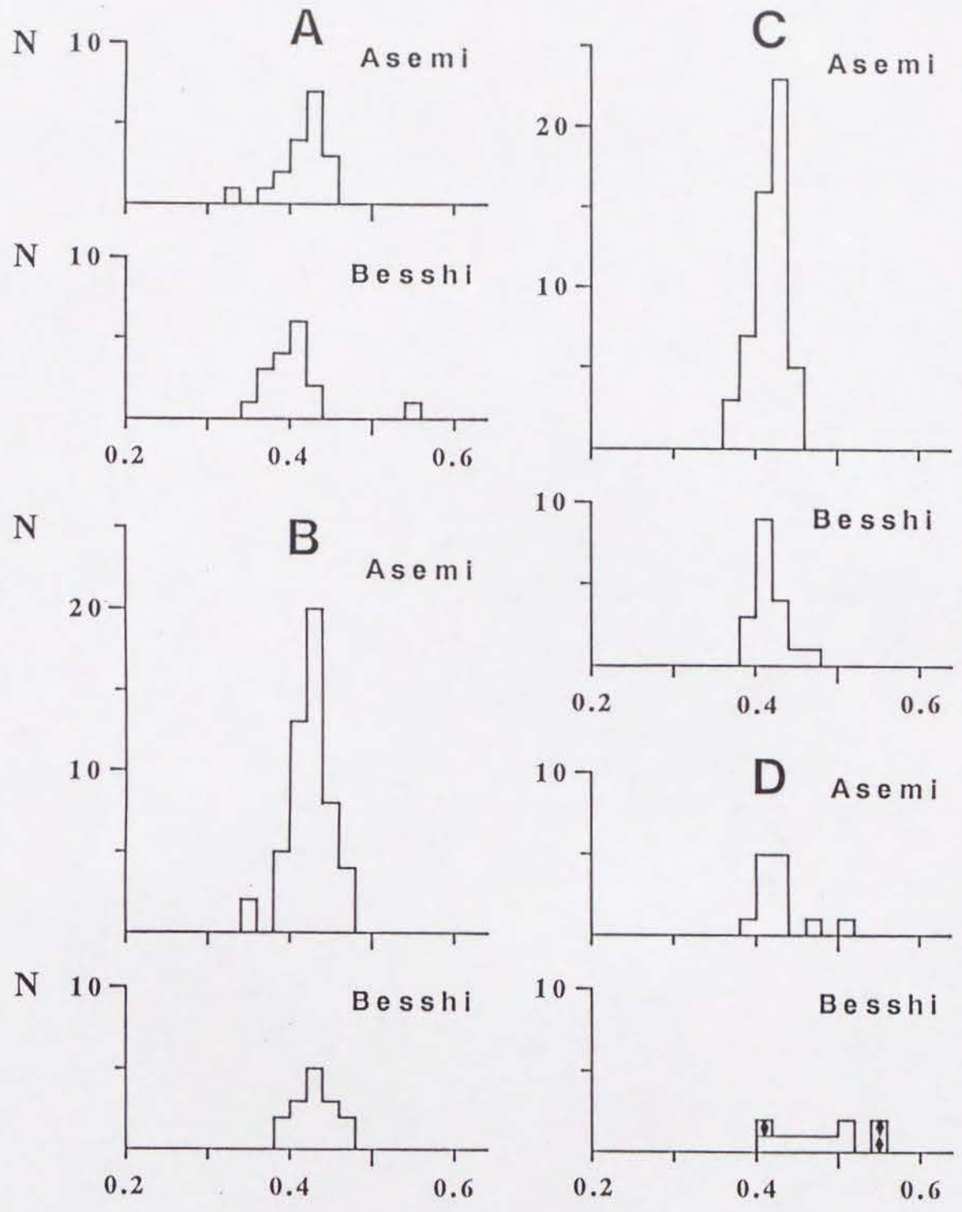

Figure 5. Frequency distribution diagrams of the mg-value, molar MgO/(MgO + FeO), of pelitic schists from the Asemi-traverse (upper) and the Besshi-traverse (lower). A: Chlorite zone samples, B: Garnet zone samples, C: Albite-biotite zone samples, D: Oligoclase-biotite zone samples and pelitic schist clasts (box with filled diamond).

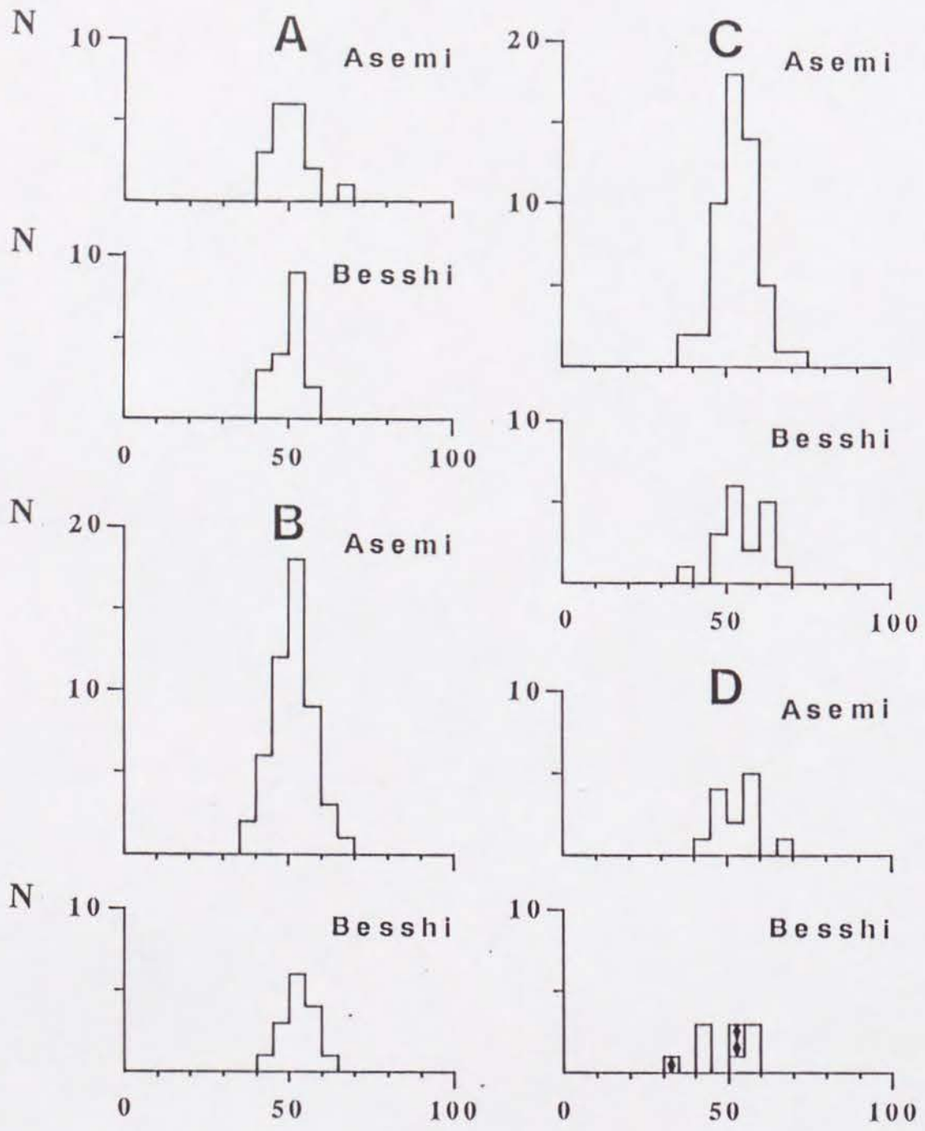

Figure 6. Frequency distribution diagrams of the K/Ba weight ratio of pelitic schists from the Asemi-traverse (upper) and the Besshi-traverse (lower). A: Chlorite zone samples, B: Garnet zone samples, C: Albite-biotite zone samples, D: Oligoclase-biotite zone samples and pelitic schist clasts (box with filled diamond).

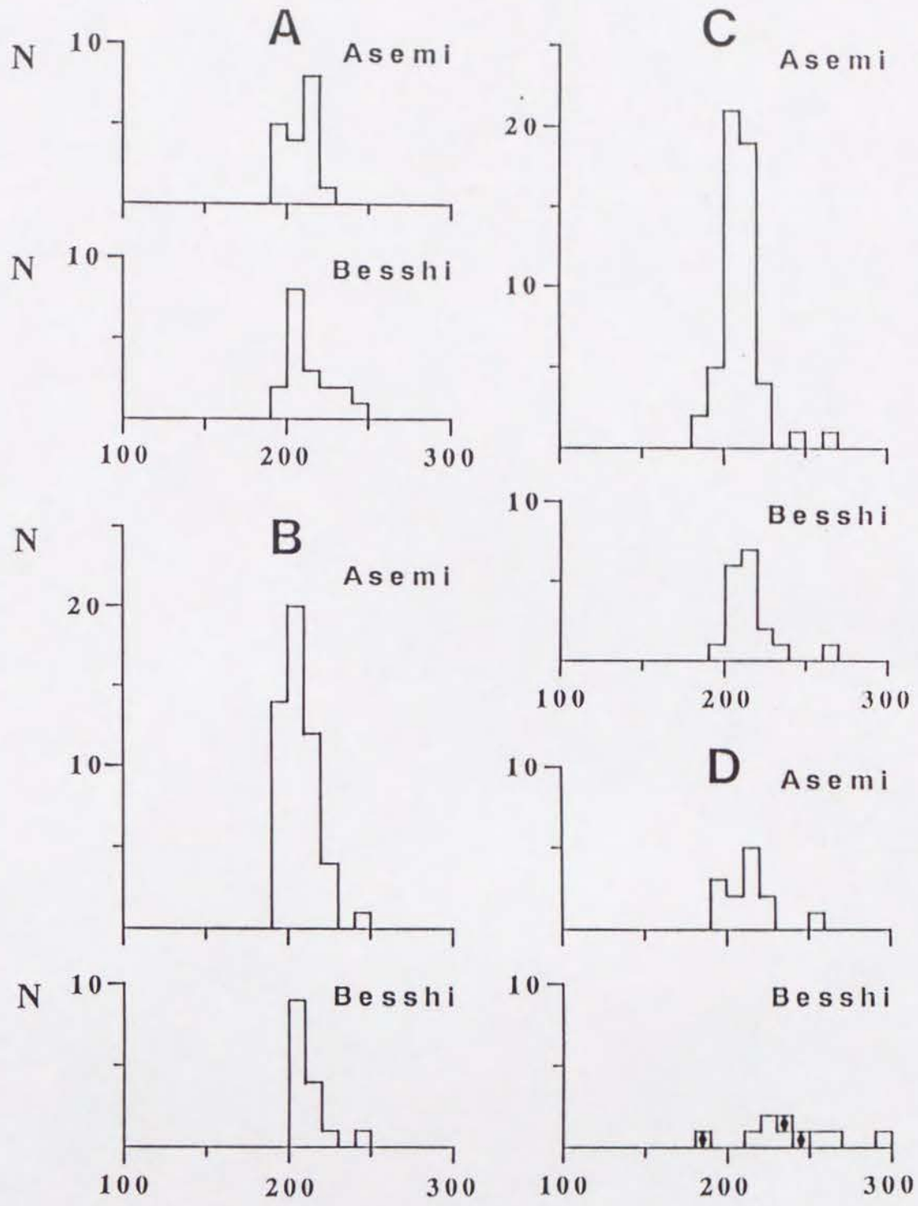

Figure 7. Frequency distribution diagrams of the K/Rb weight ratio of pelitic schists from the Aseim-traverse (upper) and the Besshi-traverse (lower). A: Chlorite zone samples, B: Garnet zone samples, C: Albite-biotite zone samples, D: Oligoclase-biotite zone samples and pelitic schist clasts (box with filled diamond).

zone schists in the Besshi-traverse (66.68 wt. % in the average SiO_2) and the pelitic schist clasts from the Kuma Group (63.03 wt. %).

- All the mineral zones except the oligoclase-biotite zone of the Besshi-traverse and the pelitic schist clasts from the Kuma Group show distinct maxima of the mg-value at 0.4-0.44 (Fig. 5). The mg-values of the latter samples are high and scattered. In addition, the averages of Fe_2O_3 and MgO of both sets of samples are higher than those of the others (Table 4).
- The averages of CaO and Sr tend to be high toward the higher grade zone (Table 4). High CaO and Sr are characteristic of the oligoclase-biotite schists in the Besshi-traverse and of the pelitic schist clasts (Fig. 4A-D).
- Although the K/Ba ratio is constant at 45-60 (Fig. 6), the K/Rb ratio of the oligoclase-biotite schists in the Besshi-traverse is considerably higher and its range is wider than those of the others (Fig. 7).

The bulk compositions of pelitic schists in the oligoclase-biotite zone of the Besshi-traverse and pelitic schist clasts from the Kuma Group differ from that of the others. The Sanbagawa pelitic schists are therefore heterochemical about CaO, Sr, the mg-value and K/Rb ratio.

2. Major elements of pelitic schists from selected metamorphic belts

The comparative study for major elements of pelitic schists from some selected metamorphic belts is required to understand the geochemistry of pelitic schists in the Sanbagawa metamorphic belt.

Table 5. Average chemical composition of pelitic schists from selected metamorphic belts.

Sanbagawa metamorphic belt (This study)

Asemi-traverse

Mineral zone	Chl-Z		Grt-Z		Abt-Z		Obt-Z	
N	18		52		54		13	
	Av.	1sigma	Av.	1sigma	Av.	1sigma	Av.	1sigma
SiO2	67.42	3.72	69.68	3.24	69.04	2.85	68.38	3.24
TiO2	0.57	0.10	0.54	0.10	0.55	0.10	0.57	0.08
Al2O3	15.70	1.37	14.92	1.26	15.17	1.06	15.14	1.07
Fe2O3	4.92	1.28	4.36	1.07	4.58	1.08	4.66	0.76
MnO	0.13	0.07	0.16	0.09	0.15	0.08	0.15	0.05
MgO	1.77	0.48	1.64	0.47	1.66	0.42	1.75	0.43
CaO	0.67	0.56	0.87	0.54	0.97	0.44	1.66	0.84
Na2O	2.92	1.03	2.42	0.73	2.38	0.86	2.50	0.47
K2O	2.82	0.71	2.99	0.54	3.11	0.54	2.87	0.22
P2O5	0.11	0.02	0.10	0.02	0.11	0.02	0.11	0.02
LOI	2.63	0.50	2.10	0.59	1.95	0.50	1.86	0.49
K2O/Na2O	0.97		1.24		1.31		1.15	
Fe2O3/MgO	2.78		2.66		2.76		2.66	

Besshi-traverse

Mineral zone	Chl-Z		Grt-Z		Abt-Z		Obt-Z	
N	18		15		18		7	
	Av.	1sigma	Av.	1sigma	Av.	1sigma	Av.	1sigma
SiO2	70.44	2.86	68.57	2.51	69.06	2.90	66.68	1.52
TiO2	0.48	0.08	0.54	0.12	0.54	0.08	0.67	0.07
Al2O3	14.47	1.31	15.46	1.13	15.04	1.11	15.42	1.32
Fe2O3	3.84	0.80	4.34	1.12	4.33	1.06	5.21	0.58
MnO	0.09	0.05	0.14	0.10	0.14	0.08	0.15	0.06
MgO	1.36	0.53	1.66	0.44	1.56	0.41	2.27	0.43
CaO	0.64	0.56	0.62	0.32	1.06	0.89	2.36	1.27
Na2O	2.82	0.75	2.44	0.88	2.31	0.86	1.78	0.62
K2O	3.03	0.63	3.24	0.50	3.11	0.56	2.88	0.35
P2O5	0.09	0.01	0.10	0.03	0.11	0.02	0.13	0.02
LOI	2.24	0.97	2.34	0.43	2.19	0.55	1.90	0.38
K2O/Na2O	1.07		1.33		1.35		1.62	
Fe2O3/MgO	2.82		2.61		2.78		2.30	

Pelitic schist clasts

N	3	
	Av.	1sigma
SiO2	63.03	2.43

TiO2	0.74	0.08
Al203	16.20	1.99
Fe203	5.65	0.40
MnO	0.12	0.04
MgO	3.01	0.94
CaO	2.82	1.86
Na20	3.07	0.85
K20	2.60	0.83
P205	0.16	0.02
LOI	2.96	0.89
K20/Na20	0.85	
Fe203/MgO	1.88	

Darladian (Yardley, 1977)

Grade	Staurolite in area A		Sillimanite in area C		Sillimanite in area D		Sillimanite in area C+D	
N	14		8		7		15	
	Av.	1sigma	Av.	1sigma	Av.	1sigma	Av.	1sigma
SiO2	57.23	3.78	53.54	2.62	50.82	2.62	52.09	3.24
TiO2	1.38	0.17	1.20	0.13	1.10	0.22	1.14	0.19
Al203	20.01	2.00	21.29	1.38	24.46	2.50	22.98	2.58
Fe203	9.80	1.21	10.34	1.19	10.59	1.27	10.47	1.20
MnO	0.13	0.02	0.18	0.03	0.19	0.05	0.19	0.05
MgO	2.51	0.34	2.67	0.37	2.75	0.25	2.71	0.30
CaO	1.21	0.77	1.72	0.78	1.69	1.89	1.70	1.43
Na20	1.76	0.59	2.42	0.99	1.59	0.68	1.98	0.92
K20	3.24	0.71	3.25	0.83	3.75	1.17	3.52	1.03
P205	0.25	0.07	0.35	0.17	0.23	0.10	0.28	0.14
H20+	3.15	0.46	3.51	0.58	3.26	0.98	3.38	0.80
K20/Na20	1.84		1.34		2.36		1.78	
Fe203/MgO	3.90		3.87		3.85		3.86	

Dalradian (Ferguson and Al-Ameen, 1986)

	St-bt		Ky-bg. st-bt		Lake marble Formation	
N	12		8		11	
	Av.	1sigma	Av.	1sigma	Av.	1sigma
SiO2	55.86	2.37	54.47	4.61	56.24	5.77
TiO2	1.28	0.11	0.80	0.22	0.81	0.33
Al203	20.12	1.83	23.04	4.35	20.77	2.60
Fe203	9.92	1.03	7.76	2.32	7.04	2.13
MnO	0.18	0.07	0.31	0.33	0.18	0.04
MgO	2.74	0.20	2.25	0.54	2.52	0.29
CaO	1.65	0.46	1.86	0.73	3.38	1.20
Na20	2.38	0.66	2.83	1.29	2.56	0.42
K20	3.19	0.58	3.36	1.37	3.73	0.71
P205	0.25	0.06	0.18	0.14	0.12	0.07
H20+	2.30	0.38	2.85	0.64	2.58	0.73
K20/Na20	1.34		1.19		1.46	

Table 5. (continued)

Fe203/MgO	3.62	3.45	2.79

Dalradian (Senior and Leake, 1978)

	Northern pelites Grt-bg.		Northern pelites Grt-free		Southern pelites		Siliceous granoblastites	
N	48		37		35		27	
	Av.	1sigma	Av.	1sigma	Av.	1sigma	Av.	1sigma
SiO2	55.34	5.75	55.46	5.30	54.32	5.95	73.52	3.46
TiO2	1.15	0.33	1.21	0.32	1.31	0.39	0.74	0.22
Al203	20.69	3.54	20.83	4.14	19.85	3.44	11.49	2.31
Fe203	1.98	0.87	3.61	2.16	2.55	1.31	1.19	0.62
FeO	7.33	2.20	5.49	1.95	6.79	3.01	3.17	1.61
MnO	0.18	0.10	0.12	0.06	0.24	0.17	0.11	0.14
MgO	2.83	0.94	3.00	1.46	3.52	1.07	1.99	1.57
CaO	1.63	1.02	1.02	0.85	1.93	1.15	1.26	0.92
Na20	1.90	0.69	1.71	0.62	2.01	0.76	2.19	1.08
K20	3.42	1.03	3.92	1.05	3.92	1.19	2.33	0.94
P205	0.25	0.20	0.24	0.12	0.21	0.11	0.13	0.11
H20	2.99	0.84	3.27	0.90	3.12	0.94	1.67	0.63
Total Fe as Fe203	10.12		9.71		10.09		4.71	
K20/Na20	1.80		2.29		1.95		1.06	
Fe203/MgO	3.58		3.24		2.87		2.37	

Appalachian The Littleton Formation (Shaw, 1956)

Grade	Low		Midium		High		Medium + High	
N	7		5		6		11	
	Av.	1sigma	Av.	1sigma	Av.	1sigma	Av.	1sigma
SiO2	62.58	3.29	61.22	2.20	58.86	5.56	60.26	4.03
TiO2	0.87	0.18	1.04	0.04	1.05	0.20	1.05	0.14
Al203	18.09	1.67	19.95	1.98	21.21	3.04	20.64	2.57
Fe203	7.24	0.91	6.80	1.83	8.11	1.45	7.51	1.69
MnO	0.04	0.02	0.07	0.02	0.11	0.04	0.09	0.04
MgO	2.18	0.97	1.90	0.42	1.96	0.30	1.93	0.34
CaO	0.16	0.11	0.52	0.32	0.52	0.29	0.52	0.29
Na20	0.81	0.45	1.72	0.68	1.10	0.31	1.38	0.58
K20	3.68	0.55	3.58	0.53	3.84	0.50	3.72	0.51
P205	0.10	0.06	0.15	0.02	0.18	0.10	0.17	0.08
H20+	3.99	0.29	2.81	0.54	2.56	0.91	2.67	0.74
K20/Na20	4.54		2.08		3.49		2.70	
Fe203/MgO	3.32		3.58		4.14		3.89	

Table 5. (continued)
Adirondack Mountains (Engel and Engel, 1958)

	Gneiss		Granitized gneiss	
N	10		13	
	Av.	1sigma	Av.	1sigma
SiO2	67.18	2.84	67.40	2.91
TiO2	0.71	0.15	0.68	0.13
Al2O3	15.84	1.52	15.50	1.41
Fe2O3	5.24	1.68	4.70	1.07
MnO	0.06	0.02*1	0.06	0.02*2
MgO	2.09	0.47	1.93	0.46
CaO	2.91	0.75	2.19	0.64
Na2O	3.53	0.27	3.32	0.51
K2O	1.96	0.60	3.75	0.68
P2O5	0.09	0.01*3	0.07	0.01*4
H2O+	0.62	0.18	0.70	0.12
K2O/Na2O	0.55		1.13	
Fe2O3/MgO	2.51		2.44	

*1, N=9: *2, N=10: *3, N=5: *4, N=8:

Abukuma (Miyashiro, 1958)

N	8		7*5	
	Av.	1sigma	Av.	1sigma
SiO2	69.86	9.51	66.99	5.37
TiO2	0.60	0.31	0.67	0.26
Al2O3	12.86	4.21	14.13	2.61
Fe2O3	6.24	2.96	6.88	2.54
MnO	0.16	0.12	0.18	0.12
MgO	2.14	1.04	2.38	0.87
CaO	2.02	1.10	2.25	0.95
Na2O	2.13	0.99	2.38	0.76
K2O	2.62	0.92	2.71	0.95
P2O5	0.21	0.16	0.22	0.17
H2O+	1.31	0.74	1.43	0.70
K2O/Na2O	1.23		1.14	
Fe2O3/MgO	2.92		2.89	

*5, excluding the sample with SiO2 = 89.33.

Table 5. (continued)
Franciscan The Pacheco Pass (Ernst et al., 1970)

N	20		16*6	
	Av.	1sigma	Av.	1sigma
SiO2	61.82	6.42	64.00	5.02
TiO2	0.95	0.42	0.81	0.20
Al2O3	14.11	2.67	13.91	2.79
Fe2O3	6.62	2.10	5.87	1.34
MnO	0.12	0.08	0.11	0.08
MgO	2.97	1.39	2.43	0.70
CaO	3.95	1.94	3.46	1.79
Na2O	3.64	1.30	3.47	1.15
K2O	1.16	0.76	1.39	0.67
P2O5	0.16	0.14	0.16	0.15
H2O+	4.03	1.15	3.92	1.23
K2O/Na2O	0.32		0.40	
Fe2O3/MgO	2.23		2.42	

*6, excluding four tuffaceous samples.

The Lachlan geosyncline

	Joplin (1942, 1946, 1947)		Vallance (1953, 1960)	
N	26		14	
	Av.	1sigma	Av.	1sigma
SiO2	59.14	5.22	66.08	11.81
TiO2	0.76	0.24*7	0.64	0.25
Al2O3	22.15	3.12	17.60	6.07
Fe2O3	6.16	1.16*8	5.91	2.43
MnO	0.05	0.04*9	0.05	0.01*10
MgO	2.25	0.68	1.87	0.98
CaO	0.43	0.28	0.37	0.31
Na2O	1.01	0.74	1.05	0.70
K2O	5.28	1.18	4.44	1.89
P2O5	0.13	0.07*11	0.15	0.07*12
H2O+	2.16	1.05*13	2.06	1.08
K2O/Na2O	5.23		4.23	
Fe2O3/MgO	2.74		3.16	

*7, N=21; *8, N=24; *9, N=19; *10, N=13; *11, N=22; *12, N=8;
*13, N=24

Table 5 lists the averages and standard deviations of the major elements of pelitic schists from the Sanbagawa belt, Connemara in the Dalradian (Yardley, 1977; Senior and Leake, 1978; Ferguson and Al-Ameen, 1986), the Littleton Formation in the Appalachian (Shaw, 1956), the Adirondack Mountains (Engel and Engel, 1958), central Abukuma plateau (Miyashiro, 1958), the Pacheco Pass in the Franciscan (Ernst et al., 1970), and the Cooma and the adjacent areas in the Lachlan geosyncline in Australia (Joplin, 1942, 1946, 1947, Vallance, 1953, 1960). Some data are divided into the metamorphic grades or into rock types, but others are undivided.

The following geochemistry for each metamorphic belt may be delineated:

- The highest SiO_2 is characteristic of the Sanbagawa pelitic schists. I also noticed the low CaO and K_2O/Na_2O ratio and the high Fe_2O_3/MgO ratio.
- The lowest SiO_2 and highest Al_2O_3 and Fe_2O_3/MgO ratio are characteristic of the Dalradian and Appalachian pelitic schists, except the siliceous granoblastites in the former (Senior and Leake, 1978). I also noticed the high Fe_2O_3 and high K_2O/Na_2O ratio. Although the bulk compositions of the two metamorphic belts have a resemblance, CaO in the Appalachian pelitic schists is clearly lower than that in the Dalradian ones.
- The gneiss and granitized gneiss in the Adirondack Mountains are high in SiO_2 and CaO. K_2O and the K_2O/Na_2O ratio of the former are systematically lower than those of the latter.
- The pelitic schists in the central Abukuma plateau are high in SiO_2 and CaO.

- The lowest K_2O/Na_2O ratio and low SiO_2 and high CaO are characteristic of the Franciscan metasedimentary rocks, called metagreywacke. Besides, Al_2O_3 is somewhat low in comparison with SiO_2.
- The Lachlan geosyncline pelitic schists are systematically different between the data of Joplin (1942, 1946, 1947) and those of Vallance (1953, 1960). Still, there shares common features in the lowest CaO and the highest K_2O/Na_2O ratio.

Discussion

1. Behavior of different groups of elements during prograde metamorphism

The division of components into volatile, excess, indifferent and independent ones is convenient in discussing chemical effects on the parageneses of the Sanbagawa pelitic schist. Devolatilization equilibria buffer the chemical compositions of metamorphic fluids (Greenwood, 1975). The excess and indifferent components influence only modal variations of metamorphic rocks. The amounts of the independent components control both the paragenesis and the mode.

Volatile components; Loss on ignition: The loss on ignition of samples includes the weight losses of volatile components and the weight gain of oxygen accompanying the change of FeO into Fe_2O_3. Still, there is no distinct change in the loss on ignition from the lower to higher grade pelitic schists (Fig. 4 and Table 4). This contradicts the tacit expectation that the volatiles fixed in metamorphic rocks must decrease with increasing metamorphic grade.

Higashino (1975) measured the modal variations of 15 pelitic schists of the garnet and biotite grades. This shows that the total amounts of modal quartz, albite and muscovite exceed 84 % with 92.7 % as the average. Moreover, they are constant regardless the metamorphic grade. Chlorite, currying a large amount of water (ca. 12 wt. %), is the main reactant mineral of dehydration reactions. Its average mode changes from 4.1 % in the garnet zone to 3.5 % in the biotite zone. A maximum modal garnet that was formed by the chlorite decomposition is 1.9 % in the

garnet zone and is 6.5 % in the biotite zone, where the average is 3.3 %. A maximum mode of biotite reaches 3.5 % in the biotite zone. The modes of chlorite eliminated by metamorphic reactions are assumed to be equal to those of garnet and biotite. Then the amount of modal garnet + biotite multiplied by the water content of chlorite makes the total amount of water released by the chlorite decomposition during the metamorphism. In the biotite zone, the maximum of the modal garnet + biotite is 10 %, and the average is about 4 %; this is obtained by the subtraction of the average modal quartz, albite, muscovite and chlorite from 100 % because the modal biotite is often less than 1 %. The maximum amount of H_2O released during the Sanbagawa metamorphism is 1.2 wt. % and the average is about 0.5 wt. %. The maximum value is much less than the average value of H_2O (2.6 wt. %) released by the metamorphic reactions of the average pelite estimated by Walther and Orville (1982). This suggests that the amount of the fluid released during the Sanbagawa metamorphism is too small to transport heat and matters effectively.

If exotic fluids infiltrate rocks, the fluid/rock volume ratios of 1:1 to 4:1 are common (Ferry, 1984). The presence of the exotic fluid reservoir around the Sanbagawa metamorphic belt leads to the high fluid/rock ratio. Still, there is no plausible external fluid reservoir around it. Thus the total amount of fluid during the Sanbagawa metamorphism is small, whereby making it hard to transport significant amount of fluid and its solutes.

Excess and indifferent components: Quartz, albite and muscovite are always present in the Sanbagawa pelitic schist. SiO_2, $NaAlO_2$ and $KAl_3O_4(OH)_2$ are thus regarded as excess components. Their

concentrations control the corresponding modal variations but do not affect the metamorphic paragenesis.

Na_2O-K_2O relations. There is a negative correlation between Na_2O and K_2O (Fig. 8). Since oligoclase and biotite are minor constituents even in the oligoclase-biotite schists, the bulk compositions of the Sanbagawa pelitic schist are projected from SiO_2 and H_2O onto the Als(Al_2SiO_5)-Ab($NaAlSi_3O_8$)-Kfs($KAlSi_3O_8$) plane (Fig. 9). They are plotted near muscovite and albite tie line. This corresponds to the petrographical evidence that the main Na- and K-bearing minerals are albite and muscovite, respectively. It also shows that paragonite and K-feldspar are rare minerals in the Sanbagawa pelitic schist (Enami, 1983). Further, I noticed that some oligoclase-biotite schists in the Besshi-traverse and pelitic schist clasts are plotted near muscovite and paragonite tie line. Layering of quartzofeldspathic and micaceous layers is common in the Sanbagawa pelitic schist. The negative correlation between Na_2O and K_2O has resulted from the difference in the proportion of quartzofeldspathic layer to micaceous layer of the analyzed samples.

The layering was formed either by the sedimentation or by the segregation of minerals during deformation and metamorphism, or both. Kawachi (1968) and Yoshida (1981) reported sedimentary structures such as the graded bedding and bedding plane in the Sanbagawa pelitic schists. The layering structure commonly found in the pelitic schists was the bedding plane particularly at the lower metamorphic grade zone, which underwent the ductile deformation in the sense of Toriumi (1990). Under his plastic deformation regime, the layering formed by the deformation had to

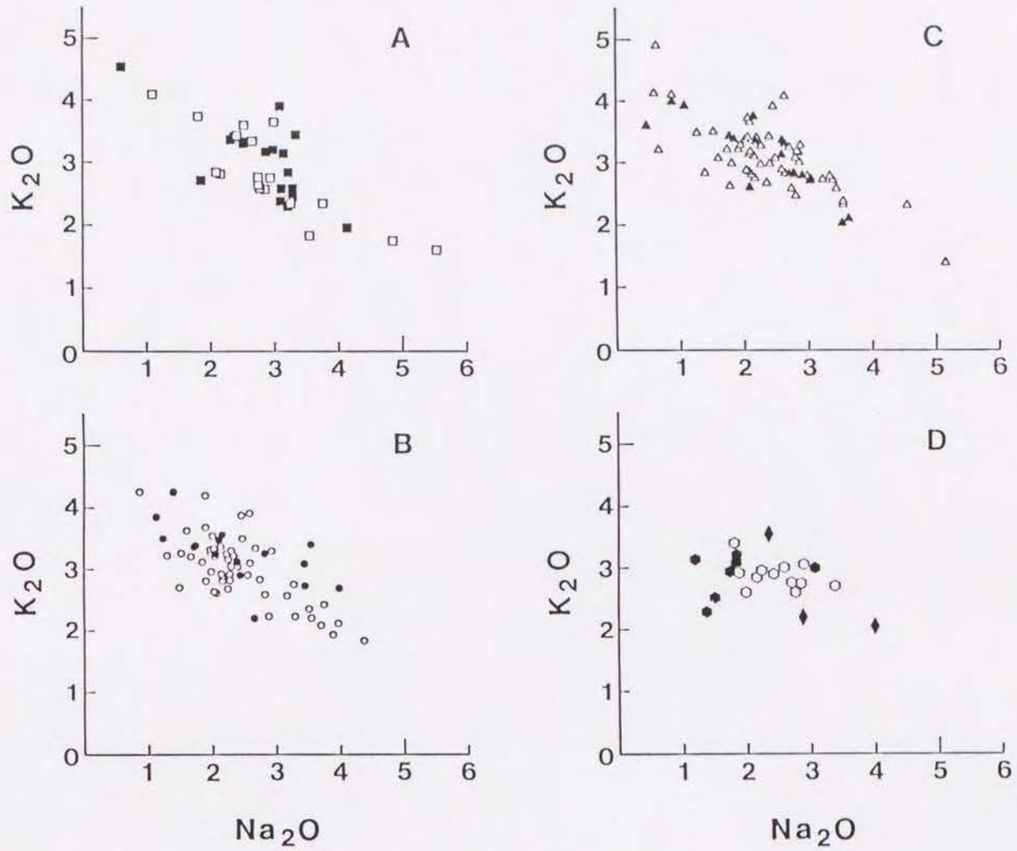

Figure 8. Na_2O-K_2O correlation diagrams. A: Chlorite zone samples, B: Garnet zone samples, C: Albite-biotite zone samples, D: Oligoclase-biotite zone samples (hexigon) and pelitic schist clasts (filled diamond). Open symbols (□,○,△,○), the Asemi-traverse; closed symbols (■,●,▲,●), the Besshi-traverse.

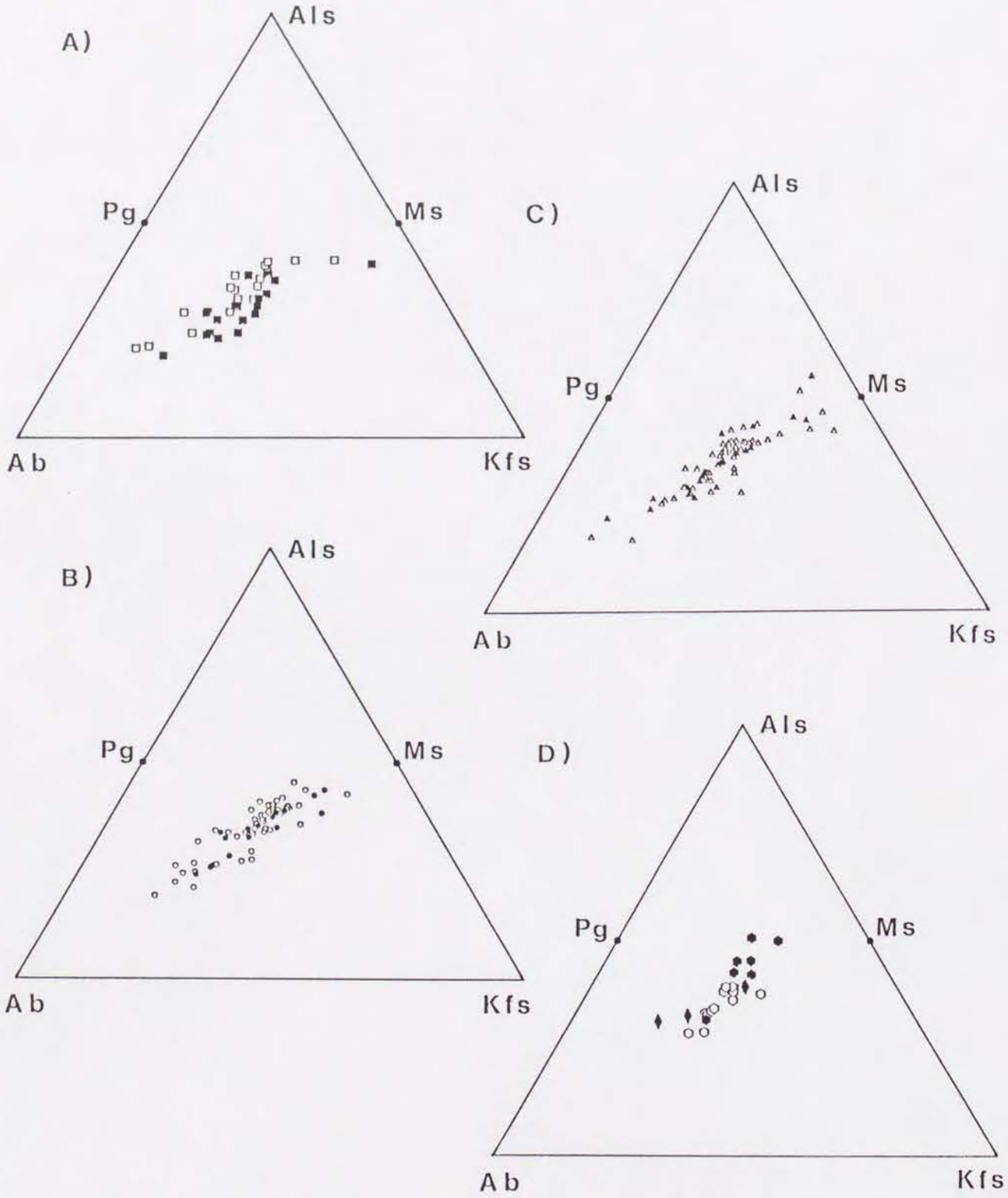

Figure 9. Projections of data onto the Als(Al_2SiO_5)-Ab($NaAlSi_3O_8$)-Kfs($KAlSi_3O_8$) plane from quartz and H_2O. A: Chlorite zone samples, B: Garnet zone samples, C: Albite-biotite zone samples, D: Oligoclase-biotite zone samples (hexagon) and pelitic schist clasts (filled diamond). Open symbols (□,○,△,⬡), the Asemi-traverse; Closed symbols (■,●,▲,⬢), the Besshi-traverse.

replace the sedimentary ones with various degrees. The chemistry of the Sanbagawa pelitic schists remains unchanged under the different deformation regimes. Thus the geochemistry of the Sanbagawa pelitic schists is found to be essentially original.

P_2O_5, entering mainly apatite in the Sanbagawa pelitic schist and never affecting their parageneses, is regarded as an **indifferent** component. TiO_2-bearing minerals in the Sanbagawa pelitic schist change from sphene through rutile to ilmenite with increasing metamorphic grade (Itaya and Banno, 1980). Thus TiO_2 is an independent component, but never is an indifferent one.

Independent components: This group includes TiO_2, Al_2O_3, FeO, MnO, MgO, and CaO, and most trace elements. Independent components influence the parageneses of metamorphic rocks. The conventional ACF, AKF and AFM diagrams represent the effect of some independent components on the metamorphic parageneses. Still, the diagrammatic representations of the parageneses have a common limit that some independent components are arbitrarily disregarded.

The trace elements are divided into two categories; one is the phase forming element such as Zr in the presence of zircon and the other is the non-phase forming element. Since zircon is a rare mineral in the Sanbagawa pelitic schist, Zr is a non-phase forming element. Non-phase forming elements follow the behavior of one or more major elements that stabilize particular phases and have similar ionic sizes (Matsui et al., 1977). Muscovite incorporates Rb and Ba into the site of K. Epidote, more specifically REE-epidote, incorporates Th into the Ca-site (Sakai et al., 1984). Sr and perhaps Y partition into the Ca-site. Ni

replaces Mg and Fe of the ferromagnesian minerals. Nb and perhaps Zr follow the site of Ti. Pb may enter muscovite. Non-phase forming element hardly influences the metamorphic paragenesis.

2. Effect of the bulk composition on the chemical trends of zoned garnet

Banno et al. (1986) examined the chemical trends of the zoned garnet, which is presumably free from intracrystalline diffusion. They assumed that the pelitic schists are isochemical from the chlorite zone to the oligoclase-biotite zone about FeO, MnO and MgO ratios, based on the data of Haramura (1961), Banno (1964) and Kurata and Banno (1974). This implies that the only one univariant curve can describe a garnet formation reaction for the Sanbagawa pelitic schists. They calculated the zoning pattern of garnet expected for the average Sanbagawa pelitic schists on the assumption that the garnet formation can be essentially described by the chlorite-garnet phase equilibria. They considered that the higher Mg trend of garnet zonation in higher-grade area is due to the lower pressure and higher temperature of crystallization.

Table 6 lists the mg-value and the molar MnO/(FeO + MnO + MgO) ratio of the rocks that include the zoned garnet examined by Banno et al. (1986). The data for 2 garnet, 1 albite-biotite, 3 oligoclase-biotite zone schists are from the Asemi-river, and 3 oligoclase-biotite zone schists are from the Besshi-area. Although the molar MnO/(FeO + MnO + MgO) ratio of rocks is scattered from sample to sample, it lacks systematic relation with the metamorphic zones.

Whereas, the mg-values of the rocks examined by Banno et al.

Table 5. The mg-values and MnO/(FeO+MnO+MgO) ratios of the pelitic schists examined the chemical trends of zoned garnet by Banno et al. (1986).

*1	Sample No.	Mineral zone	Locality	mg-value	MnO/(FeO+MnO+MgO)
1	TH71072714	Garnet	Asemi	0.432	0.0235
2	TH71072702	Garnet	Asemi	0.436	0.0132
5	CS83050908	Olg-Bt	Asemi	0.406	0.0099
6	TH71081311	Olg-Bt	Asemi	0.407	0.0210
7	TH71081315	Olg-Bt	Asemi	0.401	0.0184
8	TH71081408	Ab-Bt	Asemi	0.402	0.0206
11	TH80072307	Olg-Bt	Besshi	0.502	0.0163
12	TH80052712	Olg-Bt	Besshi	0.501	0.0112
13	TH80052705	Olg-Bt	Besshi	0.442	0.0228

*1 column represents the sample number of Banno et al. (1986).

(1986) have narrow ranges in each mineral zone. The oligoclase-biotite schists in the Besshi-traverse are the highest in mg-value ranging from 0.442 to 0.502. The mg-values of the garnet zone schists are 0.432 and 0.436. The higher grade zone schists in the Asemi-traverse are the lowest in it ranging from 0.401 to 0.407. The difference in mg-value is small but significant because it appears systematic. Thus I examine the effect of the mg-value on the garnet formation first.

The onset of the garnet formation can be drawn by a univariant curve of a pressure-temperature diagram at a fixed bulk composition when $P_{H_2O} = P_{total}$. I can compare the different mg-values keeping the other compositions the same. At the pressure range of the Sanbagawa metamorphism, the reaction curves have negative slopes for Mn-rich composition in the diagram (Banno et al., 1986). An increase in the mg-value of bulk compositions causes a rise either in pressure or in temperature of the onset of garnet formation. Three curves (thick line) in Fig. 10 represent the onset of the garnet formation reaction of three rocks with different mg-values schematically. On a univariant curve with a given mg-value, the X_{Mg} of garnet increases with a rise in temperature because of temperature dependence of the Fe-Mg partitioning between chlorite and garnet. Thus, I can also draw isopleths of the X_{Mg} of garnet (thin line) in Fig. 10. The positions of the reaction curves and the X_{Mg} isopleths are not accurate but relative.

In the Asemi-river, the garnet zone schists with higher mg-values crystallized MgO-poorer garnet than the schists of albite-biotite and oligoclase-biotite grades, although the zoned garnets

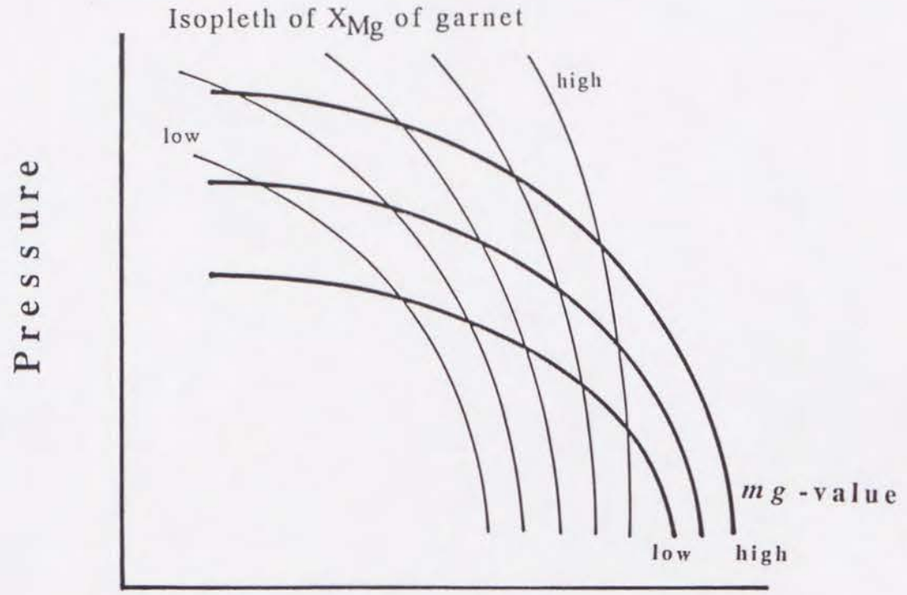

Figure 10. Schematic pressure-temperature diagram. Three curves (thick line) represent the onset of the garnet formation of three rocks with different mg-values. Thin lines show isopleths of X_{Mg} of the first crystallized garnet.

in the higher grade zones show similar chemical trend. It follows that both higher pressure and lower temperature than those proposed by Banno et al. (1986) would be required at the onset of the garnet formation in the garnet zone schists than in the higher grade zones. Thus, the difference in the pressure and temperature trajectory between the garnet zone and higher grade zones is larger than that envisaged by Banno et al. (1986). It should be concluded that the pressure and temperature conditions at the onset of the garnet formation were discontinuous at the boundary between the garnet and the albite-biotite zones in the Asemi-traverse.

The difference in the chemical trend of zoned garnet between the higher grade zone schists in the Asemi-river is primarily ascribed to the difference in the maximum conditions of the metamorphism. However the difference between the oligoclase-biotite zones in the Asemi-river and the Besshi-traverse is difficult to tell the effect of pressure and temperature from the chemical effect. The conclusion of Banno et al. (1986) that the oligoclase-biotite zone in the Besshi-traverse shows the lower pressure path is not substantiated in this study.

Next, I examine the effect of MnO on garnet formation, because garnet strongly prefers MnO. The Sanbagawa pelitic schist shows large scattering in the MnO/(FeO + MnO + MgO) ratio (Fig. 11). As other MnO-dominant mineral is absent in the Sanbagawa pelitic schists, MnO at the core of zoned garnet must increase with increasing the molar MnO/(FeO + MnO + MgO) ratio in the pelitic schists. However, the core of zoned garnet in each metamorphic grade shows similar MnO contents (Banno et al., 1986)

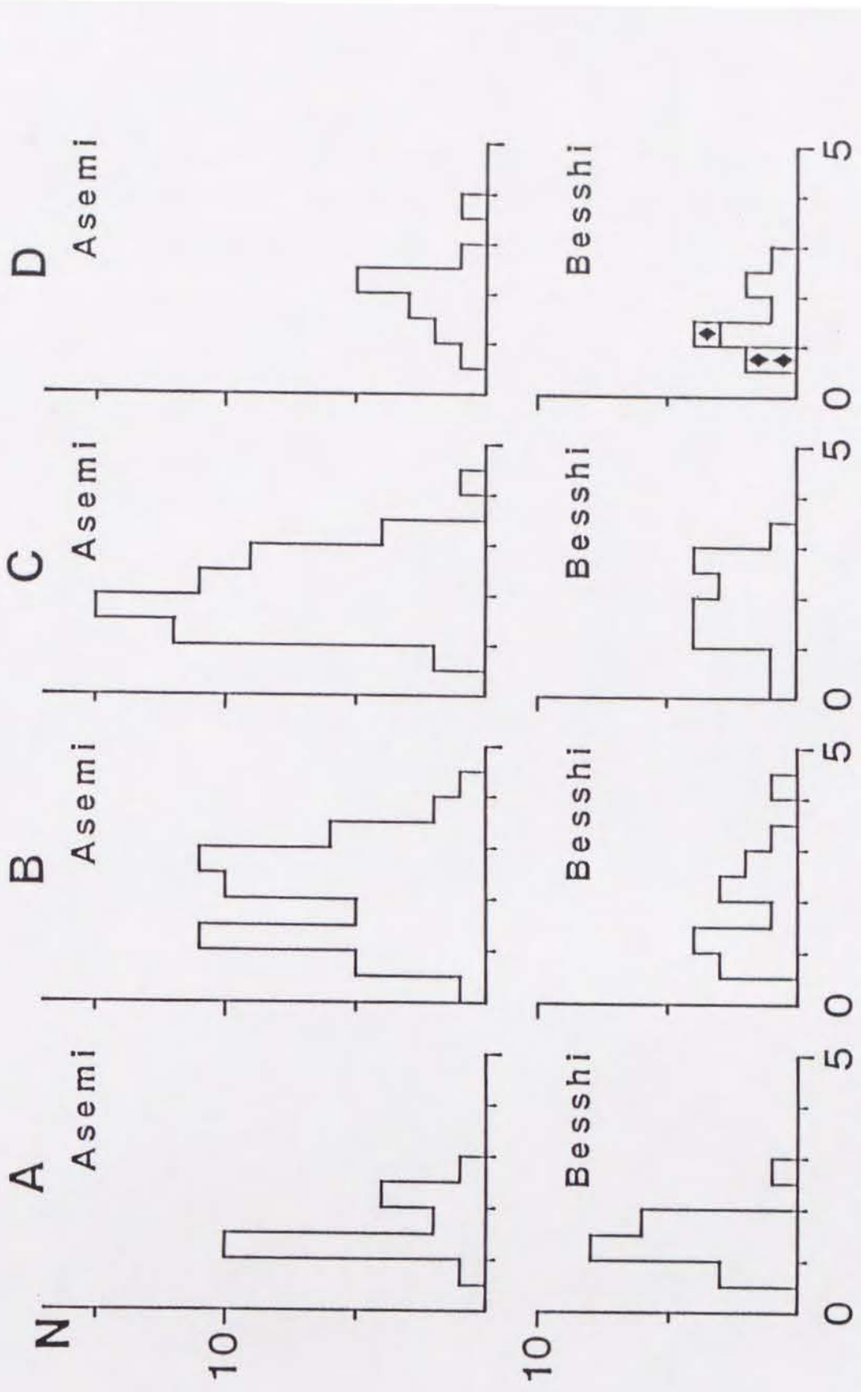

Figure 11. Frequency distribution diagrams of the Mn-ratio, percent molar MnO/(MgO + FeO + MnO), of pelitic schists from the Asemi-traverse (upper) and the Besshi-traverse (lower). A: Chlorite zone samples, B: Garnet zone samples, C: Albite-biotite zone samples, D: Oligoclase-biotite zone samples and pelitic schist clasts (box with filled diamond).

regardless the molar MnO/(FeO + MnO + MgO) ratio. This implies that the chemical compositions of chlorite is heterogeneous about the molar MnO/(FeO + MnO + MgO) ratio even in a hand specimen scale at the onset of the garnet formation, and the maximum MnO/(FeO + MnO + MgO) ratio of chlorite is roughly constant in each mineral zone. As a result, the position of the garnet formation could be that of the MnO richer chlorite.

The effect of the grossular component of garnet on its stability has been ignored and a metamorphic fluid is assumed to be pure water. In spite of the wide ranges in CaO of the pelitic schists, the Ca-(Fe + Mg)-Mn triangle (fig. 8 of Banno et al., 1986) shows similar trend in the grossular content of the zoned garnet over the whole range of metamorphic grade. To buffer the grossular content of zoned garnet, one or more CaO-dominant minerals are required and one of them may be clinozoisitic epidote. The addition of CO_2 to a metamorphic fluid phase shifts the garnet formation curves to the lower temperature side. If the X_{CO2} of the Sanbagawa metamorphism increased with increasing metamorphic grade (Itaya and Banno, 1980), the difference in pressure and temperature trajectory between garnet and higher grade zone rocks extends.

3. Material transports during the Sanbagawa metamorphism

A metamorphic fluid is supposed to be present at least during prograde metamorphism so that devolatilization of minerals should accompany a rise in metamorphic temperature. It plays important roles in transporting heat and matter, and influences the chemical and physical properties of minerals and rocks. I examine the chemical transport of material by fluids during

metamorphism using the K/Rb and K/Ba ratios of the pelitic schists.

K/Rb and K/Ba ratios: Taylor and McLennan (1985) emphasized that the K/Rb ratio of the continental upper crust is well established at 250. There are strong positive correlations between K and Rb of pelitic schists (Senior and Leake, 1978; Haack et al., 1984), of granulite facies rocks (Stähle et al., 1987), and of "Japanese Paleozoic" slates (Banno and Chappell, 1969). Stähle et al. (1987) have also reported a K-Ba positive correlation. The K/Rb and K/Ba ratios are constant even if the K-bearing mineral changes from muscovite through biotite to K-feldspar with increasing metamorphic grade (Haack et al., 1984). Thus they concluded that Rb and Ba closely follow K.

Let us consider the exchange reaction of K and Rb between muscovite and a metamorphic fluid phase:

$$2K^+ + Rb_2Al_4Al_2Si_6O_{20}(OH)_4 = K_2Al_4Al_2Si_6O_{20}(OH)_4 + 2Rb^+ \quad (1)$$

fluid muscovite$_{ss}$ muscovite$_{ss}$ fluid

where ss denotes solid solution. The K-Ba exchange reaction can be written as

$$2(K^+ + Si^{4+}) + Ba_2Al_4Al_4Si_4O_{20}(OH)_4 =$$

fluid muscovite$_{ss}$

$$K_2Al_4Al_2Si_6O_{20}(OH)_4 + 2(Ba^{2+} + Al^{3+}) \quad (2)$$

muscovite$_{ss}$ fluid.

The Ba-bearing molecule of muscovite is assumed by analogy with margarite. Although we cannot easily measure the chemical potentials of components in a metamorphic fluid phase, the apparent distribution coefficients for reactions (1) and (2) are,

$$Kd_1 = (X_K/X_{Rb})_{Ms}/(X_K/X_{Rb})_{fluid} \quad (3)$$

$Kd_2 = (X_K/X_{Ba})_{Ms}/(X_K/X_{Ba})_{fluid}$ (4)

where Xi is the concentration of component i in muscovite (Ms) and fluid phase, respectively. The apparent distribution coefficient for reaction (2), Kd_2, is more complex than Kd_1 because Kd_2 essentially contains a composition-dependent term, the activity of aluminum species in a metamorphic fluid.

In the Sanbagawa pelitic schists, the K/Rb and K/Ba ratios are those of muscovite, the main K-bearing mineral, which preferentially incorporates Rb and Ba over K. Thus, the $(X_K/X_{Rb})_{Ms}$ and $(X_K/X_{Ba})_{Ms}$ stand for the K/Rb_{rock} and K/Ba_{rock}, respectively. So we have,

$Kd_1 = (K/Rb)_{rock}/(X_K/X_{Rb})_{fluid}$ (5)

$Kd_2 = (K/Ba)_{rock}/(X_K/X_{Ba})_{fluid}$ (6).

The K/Rb and K/Ba ratios of the Sanbagawa pelitic schists are constant at 210 and 50-55, respectively, except the K/Rb ratios of some oligoclase-biotite zone schists in the Besshi-traverse (Figs. 6 and 7). To keep the K/Rb and K/Ba ratios of pelitic schists constant over a wide range of metamorphic grade, the following factors are probably envisaged:

- First, the constant K/Rb and K/Ba ratios of the pelitic schists are essentially original.
- Second, the total amount of metamorphic fluids is small, which was stated above.
- Third, the apparent distribution coefficients are independent of or insensitive to temperature and pressure.
- Finally, the concentrations of K, Rb and Ba in a metamorphic fluid are negligibly small.

When the molar Rb/(K + Rb) ratio of muscovite is lower than

0.1, Kd_2 is 2.1 at 400-600°C and 1 kbar (Iiyama, 1979). This is applicable to the compositional ranges in the Sanbagawa pelitic schists, if the pressure difference between the experiment and the Sanbagawa metamorphism is ignored. This satisfies the third factor. As the average K/Rb weight ratio of the pelitic schists is 210, I obtain 100 as the average K/Rb weight ratio of fluid at $Kd_2 = 2.1$.

Iiyama (1964) experimentally determined the ion exchange of Na and K between minerals and chloride solutions in the system Al_2O_3-$KAlSi_3O_8$-$NaAlSi_3O_8$-NaCl-KCl-H_2O at 1 kbar. The molar Na/(Na + K) ratio of fluids in the presence of albite and muscovite exceeds 0.79 at 550-600°C. Woodland and Walther (1987) experimentally determined the concentrations of Na, Al and Si in aqueous solutions in equilibrium with natural albite, paragonite and quartz between 350-500°C and 1-2.5 kbar. The log molarity of Na is lower than -2.344, i.e., Na in aqueous solution is less than 104 ppm. When the molar Na/(Na + K) ratio and Na are 0.79 and 104 ppm, respectively, K in the metamorphic fluid is 47 ppm. Thus Rb in it is 0.47 ppm. This is semi-quantitative, but clearly shows that the last factor, low concentrations of K and Rb in fluid, is valid. The chemical transport of material by the advection is, therefore, negligible during the Sanbagawa metamorphism, and the K/Rb and K/Ba ratios are essentially original.

4. Cause of an increase in X_{CO2} during the Sanbagawa metamorphism

The origin of peculiarity in bulk rock composition of some oligoclase-biotite zone schists in the Besshi-traverse and also pelitic schist clasts in the Kuma Formation will be discussed in

the phase petrological point of view.

Sphene is stable at low pressure, high temperature and low X_{CO_2}, while dolomite in quartz-bearing rocks at high pressure, low temperature and high X_{CO_2} (Fig. 12). Goto et al. (1990) stated that sphene can scarcely coexist with dolomite in quartz-bearing rocks although there lacks any direct reaction between them. Sphene occurs even in the chlorite zone (Ernst, 1972; Itaya and Banno, 1980), and it requires the low X_{CO_2} of the Sanbagawa metamorphism. Recently, Enami and Higashino (1988) reported that dolomite occurs as a matrix mineral in pelitic schists only in the oligoclase-biotite zone and it postdates sphene occurring as an inclusion of the albite porphyroblast. Yokoyama and Itaya (1990) also reported that dolomite occurs in a pelitic schist clast, showing the oligoclase-biotite grade, in the Kuma Formation. Calcite-dolomite thermometer yields the Sanbagawa peak metamorphic temperature, 600°C (Enami and Higashino, 1988). Thus, they concluded that the main reason caused the change in stability from sphene to dolomite is not a rise in pressure or a fall in temperature or both but an increase in the X_{CO_2} at the Sanbagawa peak metamorphism.

Graphite occurs commonly as inclusions in garnet, albite and micas, but rarely in the matrix of the dolomite-bearing pelitic schists (Enami, personal communication). It requires a graphite decomposition. The graphite decomposition can be written by the following reactions,

$$2C + 2H_2O = CO_2 + CH_4 \quad (7)$$

graphite water carbon-dioxide methane

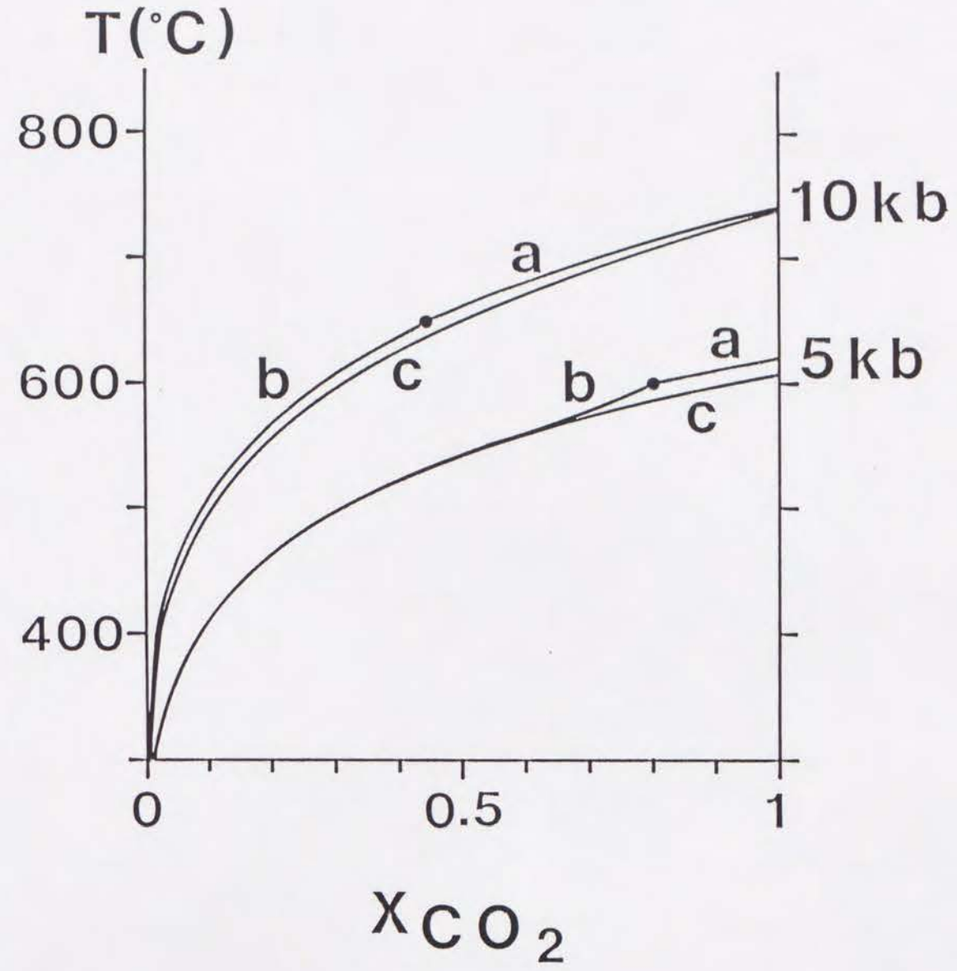

Figure 12. Temperature and X_{CO_2} ($CO_2/(H_2O + CO_2)$ molar ratio) diagram at 5 kbar and 10 kbar (after Goto et al., 1990). The reaction curves are as follows.
a: Dolomite + 2Quartz = Diopside + $2CO_2$
b: 5Dolomite + 8Quartz + H_2O = Tremolite + 3Calcite + $7CO_2$
c: Rutile + Calcite + Quartz = Sphene + CO_2

$$C + O_2 = CO_2 \quad (8).$$

graphite oxygen carbon-dioxide

Since reaction (7) buffers the maximum value of X_{H_2O} (e.g., Ohmoto and Kerrick, 1977) and increases both X_{CO_2} and X_{CH_4}, which is not the case. Thus, an increase in X_{CO_2} during the Sanbagawa metamorphism accompanies graphite oxidation as expressed by reaction (8).

As reaction (8) shows, graphite reacts with 2.67 times weight of oxygen to produce CO_2. Evidently, this amount of oxygen is too large to be introduced by a fluid with high f_{O_2}. Next, I will present an alternative idea for the source of oxygen. Fe_2O_3 is 90 wt. % FeO and 10 wt. % oxygen. The amount of oxygen is sufficient to decompose graphite. Thus, the probable reservoir of oxygen is high f_{O_2} assemblages containing Fe^{3+}-bearing minerals such as hematite, magnetite and ferric-rich epidote, which are common constituents of some Sanbagawa basic schists. Some pelitic schists of the oligoclase-biotite zone in the Besshi-traverse are exceptionally high in CaO (e.g., Table 4) amongst the samples. Thus, ferric-rich epidote is a possible oxygen reservoir to increase the X_{CO_2} of fluid in equilibrium with dolomite-bearing pelitic schists. Rocks with high f_{O_2} assemblage were mixed with graphite-bearing pelitic schists during the Sanbagawa metamorphism, and it triggered the graphite oxidation. Fe_2O_3-bearing minerals and graphite as well as hydrous and carbonate minerals are important fluid reservoirs during the metamorphism.

For basic schists in the albite-biotite and oligoclase-biotite zones of the Besshi-traverse, the low X_{CO_2} mineral, sphene, occurs in the albite porphyroblast and the higher X_{CO_2}

assemblage, dolomite-quartz, does in the matrix (Enami and Higashino, 1988). This also requires an increase in X_{CO_2} during the metamorphism. However the basic schists have no plausible CO_2 reservoir and are free from graphite. This can be explained if the dolomite-quartz assemblage is formed by the reaction of high f_{O_2} minerals in basic schists and graphite in pelitic schists, as realized by the mixing of basic and pelitic schists. The mixing of pelitic and basic schists can bring about the change in stability from sphene to dolomite. Thus, the dolomite-bearing schists are possible hybrids from pelitic and basic schists. It should be emphasized that bulk compositions of dolomite-bearing rocks in the Sanbagawa metamorphic belt are not original but secondary. The hybridization took place at the Sanbagawa peak metamorphic temperature that is obtained by dolomite-calcite thermometer. Further, it may be related to the formation of tectonic melange zones in the sense of Takasu (1984) and Kunugiza et al. (1986).

Conclusions

- The mg-value, CaO and Sr of the oligoclase-biotite schists in the Besshi-traverse and the pelitic schist clasts differ from those of the other mineral zones. The K/Rb ratio of the Besshi oligoclase-biotite schists is also different.
- Bulk compositions of the Sanbagawa pelitic schists are considered to be essentially original. However the bulk compositions of the pelitic and basic schists that recorded the change in stability from sphene to dolomite are not original. Because the stability change requires the mixing of pelitic and basic schists at the Sanbagawa peak metamorphic temperature.
- The amount of water released during the Sanbagawa metamorphism is too small to transport heat and matters effectively.
- In the Asemi-traverse, the garnet zone schists experienced much higher pressure and lower temperature than the higher grade zone schists as was envisaged previously. The difference in pressure and temperature trajectory from the oligoclase-biotite zone schists between the Asemi-traverse and the Besshi-traverse is not substantiated.
- Before garnet crystallized, chlorite heterogeneous in MnO is present in pelitic schists, and the maximum MnO is roughly constant. The crystallization of garnet was governed not by the molar MnO/(MgO + FeO + MnO) ratio of rocks but by chlorite with maximum MnO.
- When garnet commenced to crystallize, CaO dominant minerals such as clinozoisitic epidote buffers the grossular content.
- The material migration by the advective flow during the Sanbagawa high pressure metamorphism is negligibly small.

References

Banno, S., 1961. On the so-called "Soda-metasomatism" of the Sanbagawa schists in the Bessi district. J. Geol. Soc. Jpn., 67, 515-525. (In Japanese with English abstract)

Banno, S., 1964. Petrologic studies on Sanbagawa crystalline schists in the Bessi-Ino district, central Sikoku, Japan. J. Fac. Sci. Univ. Tokyo, Sec. II, 15, 203-319.

Banno, S. and Chappell, B. W., 1969. X-ray fluorescent analysis of Rb, Sr, Y, Pb and Th in Japanese Paleozoic slates. Geochem. J., 3, 127-134.

Banno, S. and Sakai, C., 1989. Geology and metamorphic evolution of the Sanbagawa metamorphic belt, Japan. In Daly, J.S., Cliff, R.A. and Yardley, B.W.D. (eds) Evolution of Metamorphic Belts. Geological Society Special Publication, 43, 519-532.

Banno, S., Sakai, C. and Higashino, T., 1986. Pressure-temperature trajectory of the Sanbagawa metamorphism deduced from garnet zoning. Lithos, 19, 51-63.

Enami, M., 1983. Petrology of pelitic schists in the oligoclase-biotite zone of the Sanbagawa metamorphic terrain, Japan: phase equilibria in the highest grade zone of a high-pressure intermediate type of metamorphic belt. J. metam. Geol., 1, 141-161.

Enami, M. and Higashino, T., 1988. Dolomite in Sanbagawa metamorphic rocks of the Bessi area, central Shikoku. J. Japan. Assoc. Mineral. Petrol. Econ. Geol., 83, 338-349. (In Japanese with English abstract)

Engel, A. E. J. and Engel, C. G., 1958. Progressive metamorphism and granitization of the major paragneiss, northwest

Adirondack Mountains, New York. Bull. Geol. Soc. Am., 69, 1369-1414.

Ernst, W. G., 1972. CO_2-poor composition of the fluid attending Franciscan and Sanbagawa low-grade metamorphism. Geochim. Cosmochim. Acta, 36, 497-504.

Ernst, W. G., Seki, Y., Onuki, H. and Gilbert, M. C., 1970. Comparative study of low-grade metamorphism in the California Coast Ranges and the outer metamorphic belt of Japan. Geol. Soc. Am. Mem., 124, 276 pp.

Ferguson, C. C. and Al-Ameen, S. I., 1986. Geochemistry of Dalradian pelites from Connemara, Ireland: new constraints on kyanite genesis and conditions of metamorphism. J. Geol. Soc. London, 143, 237-252.

Ferry, J., 1984. A biotite isograd in south-central Maine, U.S.A.: Mineral reactions, fluid transfer, and heat transfer. J. Petrol., 25, 871-893.

Goto, A., Banno, S. and Okamoto, K., 1990. Combustion of graphite and the consequential change of CO_2 pressure during the Sanbagawa metamorphism. Annual Meeting of Geol. Soc. Jpn., 97, 469. (in Japanese)

Goto, A. and Tatsumi, Y., 1991. The chemical analysis of rock sampels by XRF (I). Rigaku-Denki J., 22, 28-44. (in Japanese)

Goto, A. and Tatsumi, Y., 1992. The chemical analysis of rock samples by XRF (II). Rigaku-Denki J., (in Japanese)

Greenwood, H. J., 1975. Buffering of pore fluids by metamorphic reactions. Am. J. Sci., 275, 573-593.

Haack, U., Heinrichs, H., Boneβ, M. and Schneider, A., 1984.

Loss of metals from pelites during regional metamorphism. Contrib. Mineral. Petrol., 85, 116-132.

Haramura, H., 1961. Chemical compositions of Paleozoic slates, I. Paleozoic terrains on the Pacific side of the Sanbagawa metamorphic belt. J. Geol. Soc. Jpn., 67, 618-622.

Hide, K., Yoshino, G. and Kojima, G., 1956. Preliminary report on the geologic structure of the Besshi spotted schist zone. J. Geol. Soc. Jpn., 62, 574-584. (In Japanese with English abstract)

Higashino, T., 1975. Biotite zone of Sanbagawa metamorphic terrain in the Siragayama area, central Sikoku, Japan. J. Geol. Soc. Jpn., 81, 653-670. (In Japanese with English abstract)

Higashino, T., 1990a. The higher grade metamorphic zonation of the Sambagawa metamorphic belt in central Shikoku, Japan. J. metam. Geol., 8, 413-423.

Higashino, T., 1990b. Metamorphic zones of the Sambagawa metamorphic belt in central Shikoku, Japan. J. Geol. Soc. Jpn., 96, 703-718. (In Japanese with English abstract)

Iiyama, J. T., 1964. Etude des reactions d'echange d'ions Na-K dans la serie muscovite-paragonite. Bull. Soc. fr. Miner. Crist., 87, 532-541.

Iiyama, J. T., 1979. Trace element distribution in rock-forming silicates. The alkali and alkaline earths. In Ahrens, L. H. (ed) Origin and distribution of the elements. Pergamon Press, 161-174.

Itaya, T. and Banno, S., 1980. Paragenesis of titanium-bearing accessories in pelitic schists of the Sanbagawa metamorphic

belt, central Shikoku, Japan. Contrib. Mineral. Petrol., 73, 267-276.

Joplin, G. A., 1942. Petrological studies in the Ordovician of New South Wales. I. The Cooma complex. Proc. Linnean Soc. New South Wales, 67, 156-196.

Joplin, G. A., 1946. Petrological studies in the Ordovician of New South Wales. III. The composition and origin of the Upper Ordovician graptolite-bearing slates. Proc. Linnean Soc. New South Wales, 70, 158-172.

Joplin, G. A., 1947. Petrological studies in the Ordovician of New South Wales. IV. The northern extinction of the north-east Victorian metamorphic complex. Proc. Linnean Soc. New South Wales, 72, 87-124.

Kawachi, Y., 1968. Large-scale overturned structure in the Sanbagawa metamorphic zone in central Shikoku, Japan. J. Geol. Soc. Jpn., 74, 607-616.

Kenzan Research Group, 1984. Stratigraphy and geologic structure of the Sambagawa metamorphic belt in the Oboke area, central Shikoku, Japan. Earth Sci., 38, 53-63. (In Japanese with English abstract)

Kojima G., Hide, K. and Yoshino, G., 1956. The stratigraphical position of Kieslager in the Sambagawa crystalline schist in Shikoku. J. Geol. Soc. Jpn., 62, 30-45. (In Japanese with English abstract)

Kretz, R., 1983. Symbols for rock-forming minerals. Am. Mineral., 68, 277-279.

Kunugiza, K., Takasu, A. and Banno, S., 1986. The origin and

metamorphic history of the ultramafic and metagabbro bodies in the Sanbagawa metamorphic belt. Geol. Soc. Am. Mem., 164, 375-385.

Kurata, H. and Banno, S., 1974. Low-grade progressive metamorphism of pelitic schists of the Sazare area, Sanbagawa metamorphic terrain in central Sikoku, Japan. J. Petrol., 15, 361-382.

Matsui, Y., Onuma, N., Nagasawa, H., Higuchi, H. and Banno, S., 1977. Crystal structure control in trace element partition between crystal and magma. Bull. Soc. fr. Miner. Crist., 100, 315-324.

Miyashiro, A., 1958. Regional metamorphism of the Gosaisyo-Takanuki district in the central Abukuma Plateau. J. Fac. Sci. Univ. Tokyo, Sec. II, 11, 219-272.

Miyashiro, A., 1961. Evolution of metamorphic belts. J. Petrol., 2, 277-311.

Ohmoto, H. and Kerrick, D., 1977. Devolatilization equilibria in graphitic systems. Am. J. Sci., 277, 1013-1044.

Otsuki, M. and Banno, S., 1990. Prograde and retrograde metamorphism of hematite-bearing basic schists in the Sanbagawa belt in central Shikoku. J. metam. Geol., 8, 425-439.

Sakai, C., Higashino, T. and Enami, M., 1984. REE-bearing epidote from Sanbagawa pelitic schists, central Shikoku, Japan. Geochem. J., 18, 45-53.

Senior, A. and Leake, B. E., 1978. Regional metamorphism and the Geochemistry of the Dalradian metasediments of Connemara, western Ireland. J. Petrol., 19, 585-625.

Shaw, D. M., 1956. Geochemistry of pelitic rocks. Part III: Major elements and general geochemistry. Bull. Geol. Soc. Am., 67, 919-934.

Spear, F. S., 1988. Metamorphic fractional crystallization and internal metasomatism by diffusional homogenization of zoned garnets. Contrib. Mineral. Petrol., 99, 507-517.

Stähle, H. J., Raith, M., Hoernes, S. and Delfs, A., 1987. Element mobility during incipient granulite formation at Kabbaldurga, southern India. J. Petrol., 28, 803-834.

Takasu, A., 1984. Prograde and retrograde eclogites in the Sambagawa metamorphic belt, Besshi district, Japan. J. Petrol., 25, 619-643.

Taylor, S. R. and McLennan, S. M., 1985. The continental crust: its composition and evolution. Blackwell Scientific Publications Inc. 312 pp.

Toriumi, M., 1990. The transition from brittle to ductile deformation in the Sambagawa metamorphic belt, Japan. J. metam. Geol., 8, 457-466.

Vallance, T. G., 1953. Studies in the metamorphic and plutonic geology of the Wantabadgery-Adelong-Tumbarumba district, N.S.W. Part I. Introduction and metamorphism of the sedimentary rocks. Proc. Linnean Soc. New South Wales, 78, 90-121.

Vallance, T. G., 1960. Notes on metamorphic and plutonic rocks and their biotites from the Wantabadgery-Adelong-Tumbarumba district, N.S.W. Proc. Linnean Soc. New South Wales, 85, 94-104.

Walther, J. W. and Orville, P. M., 1982. Volatile production and transport in regional metamorphism. Contrib. Mineral. Petrol., 79, 252-257.

Woodland, A. B. and Walther, J. V., 1987. Experimental determination of the solubility of the assemblage paragonite, albite, and quartz in supercritical H_2O. Geochim. Cosmochim. Acta, 51, 365-372.

Yardley, B. W. D., 1977. Relationships between the chemical and modal compositions of metapelites from Connemara, Ireland. Lithos, 10, 235-242.

Yokoyama, K. and Itaya, T., 1990. Clasts of high-grade Sanbagawa schist in Middle Eocene conglomerates from the Kuma Group, central Shikoku, south-west Japan. J. metam. Geol., 8, 467-474.

Yoshida, S., 1981. Chert-laminite: its petrographical description and occurrence in Japanese geosynclines. J. Geol. Soc. Jpn., 87, 131-141. (In Japanese with English abstract)

主論文2

Part 2

Hydration of basic granulite to garnet-epidote amphibolite in the Sanbagawa metamorphic belt, central Shikoku, Japan

Abstract

Granulite in the Iratsu-metagabbro of central Shikoku, with color-banding defined by the presence and absence of plagioclase, is surrounded by a narrow epidote amphibolite, which itself is encased in garnet-epidote amphibolite. The epidote amphibolite formed metastably under the low P_{H_2O} conditions based on the thermodynamic considerations. The granulite-epidote amphibolite boundary is formed by the hydration reaction of plagioclase to zoisite, kyanite, and quartz, and that of clinopyroxene and orthopyroxene to amphibole. If it is assumed that temperature range of the Sanbagawa epidote amphibolite facies is 600-650°C, we obtain a lithostatic pressure of 12-15 kbar and a H_2O pressure of 1-3 kbar for the hydration conditions. The boundary between epidote amphibolite and garnet-epidote amphibolite is defined by the formation of garnet, which is more stable than epidote amphibolite assemblages. Pargasitic amphibole occurs at the garnet rim. Up to 0.32 wt.% Cl is present in amphibole from both of the hydrated facies, but is < 0.03 wt.% Cl in the granulite amphibole. During hydration, there was an overall increase in bulk-rock Na_2O and Cl contents, and localized migration of Mg and Fe across the layering of the hydrated derivatives.

It is concluded that hydration did not take place in the presence of an excess fluid phase, based on the difference of the Cl contents of amphibole between observed and expected values from a qualitative infiltration metasomatic model and also on the estimated low fluid pressure estimated. The formation of a sharp boundary between the granulite and epidote amphibolite suggests intracrystalline diffusion.

Introduction

A free fluid phase always present during hydration and also prograde metamorphism is tacit supposition for many metamorphic petrologists. This assumption allows us to apply reaction equilibria experimented under fluid-saturation conditions directly to natural parageneses. Walther and Orville (1982) have pointed out that the fluid phase released during metamorphic reactions can normally and easily escape without interacting with the surrounding rocks, and that no fluid phase is present in metamorphic rocks apart from a devolatilization site. If their argument is true, it is necessary to consider the mechanism and conditions occurring with hydration under fluid-deficient conditions.

In the Sanbagawa metamorphic belt in central Shikoku, several large peridotite and metagabbro bodies have been tectonically intruded into high-grade pelitic and basic schists (Kunugiza et al., 1986). One such body, the Iratsu mass, contains the relics of pre-Sanbagawa granulite facies rocks that have been transformed into garnet-epidote amphibolite by the Sanbagawa metamorphism, and different degrees of transition can be observed in one outcrop (Yokoyama, 1980). In this paper, we describe the chemical and mineralogical changes accompanying the hydration of this granulite and discuss the mechanism and conditions at the hydration. Mineral abbreviations used are after Kretz (1983).

Petrology, and bulk and mineral chemistries

1. Mode of occurrences

A block of garnet-epidote amphibolite containing relics of granulite was found as river float in the Nikubuchi-dani (valley), a small tributary of the Dozan-gawa (river) in the Bessi(Besshi)-yama area, Ehime prefecture (Fig. 1). The general geology of this area was described by Kunugiza et al. (1986), and the petrology of the granulite briefly by Yokoyama (1976). The material studied is almost certainly derived from the Iratsu metagabbro defined by Kunugiza et al. (1986), which Takasu and Kohsaka (1987) and Takasu (1989) suggested to be divided into three independent complexes of high-grade mafic and ultramafic bodies, all of which locally contain eclogitic rocks. The block we studied came from the newly defined "eastern-mass" of the complex, which, according to Takasu and Kohsaka (1987) and Takasu (1989), has a fairly complex thermal history; layered gabbro --> granulite --> high temperature eclogite --> low temperature eclogite --> epidote amphibolite. However, the metagabbro to be described here records mainly the granulite and the epidote amphibolite facies equilibria without the eclogite facies assemblages.

The block, whose surface as washed by running water is quite fresh, measures approximately 3 x 3.5 x 2 m^3, and is composed mostly of garnet-epidote amphibolite. It contains several smaller domains of granulite facies relics as Fig. 2A shows. The host block was broken by mining engineers for detailed study.

The domains of granulite have a long axis of 10-50 cm, and display a color-banding defined by the presence and absence of

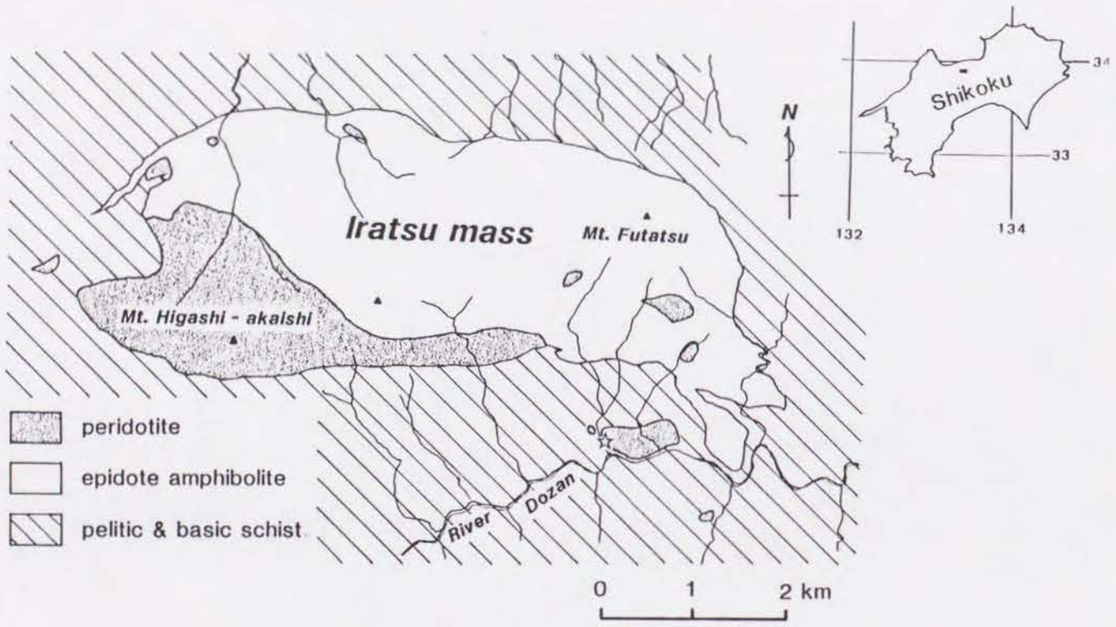

Figure 1. Index map of the Iratsu epidote-amphibolite mass. Locality of a granulite-bearing garnet-epidote amphibolite block is shown by open star.

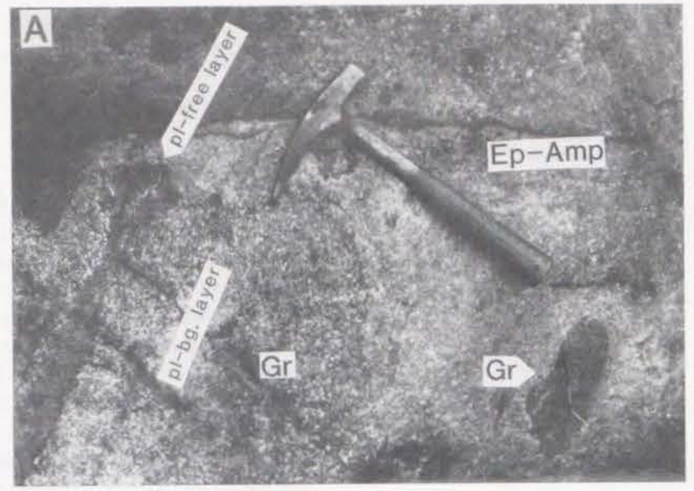

Figure 2. A: Photograph of the granulite-bearing garnet-epidote amphibolite block. Granulite (Gr) with color banding of melanocratic (pl-bearing) and hypermelanic (pl-free) layers is surrounded by epidote amphibolite (Ep-Amp).
B: Photomicrograph of boundary between granulite (right-hand side) and Grt-free epidote amphibolite (left-hand side). O=orthopyroxene, Pl=plagioclase surrounded by its hydration products, E=epidote.

plagioclase. As Figs. 2A and 3 show, this layering is inherited in the layering of garnet-bearing and garnet-free epidote amphibolites that enclose the granulite. A narrow (1-2 cm) zone of garnet-free epidote amphibolite never fails to develop between the granulite and the garnet-epidote amphibolite. These zones represent different stages of hydration reaction and will be referred to as the Grt-free zone, and Grt-bearing zone (Grt = garnet), respectively. The plagioclase-bearing layer of the granulite and its hydrated equivalents will be referred to as the melanocratic layer, as opposed to the hypermelanic layer (Shand, 1947), composed dominantly of pyroxenes or amphibole. The melanocratic and hypermelanic layers were originally plagioclase-rich and plagioclase-free, respectively, cumulate layers of gabbro (Yokoyama, 1976; Banno and Yokoyama, 1977).

2. Analytical procedures

Ten major- and 5 trace-element (Rb, Sr, Ni, Cl, S) concentrations were determined in 13 samples by X-ray fluorescence spectrometry (XRF: Rigaku Simultix System 3530 for major and Rigaku System 3370 for trace elements). The instrumental conditions and calibration techniques follow Goto and Tatsumi (1991 and in press). Table 1 lists the analyses and Table 2 compares the compositional parameters of various rock-types. Niggli's mg-value, molar MgO/(MgO+FeO), is also shown in Tables 1 and 2. Figure 3 shows the positional relation of the analyzed samples.

Mineral analyses were carried out on an energy-dispersive type electron microprobe at Kyoto University (Hitachi S550 + Kevex 7000). The analytical procedure follows Mori and Kanehira

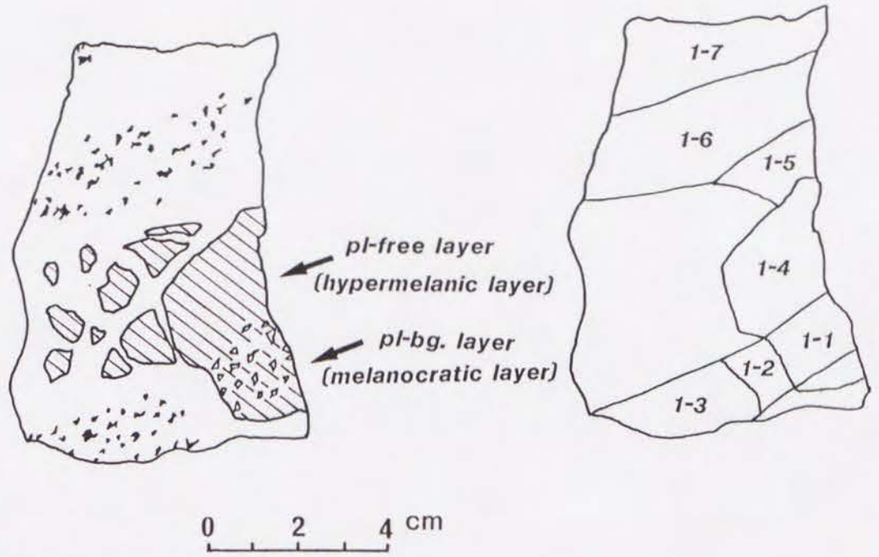

Figure 3. Schematic sketch of sample (left-hand side), and portion of the samples analyzed (right-hand side).

(1984). NaCl was the standard for Cl analysis. The analyses of the granulite facies minerals are shown in Table 3 and those of the Sanbagawa stage in Table 4 (amphibole) and Table 5 (others). The term hornblende is used in a wide sense following Hallimond (1943), but more specific amphibole names follow Leake (1978).

3. Bulk-rock chemistry

Table 2 reveals that the hydration of granulite proceeded without large changes in bulk-rock chemistry, except, of course, H_2O. There are, however, minor but significant changes. The most notable are a 6 to 8 fold increase in Cl content, and a concomitant 40% increase of Na_2O. We also notice a small but significant increase in the mg-value of the hypermelanic layer from 0.81 to 0.86.

The fact that the average value and standard deviation of the mg-value in the granulite are the same in the melanocratic and hypermelanic layers suggests that the mg-value was mainly governed by the X_{Mg} of the cumulate pyroxenes, and scarcely changed during the dry metamorphism of gabbro to granulite. The average value of the mg-value in the hydrated derivatives of the hypermelanic layers is significantly larger than that in the granulite, and suggests the migration of Mg and Fe^{2+} across the layering. The bulk-rock chemistry shows only minor compositional differences between the Grt-free (No. 1-2) and Grt-bearing (No. 1-3) samples of the same melanocratic layer (Fig. 3 and Table 1).

4. Petrography

Figure 4 shows the change in mineral assemblages from granulite through the Grt-free zone to Grt-bearing zone of the melanocratic layers.

Table 1. Bulk chemical compositions.

No.	1-1	1-2	1-3	1-4	1-5	1-6	1-7	1-8
SiO2	49.38	48.78	48.91	50.76	50.23	48.95	49.66	48.75
TiO2	0.18	0.17	0.17	0.21	0.19	0.18	0.20	0.19
Al2O3	9.72	9.58	9.33	6.68	7.87	9.82	8.00	9.73
FeO*	7.44	7.09	7.56	7.74	6.23	7.10	6.08	9.51
MnO	0.18	0.14	0.19	0.18	0.09	0.12	0.10	0.29
MgO	17.13	16.89	16.96	18.55	18.07	16.47	17.18	16.15
CaO	14.49	15.19	14.53	15.68	15.52	14.89	16.35	13.53
Na2O	0.56	0.75	0.75	0.47	0.68	0.62	0.74	0.63
K2O	0.05	0.05	0.05	0.04	0.05	0.06	0.05	0.05
P2O5	0.05	0.05	0.05	0.05	0.05	0.05	0.05	0.05
Total	99.18	98.69	98.50	100.36	98.98	98.26	98.41	98.88
mg-value	0.804	0.809	0.800	0.810	0.838	0.805	0.834	0.752
Sr(in ppm)	147	150	137	30	111	275	136	40
Rb	0.5	0.7	1.0	<0.5	<0.5	0.8	0.6	0.8
Ni	155	155	159	162	174	165	166	154
Cl	56	369	397	36	327	299	326	378
S	11	10	9	9	13	12	10	14

No.	3-1	3-2	3-3	3-4	3-5
SiO2	48.35	51.37	50.86	50.16	51.06
TiO2	0.18	0.21	0.21	0.20	0.20
Al2O3	10.22	6.27	6.20	8.54	6.91
FeO*	7.92	5.46	7.15	7.40	5.35
MnO	0.18	0.09	0.18	0.18	0.08
MgO	15.94	18.50	17.59	17.30	18.58
CaO	14.47	16.39	17.24	15.59	16.17
Na2O	0.61	0.72	0.51	0.49	0.76
K2O	0.05	0.04	0.04	0.04	0.05
P2O5	0.05	0.05	0.05	0.05	0.05
Total	97.97	99.10	100.03	99.95	99.21
mg-value	0.782	0.858	0.814	0.807	0.861
Sr	253	24	26	105	55
Rb	0.7	0.8	<0.5	0.6	0.8
Ni	156	175	163	174	175
Cl	285	285	37	41	277
S	9	9	10	11	11

*: Total Fe as FeO.

Table 1. (continued)

Granulite(1-1), garnet-free zone(1-2) and garnet-bearing zone(1-3) in the same melanocratic layer. Granulite (1-4) in the hypermelanic layer. Epidote-poor amphibole rock(1-5) near the hypermelanic layer but the part of the melanocratic layer was included in the analyzed sample. Garnet-epidote amphibolite (1-6) in the melanocratic layer. Garnet-poor epidote amphibolite(1-7). The analyzed sample contained both the layers. Garnet-epidote amphibolite(1-8) in the melanocratic layer. Garnet-epidote amphibolite(3-1) in the melanocratic layer. Epidote-poor amphibole rock(3-2) in the hypermelanic layer. Granulite(3-3) in the hypermelanic layer. Granulite(3-4) in the melanocratic layer. Epidote-poor amphibole rock(3-5) in the hypermelanic layer.

Table 2. Comparison of bulk-rock chemistry among rock-types.

	hypermelanic layer (Pl-free layer)	melanocratic layer (Pl-bg. layer)	average(1σ)
granulite			
Al2O3	6.20, 6.68	8.54, 9.72	
FeO*	7.15, 7.74	7.40, 7.44	
MgO	17.59,18.55	17.13,17.30	
Na2O	0.47, 0.51	0.49, 0.56	0.51(0.04)
Cl(ppm)	36, 37	41, 56	43(9)
mg-value	0.810,0.814	0.804,0.807	0.809(0.004)
epidote amphibolite			
Al2O3	6.27, 6.91	9.33-10.22	
FeO*	5.35, 5.46	7.09- 7.92	
MgO	18.50,18.58	15.94-16.96	
Na2O	0.72, 0.76	0.61- 0.75	0.70(0.07)
Cl(ppm)	227, 285	285- 397	338(54)
mg-value	0.858,0.861	0.782-0.809	0.819(0.033)

* Total Fe as FeO.

Granulite: The granulites are composed of an alternation of plagioclase-bearing and plagioclase-free pyroxene granulites, in which clinopyroxene predominates over orthopyroxene. The pyroxene analyses in Table 3 show Fe-Mg partitioning that is characteristic of the granulite facies. This is confirmed by the pyroxene geothermometer, which is based essentially on the miscibility gap between clino- and orthopyroxenes (Wood and Banno, 1973; Wells, 1977; Mori and Green, 1978). The pyroxene thermometer of Wells (1977) gives 750 ± 50°C for the granulite pyroxenes. Minor constituents are magnesiohornblende (AmpI) as well as the aggregate of zoisite, kyanite, quartz, and paragonite that developed at the periphery of plagioclase (An91), and cummingtonite (Cum) that occasionally replaced the orthopyroxene rim. Very minor calcite, ankerite and hematite occur interstitially.

Grt-free zone: This 1-2 cm-thick zone is developed between the granulite and Grt-bearing zone. Within this zone the melanocratic layer is epidote amphibolite and the hypermelanic layer is amphibole rock with rare epidote. The boundary against the granulite is sharp even under the microscope (Fig. 2B), but that against the Grt-bearing zone is defined mineralogically only by the appearance of garnet of 2-3 mm size in the melanocratic layer and is consequently less obvious.

The major minerals of the Grt-free zone is amphibole, ranging from actinolite to edenitic hornblende (AmpII). Aggregates of zoisite and clinozoisite that pseudomorph plagioclase, and dispersed chlorite are minor constituents. Talc, hematite, calcite and ankerite are rare. Pyroxenes (Cpx>>Opx) and

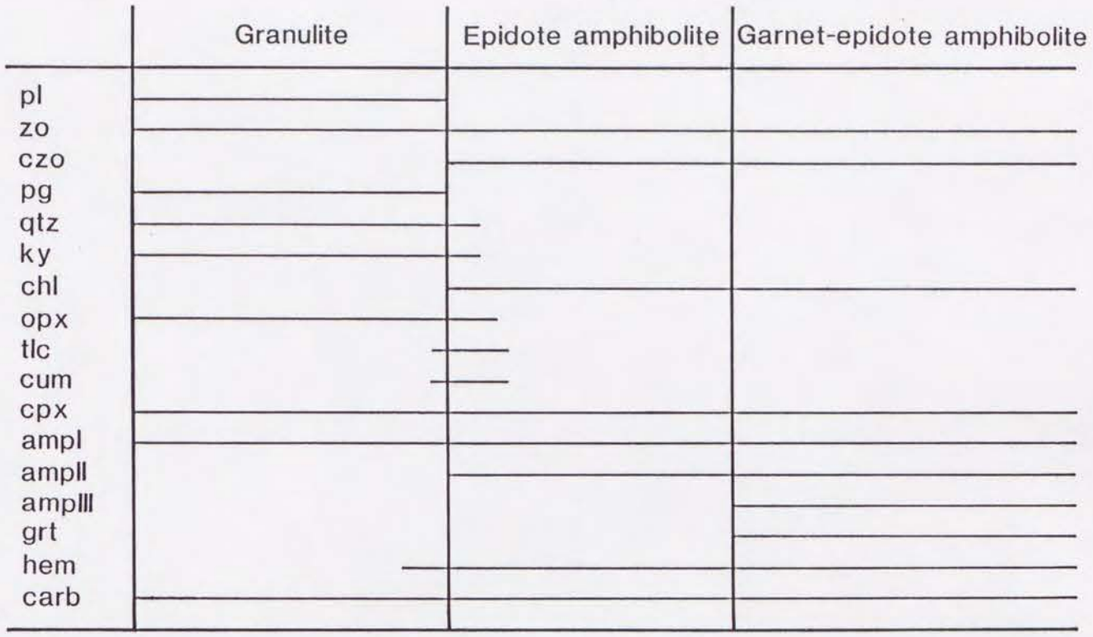

Figure 4. Changes in minerals in the melanocratic layer from granulite through epidote amphibolite to garnet-epidote amphibolite.

Table 3. Analyses of granulite minerals.

	Pl	Ampl#	Opx	Cpx
SiO2	45.05	47.06	52.47	50.89
TiO2	-	0.35	-	0.20
Al2O3	35.02	11.81	4.62	5.37
Cr2O3	-	0.32	0.17	0.27
FeO*	-	7.27	13.91	5.07
MnO	-	-	0.31	0.12
MgO	-	15.93	27.30	14.09
CaO	18.32	12.02	0.37	23.07
Na2O	1.02	1.67	-	0.56
K2O	0.12	0.13	-	-
Total	99.53	96.56	99.15	99.64
O	8	23	6	6
Si	2.087	6.751	1.893	1.879
Ti	-	0.038	-	0.006
Al	1.912	1.997	0.196	0.234
Cr	-	0.036	0.005	0.008
Fe	-	0.872	0.420	0.157
Mn	-	-	0.010	0.004
Mg	-	3.407	1.468	0.776
Ca	0.909	1.847	0.014	0.913
Na	0.092	0.465	-	0.040
K	0.007	0.024	-	-
Total	5.007	15.438	4.006	4.017
XMg		0.796	0.778	0.832
An	0.908			

-=below detection limit.
This Ampl is present in granulite.
* Total Fe as FeO.

Table 4. Analyses of amphiboles.

	AmpI		AmpII		AmpIII		Cum
SiO2	45.42	47.11	52.92	47.77	42.44	40.60	52.84
TiO2	0.16	0.34	-	0.08	0.14	0.20	-
Al2O3	10.18	9.85	4.42	9.91	14.44	15.22	5.24
Cr2O3	0.29	0.34	0.16	0.14	0.15	0.12	-
FeO*	9.93	8.69	6.05	9.03	10.98	12.39	12.50
MnO	0.12	0.12	0.14	0.13	0.12	0.14	0.37
MgO	15.24	16.11	20.02	16.58	13.75	12.56	21.47
CaO	12.66	12.12	12.08	12.70	12.44	12.44	3.31
Na2O	1.88	1.72	0.90	1.87	2.74	2.91	0.73
K2O	-	0.04	-	-	-	-	-
Cl	0.14	0.02	0.03	0.12	0.19	0.32	-
Total	96.02	96.46	96.72	98.33	97.39	96.90	96.46
O	23	23	23	23	23	23	23
Si	6.699	6.831	7.482	6.818	6.235	6.068	7.503
Ti	0.018	0.037	-	0.009	0.015	0.022	-
Al	1.770	1.683	0.736	1.667	2.500	2.681	0.877
Cr	0.034	0.039	0.018	0.016	0.017	0.014	-
Fe	1.225	1.054	0.715	1.078	1.349	1.549	1.484
Mn	0.015	0.015	0.017	0.016	0.015	0.018	0.044
Mg	3.351	3.483	4.220	3.528	3.011	2.798	4.545
Ca	2.001	1.883	1.830	1.942	1.958	1.992	0.503
Na	0.538	0.484	0.247	0.517	0.780	0.843	0.201
K	-	0.007	-	-	-	-	-
Total	15.651	15.516	15.265	15.591	15.880	15.985	15.157
XMg	0.732	0.832	0.855	0.766	0.691	0.644	0.754

-= below detection limit
* Total Fe as FeO.

AmpI occur only as relics from the granulite facies metamorphism. Some clinopyroxenes are zoned with an Al-poorer and Mg-richer rim. Both epidote and AmpII occur as irregularly shaped blebs within clinopyroxene, implying that the sporadic epidote in AmpII was derived from clinopyroxene.

Grt-bearing zone: This encloses the granulite relics. In this zone, the melanocratic layer is garnet-epidote amphibolite and the hypermelanic layer is composed essentially of hornblende as is in the Grt-free zone of it. Major constituents are AmpII, as in the Grt-free zone, garnet and clinozoisite. The garnet is generally 2-3 mm in size, but may reach a maximum size of up to 8 mm. It is anhedral, rather high in Mg for garnet (X_{Mg}=0.25-0.35), slightly heterogeneous but not systematically zoned, and contains abundant inclusions of zoisite, clinozoisite, AmpII, and opaques. The garnet is often armored by green pargasitic hornblende (AmpIII). When its periphery is replaced by the aggregate of chlorite + epidote, the rim of the garnet is depleted in Mg (X_{Mg}=0.25) compared with the core (X_{Mg}=0.3-0.35). Kyanite, quartz and paragonite do not occur. Even in this zone, relict clinopyroxene and AmpI are present.

Amphiboles: The compositions of three kinds of amphiboles are shown in a Hallimond (1943) diagram as Fig. 5. AmpI in the granulite, colorless magnesiohornblende, is homogeneous, and sometimes as coarse-grained as the pyroxene but sometimes replaces the rim of the latter. It persists into the Grt-free and Grt-bearing zones, where AmpI contains abundant fine-grained rutile and ilmenite, suggesting its adjustment to a lower-temperature environment. AmpI was formed in the period between

Table 5. Analyses of other constituent minerals.

	Ep#1	Ep	Chl	Grt		Cpx#2	Tlc	Pg
SiO2	38.95	37.31	27.64	38.68	37.92	53.29	55.98	44.94
Al2O3	32.93	25.37	21.41	21.56	21.10	1.32	3.24	39.00
Cr2O3	-	-	-	-	0.09	0.35	0.19	-
Fe2O3	0.19	9.95						
FeO*			10.05	22.25	22.27	3.80	4.17	-
MnO	-	-	-	1.63	1.89	-	-	-
MgO	-	-	27.58	5.39	4.21	15.85	28.11	-
CaO	24.58	23.48	-	10.36	11.70	24.03	-	1.62
Na2O	-	-	-	-	-	0.67	-	6.72
K2O	-	-	-	-	-	-	-	0.20
Total	96.65	96.11	86.68	99.87	99.18	99.31	91.68	92.48
O	25	25	28	12	12	6	11	22
Si	5.986	5.985	5.425	3.002	2.988	1.967	3.771	5.913
Al	5.964	4.796	4.953	1.972	1.960	0.057	0.257	6.048
Cr	-	-	-	-	0.006	0.010	0.010	-
Fe3+	0.022	1.201						
Fe			1.650	1.444	1.468	0.117	0.235	-
Mn	-	-	-	0.107	0.126	-	-	-
Mg	-	-	8.071	0.624	0.495	0.872	2.823	-
Ca	4.047	4.035	-	0.862	0.988	0.950	-	0.228
Na	-	-	-	-	-	0.048	-	1.714
K	-	-	-	-	-	-	-	0.034
Total	16.019	16.017	20.099	8.011	8.031	4.021	7.096	13.937
XMg			0.830	0.302	0.252	0.881	0.923	
XFe3+	0.004	0.200						

-=below detection limit.
#1: This occurs at the periphery of plagioclase in granulite.
#2: This shows the rim composition of clinopyroxene in the hydrated equivalent.
* Total Fe as FeO except epidote. Total Fe as Fe2O3 for epidote.

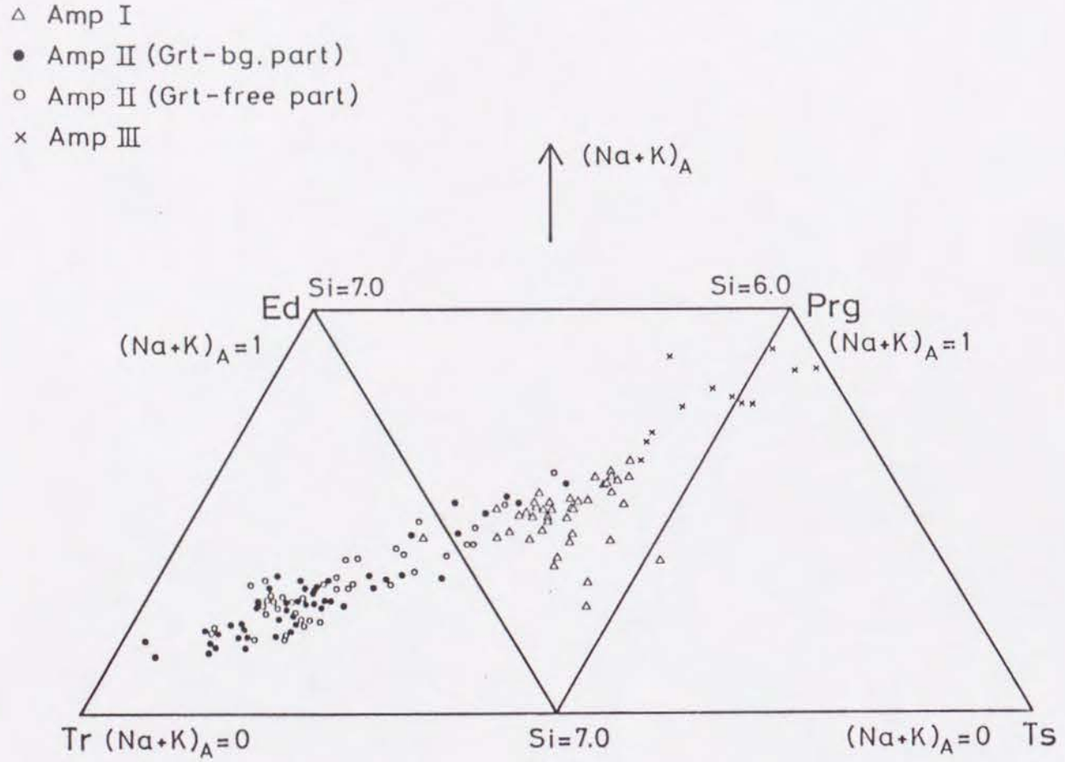

Figure 5. Compositional variation of amphiboles shown in the Hallimond diagram.

the granulite and the Sanbagawa metamorphism.

AmpII has a wide compositional range, from 30 to 90 % of actinolite, but is usually zoned with an actinolite core and hornblende rim. Rarely, it incipiently develops in the granulite along the pyroxene grain boundary, or occurs as vein, but its appearance is rather abrupt at the hydration front as seen in Fig. 2B. AmpIII is green pargasite and is confined to the periphery of the garnet. It has the highest Al content among the three amphibole types and postdates the formation of the metasomatic zone.

Figure 6 is an X_{Mg}-Al diagram for amphiboles. The range of X_{Mg} is the same for epidote amphibolite and garnet-epidote amphibolite, but the scatter of Al content is smaller for AmpII coexisting with garnet than that without garnet. Aluminum in the octahedral site of amphibole may be substituting Mg rather than Fe because of the negative correlation between X_{Mg} and Al content of amphiboles in Fig. 6.

Chlorine is mainly fixed in amphibole. A search for Cl in other minerals failed to record it. Figure 7 shows a strong correlation between the Na and Cl contents of the amphiboles. As there is a strong correlation between Na and Al (Fig. 5), there also is a correlation between Al and Cl.

Epidote: The relationships between the compositions and mode of occurrence of the epidote group minerals are shown in Fig. 8. The $Fe^{3+}/(Fe^{3+}+Al)$ ratio of epidote increases from the granulite to the Grt-bearing zone. In the epidote amphibolite and the garnet-epidote amphibolite, ferric-rich epidotes occur at the margins of pseudomorphs after plagioclase, as inclusions within AmpII and

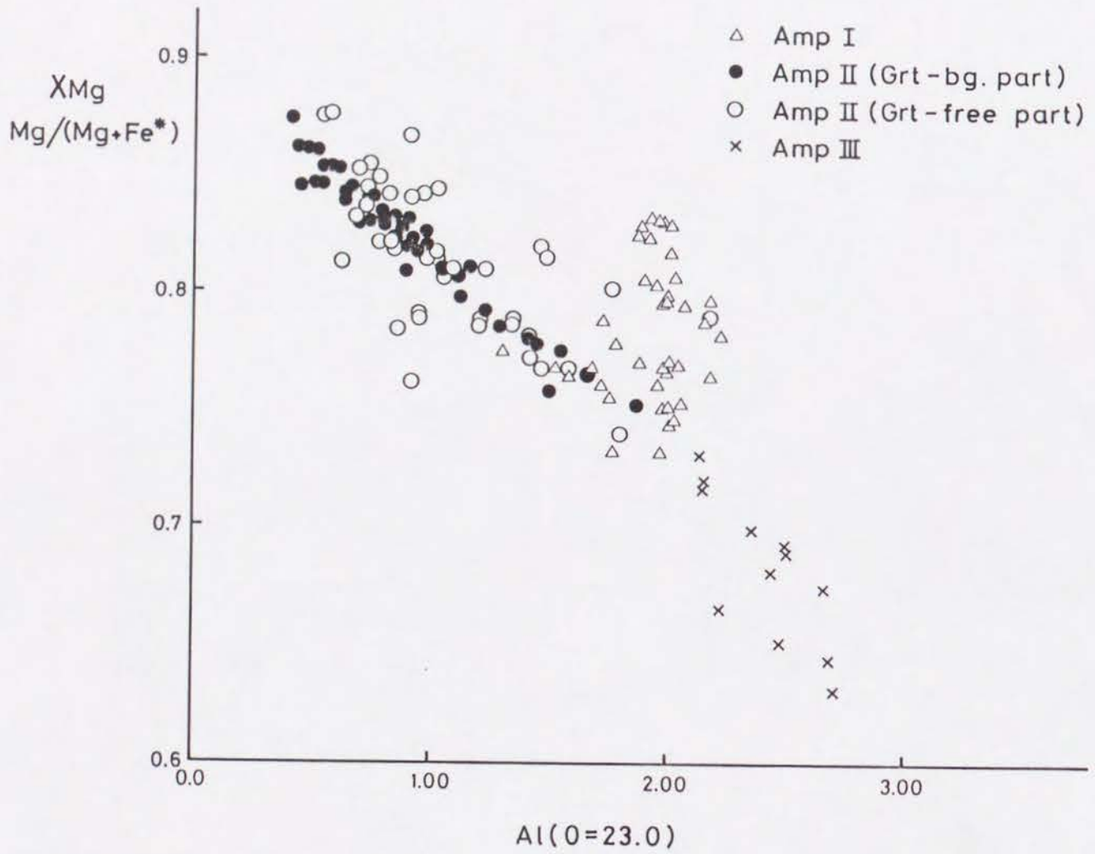

Figure 6. Correlation of the Al contents with X_{Mg} of amphiboles.

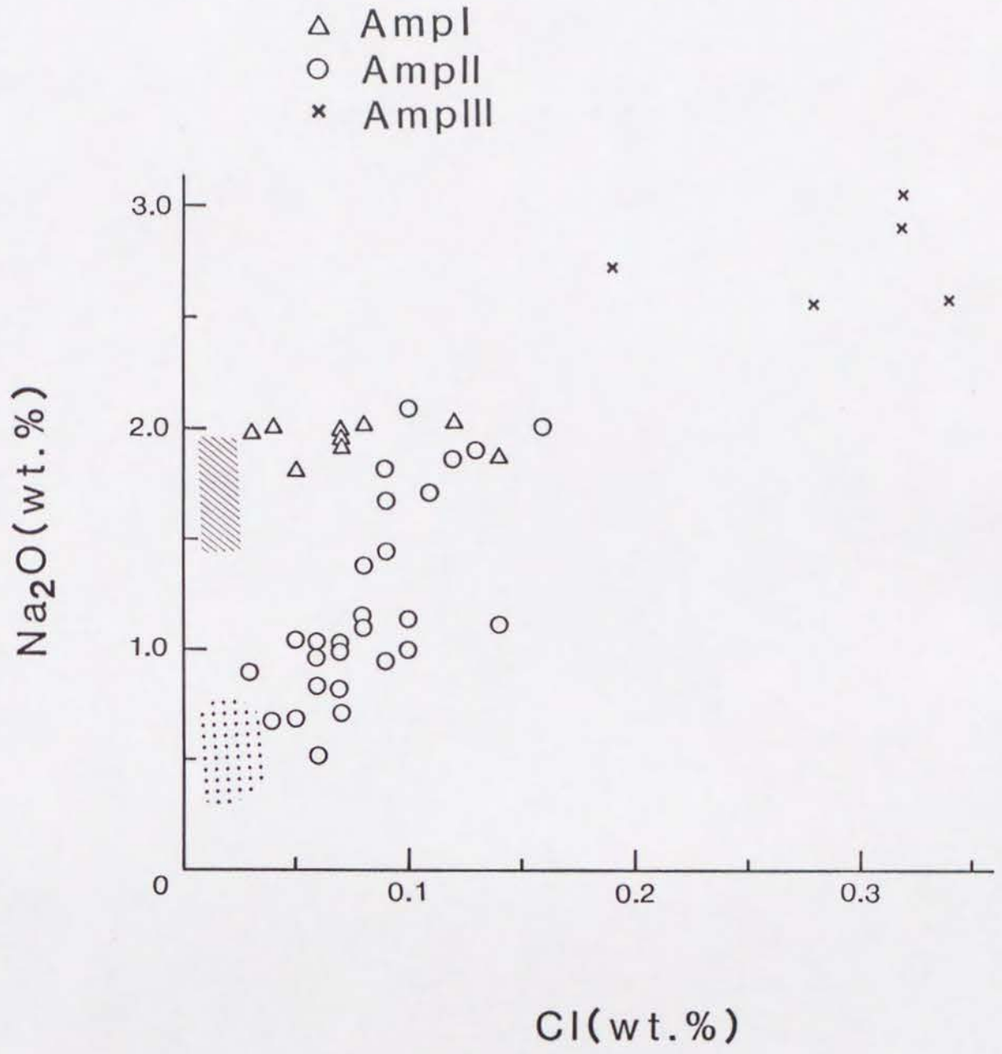

Figure 7. Na_2O vs. Cl of amphiboles. Hatched and dotted areas show compositional ranges of AmpI in the granulite and most of low Cl of AmpII, respectively. AmpI by open triangle occurs in epidote amphibolite and garnet-epidote amphibolite.

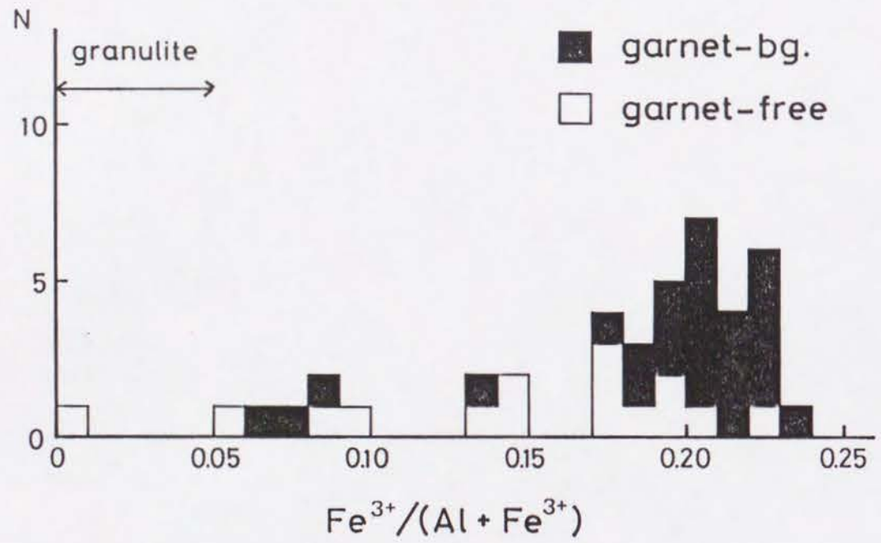

Figure 8. Frequency diagram of $X_{Fe}3+$ of epidote group minerals. Compositional range of zoisite in the granulite is shown by arrow.

garnet, lamellae within clinopyroxene, and as pseudomorphs after garnet. Zoisite is confined to the periphery of the plagioclase in the granulite, and in the center of clinozoisite aggregates that pseudomorph plagioclase in the hydrated derivatives of the granulite.

Advance of hydration zones

The first mineral formed after the granulite equilibration but before the Sanbagawa metamorphism was AmpI. It also occurs in the Grt-free and Grt-bearing epidote amphibolite zones as relics, which contains higher Cl content (up to 1300 ppm) than that in the granulite (< 300 ppm). The first hydrous minerals formed during the Sanbagawa metamorphism were zoisite and paragonite, which were co-occurring with quartz and kyanite replacing the margins of plagioclase. Rarely, AmpII vein occurs in the granulite, but generally the boundary of the Grt-free epidote amphibolite against the granulite is very sharp (Fig. 2B).

The Grt-bearing zone starts with the formation of garnet at the expense of AmpII and epidote from the melanocratic layer of the Grt-free zone. Garnet is anhedral and little zoned, compared with euhedral and zoned garnet in the prograde garnet-bearing basic schists. With the advance of hydration, the Fe^{3+} content of the epidote group minerals increases, suggesting that the oxidation gave rise to the larger degree of substitution of Fe^{3+} for Al and also the formation of hematite in the hydrated derivatives.

During hydration, pressure and temperature differences between the metasomatic zones could hardly have been significant over a distance of 1 m or so. Hydration was due to the reaction between the granulite and the migrating fluid. The resultant chemical change may be summarized as follows:

(1) The Cl content of the epidote amphibolite is as much as 8 times that of granulite (Table 2).

(2) The Na_2O increased by about 40%.

(3) The mg-values of the melanocratic and hypermelanic layers of the Grt-bearing zone show slight but statistically significant difference. However, the mg-values are the same between the corresponding layers in the granulite.

(4) The X_{Mg} of hornblende is almost the same between the hornblendes in both the melanocratic and hypermelanic layers of the Grt-bearing zone.

(5) The Fe^{3+} content of epidote increases.

Discussion

1. H_2O pressure

The Grt-free and the Grt-bearing zones derived from the same melanocratic layer have similar bulk compositions across the front of garnet formation. The boundary between the Grt-free and the Grt-bearing zones of the melanocratic layer is described by the following reaction:

amphibole II + epidote = garnet + H_2O.

Grt-free zone Grt-bearing zone (1).

Figure 9 schematically shows free energy changes among granulite, epidote amphibolite, and garnet-epidote amphibolite assemblages in the melanocratic layer at constant pressure, temperature and bulk composition in response to P_{H_2O}. Clearly, the granulite assemblage becomes unstable and is to be replaced by hydrated assemblages with increasing P_{H_2O}. Moreover, if the epidote amphibolite assemblage is stable at the hydration front, the garnet-epidote amphibolite assemblage could never form at any P_{H_2O}. Therefore we envisage that the granulite was first replaced metastably by epidote amphibolite that was in turn transformed to the more stable garnet-epidote amphibolite. It seems easy to transform the granulite to the epidote amphibolite metastably rather than to transform the granulite to the garnet-epidote amphibolite at the hydration front. Tha metastable reactions between pyroxene and amphibole may be partly responsible to the similarity of their crystal structures. Note that P_{H_2O} for the stable transition of the granulite assemblage to the garnet-epidote amphibolite assemblage is lower than that for the the metastable transition observed.

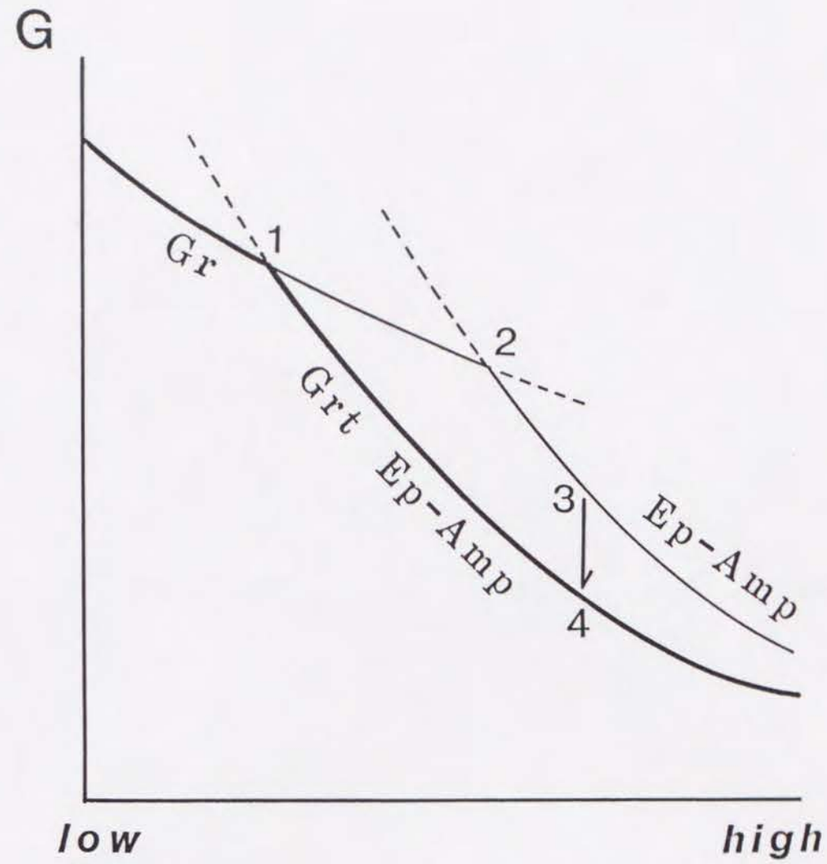

Figure 9. Schematic diagram of the free energy changes among granulite (Gr), epidote-amphibolite (Ep-Amp), and garnet epidote-amphibolite (Grt Ep-Amp) of the melanocratic layer in response to P_{H_2O}. Thick, thin, and broken curves correspond to stable, metastable, and unstable conditions, respectively. Points 1 and 2 show the stable (expected) hydration front and the metastable (observed) hydration front, respectively. The arrow from point 3 to point 4 represents the free energy change of the garnet formation in the melanocratic layer.

Although the hydration front represents the metastable interface between granulite and epidote amphibolite, its physical conditions can be determined. At the hydration front, zoisite and AmpII coexist with pyroxenes and plagioclase. As AmpII includes actinolitic hornblende, the H_2O partial pressure can be estimated by using two chemical reactions in relation to the formation of the zoisite and AmpII.

As zoisite coexists typically with kyanite and quartz at the hydration front, its formation is described quantitatively by the following reaction:

$4CaAl_2Si_2O_8 + H_2O = 2Ca_2Al_3Si_3O_{12}(OH) + Al_2SiO_5 + SiO_2$

anorthite water zoisite kyanite quartz (2).

The formation of amphibole is rather complex, but we may simplify the reaction as the formation of actinolite from Al-poor and Fe-free pyroxenes, since actinolite usually occupies the core of the amphibole, suggesting that it is the first amphibole to be formed. Furthermore, the high X_{Mg} of actinolite (Fig. 6) allows us to use tremolite instead of actinolite in the calculation. The amphibole formation may then be described by either of the following equations:

$2CaMgSi_2O_6 + 1.5Mg_2Si_2O_6 + SiO_2 + H_2O = Ca_2Mg_5Si_8O_{22}(OH)_2$

diopside enstatite quartz water tremolite (3).

$2CaMgSi_2O_6 + 2.5Mg_2Si_2O_6 + H_2O = Mg_2SiO_4 + Ca_2Mg_5Si_8O_{22}(OH)_2$

diopside enstatite water forsterite tremolite (4).

AmpII is not associated with quartz (Qtz occurs only in zoisite aggregates in the granulite and around the hydration front), so that we may regard the reaction as having taken place somewhere between the univariant lines of the above two reactions

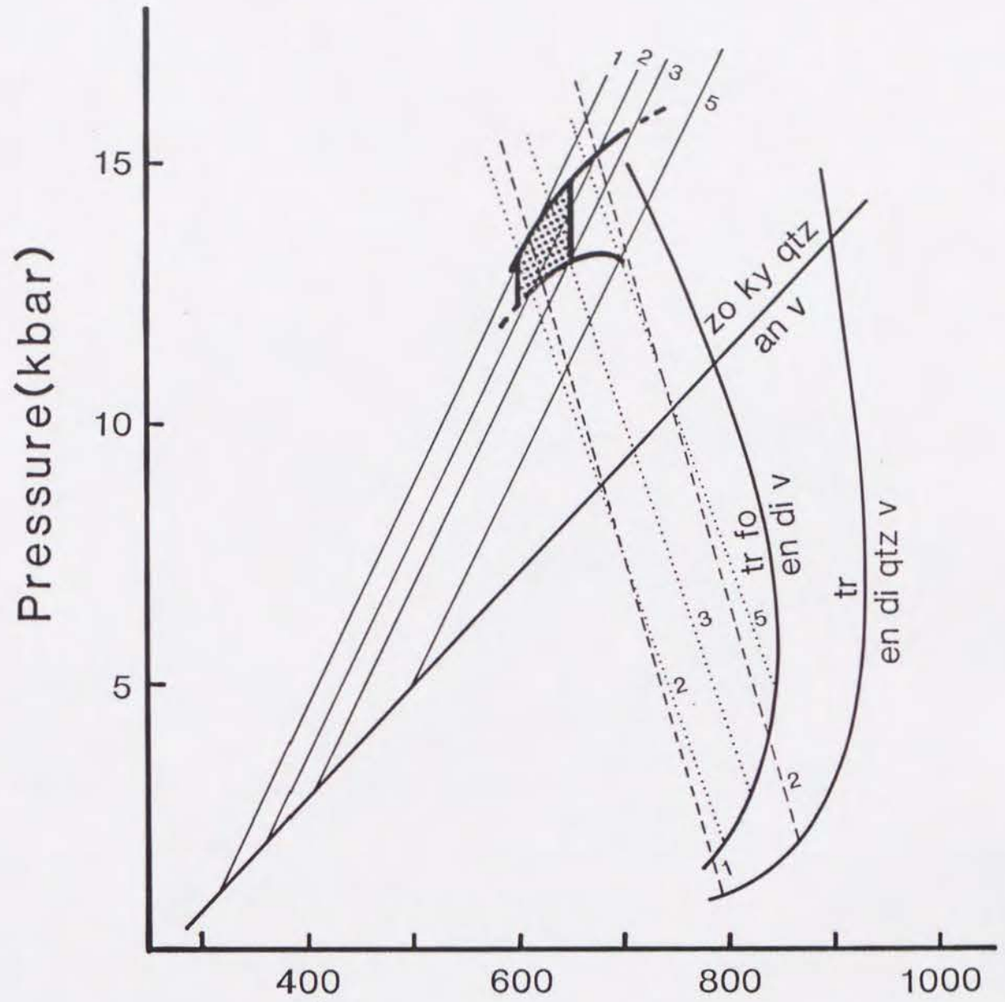

Figure 10. Estimated P-T conditions of granulite hydration: tremolite = enstatite + diopside + quartz + H_2O (Boyd, 1959; Helgeson et al., 1978): tremolite + forsterite = enstatite + diopside + H_2O (Jenkins, 1983): zoisite + kyanite + quartz = anorthite + H_2O (Jenkins et al., 1983). Broad lines show the dehydration curves under $P_{total} = P_{H_2O}$ conditions. $P_{H_2O} < P_{total}$ lines also show with a given P_{H_2O}. Temperature range is quoted from Kunugiza et al. (1986). Two thick lines represent the traces of the upper and the lower pressure limits in response to P_{H_2O}. The conditions of the granulite hydration are approximately estimated to be in the dotted region.

(3) and (4), although no olivine was observed in the amphibolite. Figure 10 shows the reaction curves for different values of P_{H_2O}. The relevant phase relations and thermodynamic properties are taken from Boyd (1959), Helgeson et al. (1978), Jenkins (1983) and Jenkins et al. (1983). Assuming 600°C-650°C for epidote amphibolite, the value given by Kunugiza et al. (1986) as the formation temperature for the eclogite-epidote amphibolite association of the Iratsu mass, we obtain 12-15 kbar as the rock pressure, and 1-3 kbar as the nominal H_2O pressure for the zoisite-AmpII assemblage. The latter value hardly exceeds 5 kbar, even if ample allowance is made for the uncertainty of calculations, as is seen in Fig. 10. The very low partial pressure of H_2O we obtained may be realized if the fluid contains fluid species other than H_2O. Stability of diopside in the presence of CO_2-H_2O binary fluid is governed by the following reaction:

$$CaMgSi_2O_6 + 2CO_2 = CaMg(CO_3)_2 + 2SiO_2 \quad (5).$$

diopside carbon-dioxide dolomite quartz

The diopside-bearing assemblage at 650°C is confined to rocks with $X_{CO_2} < 0.35$ at 12 kbar following the thermodynamic properties of minerals from Holland and Powell (1985) and the f_{CO_2} from Powell and Holland (1985). This is consistent with the general low P_{CO_2} of fluid coexisting with the Sanbagawa schists (Ernst, 1972; Itaya and Banno, 1980).

We obtain maximum values for X_{CO_2} of 0.35 and X_{H_2O} of 0.25. The result suggests that the granulite hydration did not take place under fluid-excess conditions, but did so under fluid-deficient conditions. This conclusion will be supported by the

inconsistency between the mineral chemistries observed and estimated assuming infiltration metasomatic equilibrium.

2. Model of transportation of excess fluid

The simplest hypothesis for the hydration of the granulite is based on a 1-dimensional model (Fig. 11). Granulite (Gr) is surrounded by epidote amphibolite (Ep-Amp) which is in turn surrounded by some external environment (Ext). The Grt-free and Grt-bearing epidote amphibolites are jointly represented by Ep-Amp. We first try to explain this metasomatic column by infiltration metasomatism, which is modeled as follows:

(1) Amphibole (Amp_{ss}) is equivalent to pyroxenes (Px) + fluid (Fld).

(2) Fluid is an H_2O-Cl mixture because of the low CO_2 pressure estimated.

(3) Amphibole preferentially incorporates H_2O over Cl, i.e.:

$K = (X_{OH}/X_{Cl})^{Amp_{ss}}/(X_{OH}/X_{Cl})^{Fld} > 1.$ (6).

(4) Excess fluid is present.

(5) Local equilibrium is achieved everywhere.

The phase relations of the model system taking the assumptions of (1)-(4) into account are shown in Fig. 12, in which the triangle Px-Amp_{ss}-Fld shows the compositions of amphibole saturated with Cl. Compositional changes of amphibole and fluid have been qualitatively calculated to obtain insight of what should happen in the natural system. As the model is crude and adequate initial values of fluid are not available, we arbitrarily chose the following values: K of eq.(6) is 2, X_{Cl} of initial fluid is 0.1 (i.e. X_{Cl} of amphibole coexisting with it is 0.053) and amphibole saturates in Cl when X_{Cl} of amphibole

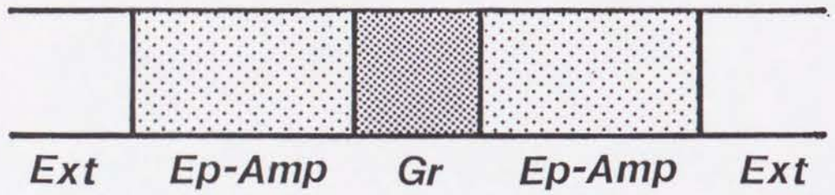

Figure 11. One-dimensional model for granulite hydration. Granulite (Gr) is surrounded by epidote amphibolite (Ep-Amp) which in turn is surrounded by external environment (Ext). Cl-bearing fluid is supplied from the external environment.

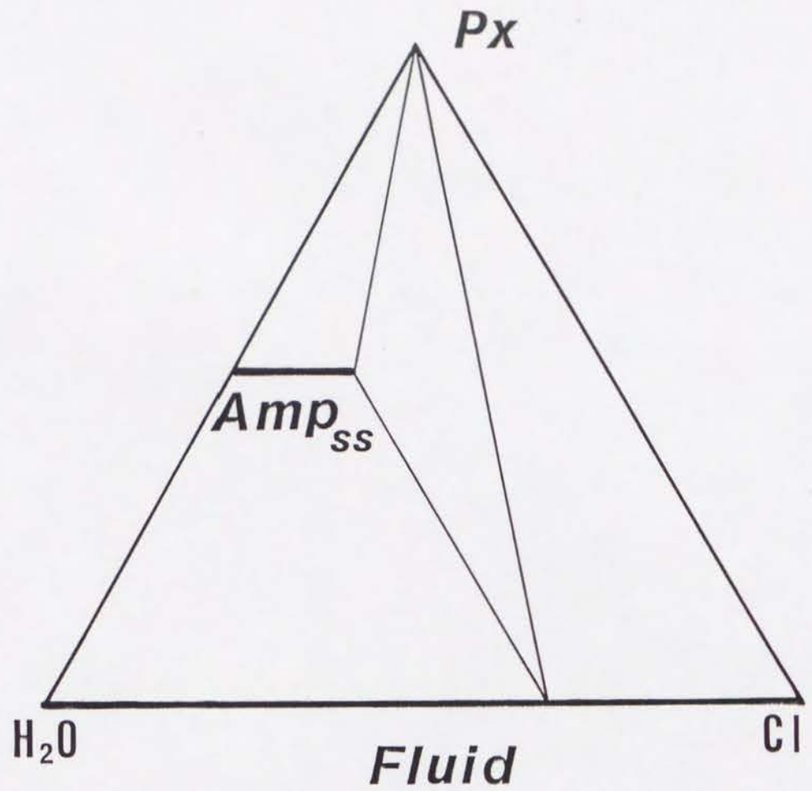

Figure 12. Schematic phase relation among pyroxene (Px), amphibole solid solution (Amp_{ss}), and H_2O-Cl binary fluid.

reaches 0.3 (i.e. X_{Cl} of fluid coexisting with the saturated amphibole is 0.462). We further assume that H_2O and Cl mix ideally.

Figures 13A and 13B show how the compositional change in the model infiltration column is calculated. We divided the system into cells, and fluid moves step by step by transferring the fluid from one cell to the other. The first fluid entering the first cell is consumed to hydrate pyroxene to amphibole with X_{Cl} of 0.1. At the next step the amphibole in the first cell reacts with the incoming fluid with X_{Cl} of 0.1 and exchanges Cl with it to give rise to the amphibole with X_{Cl} of 0.07 and fluid with X_{Cl} of 0.13 which is transferred to the second cell where it precipitates forming amphibole with X_{Cl} of 0.13. The X_{Cl} of amphibole in the cell of pyroxene first infiltrated by fluid is high because all the fluid with high X_{Cl} is fixed in amphibole. Further, the X_{Cl} of amphibole in a given cell decreases as the result of exchange of Cl and (OH) with the incoming fluid till it becomes 0.053, the value to be in equilibrium with initial fluid with X_{Cl} of 0.1. When the step continues, the X_{Cl} of fluid infiltrating into the cell of the hydration front increases. Figure 13A shows the compositions of the fluid and amphibole at the sixth step of the infiltration process.

With further advance of the infiltration, the amphibole becomes saturated in Cl. Then the fluid with X_{Cl} of 0.462, that coexists with both the amphibole saturated with Cl and pyroxene, enters the pyroxene cell and forms amphibole without changing neither the X_{Cl} of fluid nor that of amphibole. Eventually, the fluid with X_{Cl} of 0.462 entering granulite cannot hydrate the

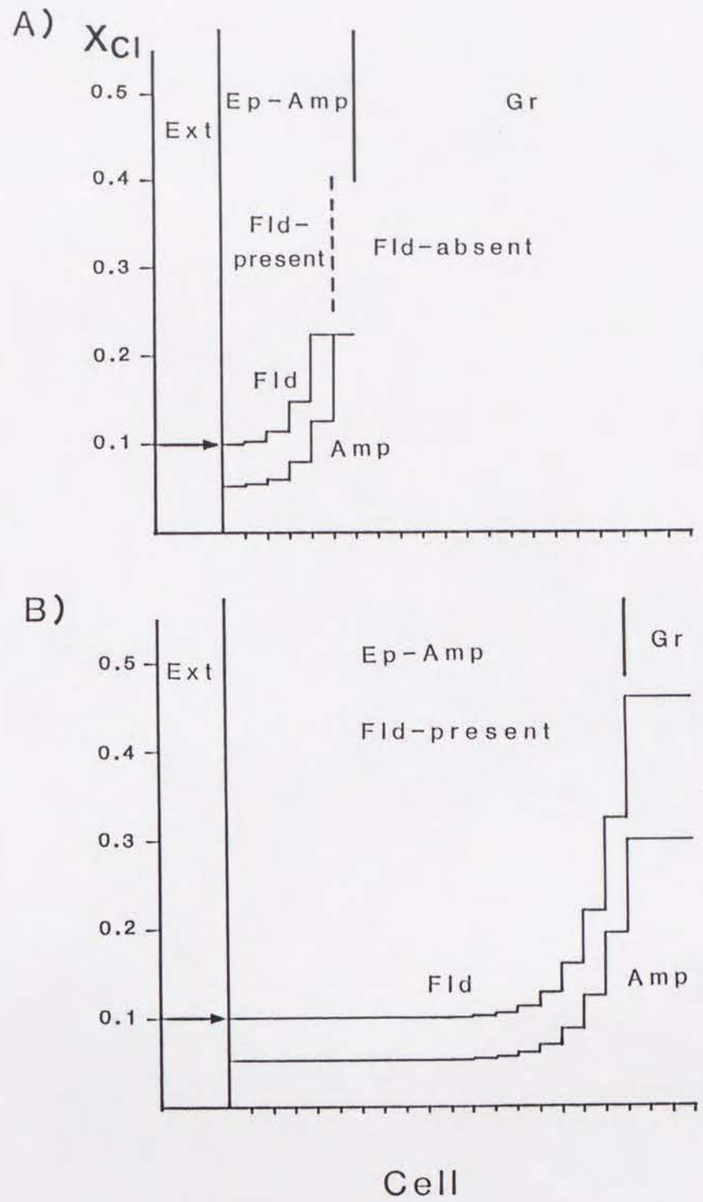

Figure 13. Compositional changes in amphibole (Amp) and fluid (Fld) calculated by an infiltration metasomatic column model. Compositions of fluid and amphibole at the 6th step (A) and at the n-th step (B) of the infiltration process. Vertical lines represent zone boundaries. Broken line in (A) indicates the boundary between fluid-present and -absent cells. Fluid is in equilibrium with both epidote-amphibolite (Ep-Amp) and granulite (Gr) in the case of (B). See text for detail.

pyroxene at all. Thus, at this stage, the front of infiltrating fluid overtakes that of the hydration. The front of hydration further advances because X_{Cl} of amphibole ahead of the hydration front must decrease as the infiltration proceeds, or in other words, the formation of the fluid coexisting with amphibole saturated with Cl must be compensated by the formation of Cl-poor amphibole.

Figure 13B shows the compositions of fluid and amphibole at the n-th step of calculation. The figure shows that it needs only 5 cells for the change of X_{Cl} of amphibole from approximately 0.06 to 0.30. Although the size of cell is chosen arbitrarily in the calculation, it should be infinitesimal small to simulate the natural process. Thus the gradient of X_{Cl} of amphibole in front of the saturation front is vertical.

Our model of infiltration metasomatism of the Cl-bearing fluid can explain how the pyroxene-rich granulite changes to amphibole with high X_{Cl}. Ito and Anderson (1983) demonstrated that in the alteration zone of submarine gabbros, the Cl-content of rocks gradually increases from 100 ppm to 500 ppm in samples taken from depths between about 2900 m to 3100 m, and rapidly declined at deeper levels. This compositional trend corresponds to that of our model and suggests that the hydrothermal alteration in the ocean floor might be an infiltration metasomatic process.

Next, let us assume that some Cl-poor amphibole is dispersed in the granulite. In the amphibole zone, this amphibole has the same X_{Cl} as the associated amphibole. In the zone where saturated fluid and pyroxene coexist, the primary amphibole should exchange

Cl with the fluid and be saturated in Cl. However, as described in preceding sections this is not the case. The amphibole in the granulite is virtually free from Cl, whereas in the hydrated derivatives, it contains up to 1300 ppm of Cl. As the Al_2O_3 content of relict amphibole, AmpI, is higher than those of newly formed amphibole, AmpII, the compositional effect shown in Fig. 7 cannot explain the observed difference. The observation can be explained if the fluid did not reach AmpI, but the volume of granulite relic is negligible as compared with that of the epidote amphibolite, making it difficult to envisage that the saturated fluid did not soak the granulite.

Therefore, we must conclude that the infiltration of Cl-bearing fluid into the granulite cannot explain the Cl content of AmpI. Further, we must accept the material transfer with fluid pressure lower than solid pressure, a conclusion reached by estimating the equilibrium calculations.

3. Fluid migration under fluid-deficient conditions

If we accept that the fluid pressure is lower than that of the solid, we may model the system to be penetrated by capillaries surrounded with semi-permeable membrane through which H_2O and Cl migrate (Thompson, 1955). The metasomatic column and concentration gradient are similar to those for excess fluid, but now the total fluid pressure is less than the confining pressure, and the material moves through the capillaries. The sum of partial pressure of H_2O, CO_2 and Cl is lower than lithostatic pressure. The fluid species exist beyond the hydration front, but their pressures are too low to hydrate the granulite. Provided that the diffusion rate, and not the reaction rate, controls the

hydration process, not only the pressure but also the amount of fluid species to diffuse ahead of the hydration front is small. We may then transpose the capillary model into the intracrystalline diffusion model, as judged from the fact that the sharp hydration front is not overtaken by the grain boundary system.

Consideration of the transport system does not present any compelling conclusion, but we consider the fluid-deficient model to be more logical than the excess fluid model, even though it may appear speculative.

4. Some additional comments

Soda metasomatism: Even though the concept of soda metasomatism has failed to explain the origin of glaucophane schists (Miyashiro and Banno, 1958), widespread occurrences of jadeite veins and nodules in mafic and ultramafic rocks suggest that Na_2O is mobile, at least locally, in the environment of high pressure regional metamorphism. We have shown that migration of Na_2O on a scale of 10 to 100 m took place, accompanied by the hydration of the basic granulite. Even if Na_2O migrated over a considerable distance in the Sanbagawa belt, it may not be detected usually, since Na_2O is a major component of the schists, whose Na_2O content varies greatly from one rock to another. We could detect the addition of Na_2O because the granulite was very low in Na_2O and the banding of melanocratic and hypermelanic layers could be traced from the anhydrous granulite to fully hydrated garnet-epidote amphibolite.

Yokoyama and Mori (1975) demonstrated that the formation of pargasite in a spinel-bearing metagabbro from the Nikubuchi body

of the same Iratsu complex required transport of Na_2O. This is essentially the same as the addition of Na_2O revealed in this study. Supply of Na_2O in the formation of hornblende has also been described from a garnet websterite from the Basal Gneiss region of Norway (Banno and Mori, 1976). The migration of Na_2O was not a local phenomenon, moreover it could be a fairly common phenomenon.

Mg and Fe migration across the layering: The formation of garnet occurred due to the high Al_2O_3 content of the melanocratic layer, and then a stable alternation of garnet-bearing and garnet-free epidote amphibolites was formed. Originally, the mg-values in them had been the same, so that the amphiboles in the garnet-bearing melanocratic layer had a higher X_{Mg} than those in the hypermelanic layer free from garnet, because Fe in the former layer was preferentially fixed in garnet. This led to a difference in chemical potentials of the amphibole end-members, and those of the constituent oxides such as FeO, MgO etc., between two layers. Thus bimetasomatism took place, and gave rise to the same X_{Mg} of amphibole and different mg-values between the melanocratic and hypermelanic layers.

Source of fluid: The hydrating fluid was high in Na_2O, Cl and f_{O_2}, and low in F and S. Ito and Anderson (1983) and Nakamura (1986) attributed the high Cl and low F amphiboles in ophiolitic rocks to their reaction with seawater, which migrated around oceanic ridges. However, fluid directly derived from seawater is not envisaged in the hydration of the granulite in question, as it took place in the epidote amphibolite facies that is at too high a pressure to be expected in the oceanic ridge region. The

fluid in the Sanbagawa metamorphism may ultimately have been of seawater origin, but it was significantly modified, as it experienced complex fixation by, and liberation from, the Sanbagawa schists.

Concluding remarks

By tracing the chemical changes accompanying the hydration of granulite to garnet-epidote amphibolite in the area of the epidote amphibolite facies of the Sanbagawa metamorphic belt, addition of Na_2O and Cl was clearly detected, but no remarkable change in the other components was confirmed. Slight migration of Mg and Fe across the layering took place due to bimetasomatism between garnet-epidote amphibolite and epidote amphibolite. During the hydration, metastable epidote amphibolite preceded garnet-epidote amphibolite, which was the stable final product.

The mechanism of hydration has been discussed, based on the behavior of Cl in amphibole, and the difficulty of applying the concept of infiltration metasomatism to the hydration of the granulite in the Sanbagawa belt, is pointed out.

References

Banno, S. and Mori, T., 1976. Compositional gradient in interstitial hornblende from a Norwegian garnet websterite. Norsk. Geologisk. Tidsskrift., 56, 309-314.

Banno, S. and Yokoyama, K., 1977. Peridotite-metagabbro complex in central Shikoku. In: K. Hide (Editor), The Sambagawa belt. Hiroshima University Press, Hiroshima, 57-68 (in Japanese with English abstract).

Boyd, F. R., 1959. Hydrothermal investigation of amphiboles. In: P.H. Abelson (Editor), Researches in geochemistry. John Wiley & Sons, Inc., New York, 1, 377-396.

Ernst, W. G., 1972. CO_2-poor composition of the fluid attending Franciscan and Sanbagawa low-grade metamorphism. Geochim. Cosmochim. Acta, 36, 497-504.

Goto, A. and Tatsumi, Y., 1991. The chemical analysis of rock samples by XRF (I). Rigaku-Denki J., 22, 28-44. (In Japanese)

Goto, A. and Tatsumi, Y., in press. The chemical analysis of rock samples by XRF (II). Rigaku-Denki J. (In Japanese)

Hallimond, A. F., 1943. On the graphical representation of the calciferous amphiboles. Am. Mineral., 28, 65-89.

Helgeson, H. C., Delany, J. M., Nesbitt, H. W. and Bird, D. K., 1978. Summary and critique of the thermodynamic properties of rock-forming minerals. Am. J. Sci., 278-A, 1-229.

Holland, T. J. B. and Powell, R., 1985. An internally consistent thermodynamic dataset with uncertainties and correlations: 2. Data and results. J. meta. Geol., 3, 343-370.

Itaya, T. and Banno, S., 1980. Paragenesis of titanium-bearing accessories in pelitic schists of the Sanbagawa metamorphic

belt, central Shikoku, Japan. Contrib. Mineral. Petrol., 73, 267-276.

Ito, E. and Anderson, A. T. Jr., 1983. Submarine metamorphism of gabbros from the Mid-Clayton Rise: Petrographic and mineralogic constraints on hydrothermal processes at slow-spreading ridges. Contrib. Mineral. Petrol., 82, 371-388.

Jenkins, D. M., 1983. Stability and composition relations of calcic amphiboles in ultramafic rocks. Contrib. Mineral. Petrol., 83, 375-384.

Jenkins, D. M., Newton, R. C. and Goldsmith, J. R., 1983. Fe-free clinozoisite stability relative to zoisite. Nature (London), 304, 622-623.

Kretz, R., 1983. Symbols for rock-forming minerals. Am. Mineral., 68, 277-279.

Kunugiza, K., Takasu, A. and Banno, S., 1986. The origin and metamorphic history of the ultramafic and metagabbro bodies in the Sanbagawa metamorphic belt. In: B.W. Evans and E.H. Brown (Editors), Blueschists and Eclogites. Geol. Soc. Am. Mem., 164, 375-385.

Leake, B. E., 1978. Nomenclature of amphiboles. Am. Mineral., 63, 1023-1052.

Miyashiro, A. and Banno, S., 1958. Nature of glaucophanitic metamorphism. Am. J. Sci., 256, 97-110.

Mori, T. and Green, D. H., 1978. Laboratory duplication of phase equilibria observed in natural garnet lherzolites. J. Geol., 86, 83-97.

Mori, T. and Kanehira, K., 1984. X-ray energy spectrometry for electron-probe analysis. J. Geol. Soc. Jpn., 90, 271-285.

Nakamura, Y., 1986. Rocks of the seamount interior. Gekkan Chikyu (The Earth Monthly), 8, 485-488. (in Japanese)

Powell, R. and Holland, T. J. B., 1985. An internally consistent thermodynamic dataset with uncertainties and correlations: 1. Methods and a worked example. J. meta. Geol., 3, 327-342.

Shand, S. J., 1947. Eruptive rocks. John Wiley & Sons, Inc., New York, 488pp.

Takasu, A., 1989. P-T histories of peridotite and amphibolite tectonic blocks in the Sanbagawa metamorphic belt, Japan. In: J.S. Daly, R.A. Cliff, and B.W.D. Yardley (Editors), Evolution of metamorphic belts. Geol. Soc. London, Special Publication, 43, 533-538.

Takasu, A. and Kohsaka, Y., 1987. Eclogites from the Iratsu epidote amphibolite mass in the Sambagawa metamorphic belt, Besshi district, Japan. J. Geol. Soc. Jpn., 93, 517-520. (in Japanese)

Thompson, J. B. Jr., 1955. The thermodynamic basis for the mineral facies concept. Am. J. Sci., 253, 65-103.

Walther, J. V. and Orville, P. M., 1982. Volatile production and transport in regional metamorphism. Contrib. Mineral. Petrol. 79, 252-257.

Wells, P. R. A., 1977. Pyroxene thermometry in simple and complex systems. Contrib. Mineral. Petrol., 62, 129-139.

Wood, B. J. and Banno, S., 1973. Garnet-orthopyroxene and orthopyroxene-clinopyroxene relationships in simple and complex systems. Contrib. Mineral. Petrol., 42, 109-124.

Yokoyama, K., 1976. Finding of plagioclase-bearing granulite from the Iratsu epidote amphibolite mass in central Shikoku. J. Geol. Soc. Jpn., 82, 549-551.

Yokoyama, K., 1980. Nikubuchi peridotite body in the Sanbagawa metamorphic belt; Thermal history of the 'Al-pyroxene-rich suite' peridotite body in high pressure metamorphic terrain. Contrib. Mineral. Petrol., 73, 1-13.

Yokoyama, K. and Mori, T., 1975. Spinel-garnet-two pyroxene rock from the Iratsu epidote amphibolite mass, central Shikoku. J. Geol. Soc. Jpn., 81, 29-37.

主論文3

Part 3

Stability of chlorite in the upper mantle

Abstract

Stability of chlorite in the presence of orthopyroxene under upper-mantle conditions has been thermodynamically examined in the model system MgO-Al_2O_3-SiO_2-H_2O (MASH). All minerals were assumed to be pure in the MASH system. Calculation of the reaction curve took into account heat capacity (Cp), thermal expansion (αV), and isothermal compressibility (βV). If it is assumed that $\Delta\alpha V = \Delta\beta V = 0$, the stability of chlorite in the upper mantle is slightly pressure dependent; the upper stability curve for chlorite is located at 800°C, 650°C, and 500°C, at 2.9 GPa, 4.2 GPa, and 5.0 GPa, respectively. On the other hand, the assumption that $\Delta\alpha V \neq 0$ and $\Delta\beta V \neq 0$ yields a more temperature-dependent curve for the chlorite stability; 800°C at 3.9 GPa, and 700°C at 5.5 GPa. The present calculation indicates that chlorite crystallized in down-dragged hydrous peridotite at the base of a mantle wedge decomposes at pressures of 3.0-3.5 GPa. Therefore, H_2O released from chlorite may play a partial role in producing magmas beneath a volcanic front which lies about 110 km above a subducted slab.

Introduction

Chlorite must crystallize during hydration processes in an ultramafic system and may be one of the main hydrous phases in both the lower crust and the upper mantle. Phase relations of chlorite have been examined in natural metamorphosed ultramafic rocks formed at low pressures or under lower-crustal conditions (e.g., Springer, 1974). However, very little is known about the stability of chlorite in the upper mantle, probably because chlorite is relatively uncommon in high-pressure hydrous ultramafic rocks which commonly contain amphibole and/or phlogopite. The stability of chlorite, which carries a large amount of water (ca. 13 wt%), should yield important information pertinent to the understanding of the distribution and circulation of water in the upper mantle.

In this paper, we examine the stability limit of chlorite in the upper mantle in terms of thermodynamic calculations and discuss the role of chlorite in magma genesis in subduction zones. Mineral abbreviations in the text and figures are after Kretz (1983).

Previous work

Staudigel and Schreyer (1977) conducted high-pressure experiments on the stability limit of 14Å-clinochlore, which is the thermally most stable mineral among Mg-rich chlorites, in the water-pressure range 1.0-3.5 GPa in the system MgO-Al_2O_3-SiO_2-H_2O (MASH). Their results revealed that clinochlore disintegrates through strongly temperature-dependent reactions to forsterite, enstatite, spinel and aqueous fluid at pressures below 2.0 GPa, that is, within the spinel-peridotite field. In the garnet peridotite field, it breaks down to spinel, pyrope, forsterite and aqueous fluid (Fig. 1). However, the reaction does not govern the stability limit of chlorite in a natural garnet peridotite, because chlorite is stable only under P-T conditions below those of the univariant curve of the reaction

$$Mg_{10}Al_2Al_2Si_6O_{20}(OH)_{16} + 2Mg_2Si_2O_6$$
clinochlore enstatite
$$= 2Mg_3Al_2Si_3O_{12} + 4Mg_2SiO_4 + 8H_2O. \quad (1)$$
pyrope forsterite fluid

Delany and Helgeson (1978) calculated univariant curves for a number of dehydration reactions taking place in the subducted oceanic crust in the system K_2O-Na_2O-MgO-FeO-Al_2O_3-SiO_2-H_2O up to 10 GPa and presented the decomposition reaction of clinochlore. They argued that anhydrous assemblages after dehydration of 14Å-clinochlore at pressures up to 10 GPa are clinoenstatite, forsterite, spinel and H_2O (Fig. 1). However, the assemblage enstatite + spinel can only be stable in the spinel peridotite stability field. It is stressed, therefore, that the dehydration curve of clinochlore after Delany and Helgeson (1978) is not

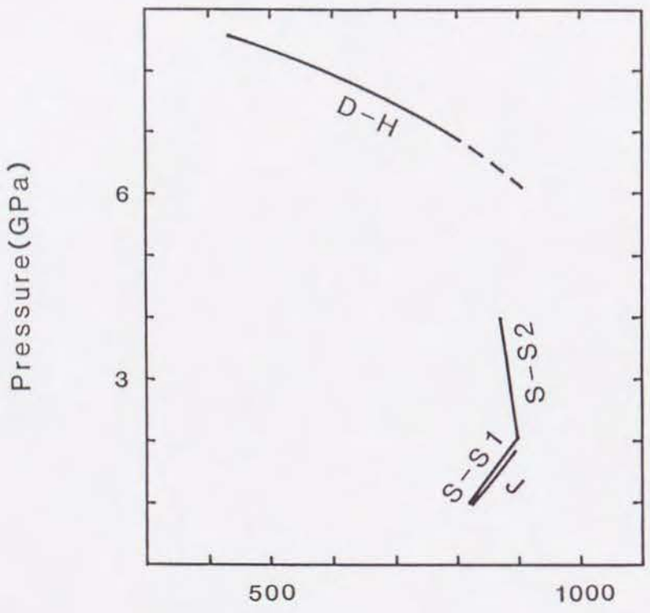

Figure 1. Previous work bearing on chlorite stability at high pressures. **S-S1**; 14Å-clinochlore ⟶ enstatite + forsterite + spinel + H_2O (Staudigel and Schreyer, 1977). **S-S2**; 14Å-clinochlore ⟶ pyrope + forsterite + spinel + H_2O (Staudigel and Schreyer, 1977). D-H; 14Å-clinochlore ⟶ clinoenstatite + forsterite + spinel + H_2O (Delany and Helgeson, 1978). J; 14Å-clinochlore ⟶ enstatite + forsterite + spinel + H_2O (Jenkins, 1981).

applicable to the consideration of hydrous phase relations in the upper mantle at pressures grater than 2 GPa.

Obata and Thompson (1981) made a first attempt to construct a petrogenetic grid for hydrous mafic and ultramafic rocks combining the method of Schreinemakers with available experimental data in the model system CaO-MgO-Al_2O_3-SiO_2-H_2O (CMASH). They chose the following reactions from the grid obtained for the chlorite-bearing reactions.

Chl + Grt = Fo + Spl + Opx + H_2O (2)

Chl + Amp = Fo + Spl + Opx + H_2O (3)

Chl + An = Fo + Spl + Opx + H_2O (4)

Chl + Cpx = Fo + Spl + Opx + H_2O (5)

Garnet, amphibole, anorthite and clinopyroxene on the left hand sides of reactions, and orthopyroxene on the right hand sides of all reactions are CaO-bearing phases. However, the maximum stability of chlorite under spinel peridotite conditions expressed by

$Mg_{10}Al_2Al_2Si_6O_{20}(OH)_{16}$

clinochlore

$= 2MgAl_2O_4 + 2Mg_2SiO_4 + 2Mg_2Si_2O_6 + 8H_2O.$ (6)

spinel forsterite enstatite fluid

should be adopted in the grid instead of the reactions 2-5, because the effect of CaO-solubility in orthopyroxene on reaction 6 is negligible in this temperature range (ca. less than 900°C).

Jenkins (1981) determined the location of the reaction 6 and discussed the stability of chlorite-lherzolite. As reaction 6 shows, Jenkins's (1981, 1983) chlorite-lherzolite is stable only at the spinel peridotite field, not at the garnet peridotite

field.

Thermodynamic considerations

The aluminous phase in an upper-mantle peridotite changes from plagioclase through spinel to garnet with increasing pressure. Determining the stability of chlorite must take the coexisting aluminous phase into account; reactions 1 and 6 define the stability of chlorite in a garnet peridotite system and a spinel peridotite system, respectively.

The dehydration curve of reaction 6, which was experimentally determined by Staudigel and Schreyer (1977) and Jenkins (1981), is directly applicable to consideration of the stability of 14Å-clinochlore in spinel peridotites, because the dehydration products of clinochlore include the spinel peridotite minerals forsterite + enstatite + spinel.

In order to clarify the stability of chlorite in a garnet peridotite system, we examine the equilibrium conditions for reaction 1 in terms of equilibrium constant and activities.

$$\Delta G^{O} = \Delta_f H - T\Delta S + \int_{298}^{T} \Delta Cp\,\underline{dT} - T\int_{298}^{T} (\Delta Cp/T)\,\underline{dT}$$
$$+ P[\Delta V + (\Delta\alpha V)(T-298) - (\Delta\beta V)P/2] + 8RT\ln \underline{f}_{H_2O} + RT\ln K$$

$$K = \frac{(\underline{a}^{grt}_{Mg_3Al_2Si_3O_{12}})^2 (\underline{a}^{ol}_{Mg_2SiO_4})^4}{(\underline{a}^{chl}_{Mg_{10}Al_2Al_2Si_6O_{20}(OH)_{16}})(\underline{a}^{opx}_{Mg_2Si_2O_6})^2}.$$

Symbols are listed in Table 1; $\underline{a}^{\underline{j}}_{\underline{i}}$ is the activity of component $\underline{i}$ in phase $\underline{j}$. As the behavior of H_2O differs markedly from that predicted from the perfect gas laws, the fugacity of H_2O($\underline{f}_{H_2O}$) tabulated by Burnham et al. (1969) up to 1.0 GPa pressures and Delany and Helgeson (1978) up to 10 GPa pressures are used for the present calculations. The thermodynamic data of minerals after Holland and Powell (1985) are also used (Table 2).

Table 1. Symbols used in an equilibrium calculation.

$\Delta_f H$	enthalpy of formation from the elements at 1 bar and 298 K
S	entropy at 1 bar and 298 K
V	volume at 1 bar and 298 K
Cp	heat capacity: $Cp = a + bT + cT^{-2} + dT^{-1/2}$, with T in K
α	coefficient of thermal expansion
β	coefficient of isothermal compressibility
ΔG^{o}	Gibbs energy change for a reaction among pure-end member phases at the temperature and pressure of interest
K	equilibrium constant for a balanced reaction

Note: Themodynamic properties are in units of kilojoules, kelvins, and kilobars.

Table 2. Thermodynamic properties used in this study.

Mineral	enstatite	clinochlore	forsterite	pyrope	H_2O
H	-3090.08	-17742.12	-2173.02	-6284.49	-241.81
S $x10^{-3}$	132.5	924.0	94.1	266.3	188.8
V	6.262	42.280	4.379	11.327	
a	0.3562	1.4494	0.2349	0.5450	0.0401
b $x10^{-5}$	-0.299	23.074	0.107	2.068	0.866
c	-597	-40618	-543	-8331	488
d	-3.185	0.646	-1.906	-2.283	-0.251
αV $x10^{-5}$	18.0	136.0	16.0	28.0	
βV $x10^{-3}$	4.6	76.0	3.2	7.6	

Note: Units are kilojourles, kelvins, and kilobars.

For the purpose of solving the equilibrium conditions for reaction 1, the following simplified treatment may be sufficient. All phases treated here are assumed to be pure, although orthopyroxene can contain tschermakite components. Thus, the equilibrium constant K can be unity.

Figures 2A and 2B show the calculated stability limit of chlorite in the presence of orthopyroxene in the MASH system. The results in Fig. 2A are based on the assumption of $\Delta\alpha V = \Delta\beta V = 0$, and those in Fig. 2B on $\Delta\alpha V \neq 0$ and $\Delta\beta V \neq 0$.

Because of the metastable extension of spinel peridotite assemblages into the garnet peridotite field, the univariant line of chlorite decomposition calculated by Delany and Helgeson (1978) is located at the highest P-T region (Fig. 1). Both the experiments by Staudigel and Schreyer (1977) and by Jenkins (1981) obtained similar dehydration curves of chlorite in the spinel peridotite field (Fig. 1). Since the Al_2O_3 content of chlorite is too high to decompose into garnet lherzolite minerals, the maximum stability of chlorite with more temperature-dependent reactions (**S-S2** in Fig. 1) is wider than that of chlorite in peridotite in Figs. 2A and 2B. It is suggested that chlorite in peridotite assemblages decomposes through a reaction with a positive $\underline{dP}/\underline{dT}$ slope within the spinel peridotite field (Fig. 1) and through a reaction with a negative $\underline{dP}/\underline{dT}$ slope under conditions corresponding to the garnet-peridotite field (Figs. 2A, 2B).

Although chlorite has been recognized in only a few ultramafic rocks, it does crystallize under some upper mantle conditions. In the Ochiai-Hokubo ultramafic complex,

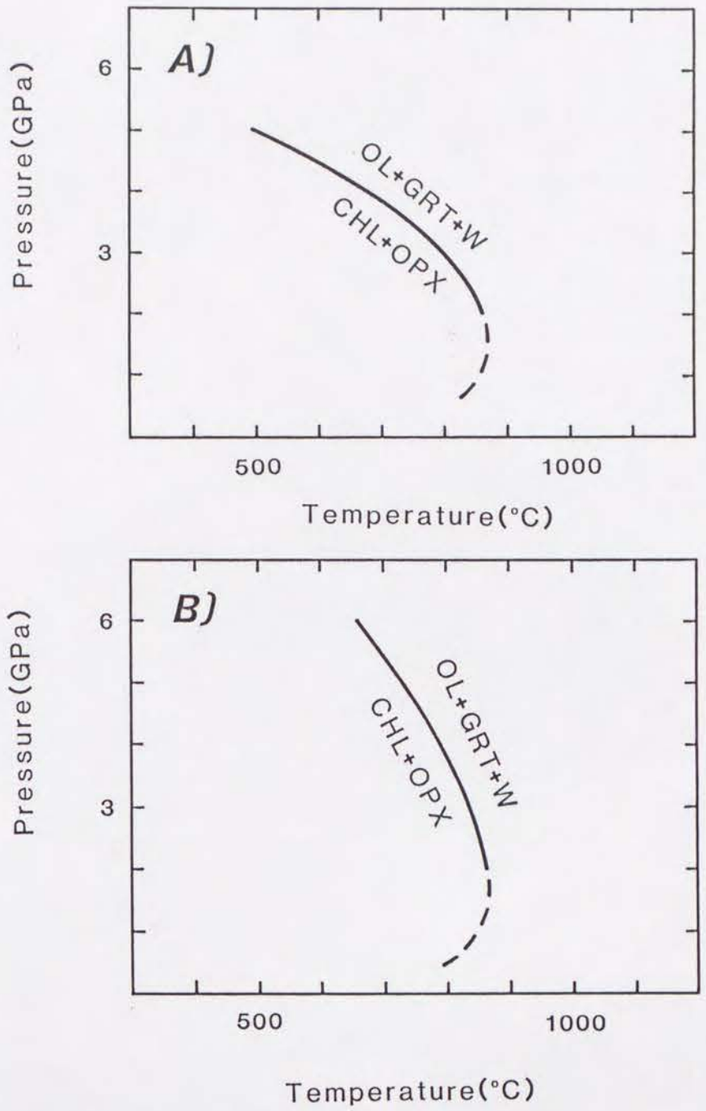

Figure 2. Calculated stability limits of chlorite + orthopyroxene, based on the assumptions (**A**) $\Delta\alpha V = \Delta\beta V = 0$ and (**B**) $\Delta\alpha V \neq 0$ and $\Delta\beta V \neq 0$.

southwestern Japan, a chlorite corona around chromian spinel was commonly observed even if the peridotite was almost free from serpentinization (Arai, 1978). Medaris (1980, 1984) also described the assemblage chlorite + orthopyroxene in Norwegian peridotite. These lines of evidence indicate that chlorite is stable under higher P-T conditions than both serpentine and talc.

Implication for magma genesis

A knowledge of the stability of hydrous phases in peridotite systems is essential to an understanding of magma genesis in the upper mantle, because H_2O released from hydrous phases drastically lowers the solidus temperature of peridotite. In particular, the origin of subduction-zone magmas has been related to the decomposition of hydrous minerals in subducted oceanic lithosphere (e.g., Fyfe and Mcbirney, 1975). Therefore, attention must be paid to the contribution of chlorite to the production of magmas in subduction zones. Tatsumi (1986, 1989) emphasized that the downgoing slab is anhydrous beneath a volcanic arc and proposed a mechanism in which hydrous peridotites, formed at the base of the fore-arc mantle wedge by the addition of slab-derived H_2O, are dragged downward on the slab. The mechanism implies that the stability of hydrous phases in a peridotite system strongly controls the position of magma generation in the mantle wedge.

Figure 3 shows the calculated stability limits of chlorite in the MASH system together with decomposition curves of amphibole (AMP; Millhollen et al., 1974) and phlogopite (PHL; Sudo and Tatsumi, 1990) in a peridotite. Temperature distributions at the top (TMJ) and at 5km below the top (TMJ5) of the subducted slab (Toksöz et al., 1971) are also shown in Fig. 3. It should be noted that the decomposition of chlorite takes place under P-T conditions close to the maximum stability of amphibole in the down-dragged hydrous peridotite; both chlorite and amphibole break down at pressures of 3-3.5 GPa under the geothermal gradient shown on Fig. 3. This pressure is equivalent to the depth of the base of the mantle wedge or the surface of

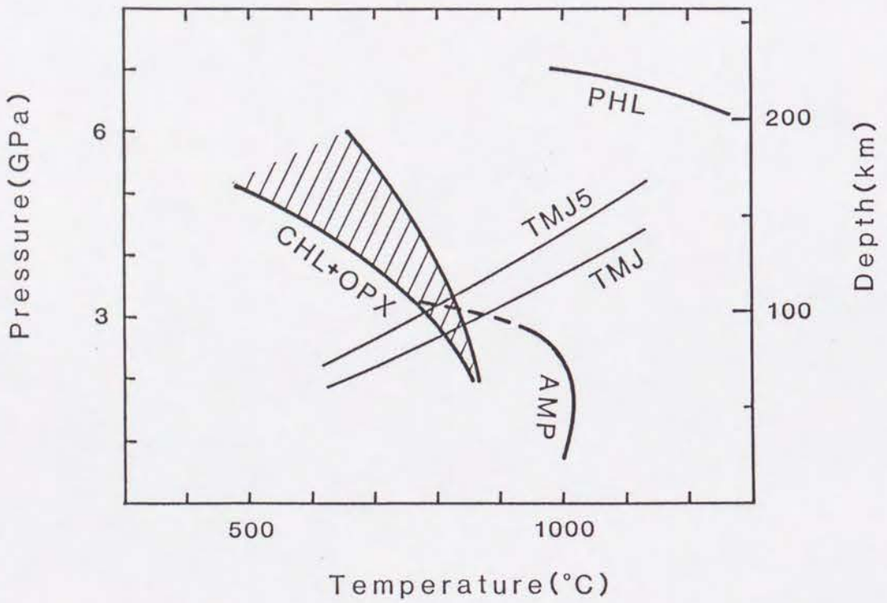

Figure 3. Dehydration curves of phlogopite in a peridotite (PHL; Sudo and Tatsumi, 1990), amphibole in a peridotite (AMP; Millhollen et al., 1974) and chlorite + orthopyroxene in the MASH system (CHL + OPX). Temperature distributions at the top (TMJ) and at 5 km below the top (TMJ5) of the subducted slab (Toksöz et al., 1971) are also indicated.

the slab immediately beneath a volcanic front in most subduction zones [112±19(1σ) km; Tatsumi, 1986]. Therefore, it is suggested that generation of magmas beneath the volcanic front is governed by the dehydration of both chlorite and amphibole in the down-dragged hydrous peridotite. Chlorite decomposes through less pressure-dependent reaction than amphibole in a peridotite system (Fig. 3), which may yield the variety in depth of the subducted slab beneath the volcanic front. Phlogopite remains stable to deeper levels (Fig. 3) and its dehydration may be related to volcanism in volcanic arcs away from (behind) the volcanic front (Tatsumi, 1989; Sudo and Tatsumi, 1990).

References

Arai, S., 1978. Formation of the chlorite corona around chromian spinel in peridotite and its significance. Geosci. Reports Shizuoka Univ., 3, 9-15. (in Japanese with English abstract)

Burnham, C. W., Holloway, J. R. and Davis, N. F., 1969. Thermodynamic properties of water to 1000^{o}C and 10000 bars. Geol. Soc. Am. Special Paper, 132, 1-96.

Delany, J. M. and Helgeson, H. C., 1978. Calculation of the thermodynamic consequences of dehydration in subducting oceanic crust to 100 kb and >800^{o}C. Am. J. Sci., 278, 638-686.

Fyfe, W. S. and McBirney, A. R., 1975. Subduction and the structure of andesitic volcanic belts. Am. J. Sci., 275-A, 285-297.

Holland, T. J. B. and Powell, R., 1985. An internal consistent thermodynamic dataset with uncertainties and correlations: 2. Data and resu;ts. J. metam. Geol., 3, 343-370.

Jenkins, D. M., 1981. Experimental phase relations of hydrous peridotites modelled in the system H_2O-CaO-MgO-Al_2O_3-SiO_2. Contrib. Mineral. Petrol., 77, 166-176.

Jenkins, D. M., 1983. Stability and composition relations of calcic amphiboles in ultramafic rocks. Contrib. Mineral. Petrol., 83, 375-384.

Kretz, R., 1983. Symbols for rock-forming minerals. Am. Mineral., 68, 277-279.

Medaris, L. G. Jr., 1980. Petrogenesis of the Lien peridotite and associated eclogites, Almklovdalen, Western Norway. Lithos, 13, 339-353.

Medaris, L. G. Jr., 1984. A geothermobarometric investigation of garnet peridotites in the Western Gneiss Region of Norway. Contrib. Mineral. Petrol., 87, 72-86.

Millhollen, G. L., Irving, A. J. and Wyllie, P. J., 1974. Melting interval of peridotite with 5.7 percent water to 30 kilobars. J. Geol., 82, 575-587.

Obata, M. and Thompson, A. B., 1981. Amphibole and chlorite in mafic and ultramafic rocks in the crust and upper mantle. A theoretical approach. Contrib. Mineral. Petrol., 77, 74-81.

Springer, R. K., 1974. Contact metamorphosed ultramafic rocks in the western Sierra Nevada Foothills, California. J. Petrol., 15, 160-195.

Staudigel, H. and Schreyer, W., 1977. The upper thermal stability of clinochlore, $Mg_5Al(AlSi_3O_{10})(OH)_8$, at 10-35kb P_{H_2O}. Contrib. Mineral. Petrol., 61, 187-198.

Sudo, A. and Tatsumi Y., 1990. Phlogopite and K-amphibole in the upper mantle: Implication for magma genesis in subduction zones. Geophys. Res. Lett., 17, 29-32.

Tatsumi, Y., 1986. Formation of the volcanic front in subduction zones. Geophys. Res. Lett., 13, 717-720.

Tatsumi, Y., 1988. Migration of H_2O and genesis of basaltic magmas in subduction zones. J. Geophys. Res., 94, 4697-4707.

Toksöz, M. N., Minear, J. W. and Julian, B. R., 1971. Temperature field and geophysical effects of a downgoing slab. J. Geophys. Res., 76, 1113-1138.